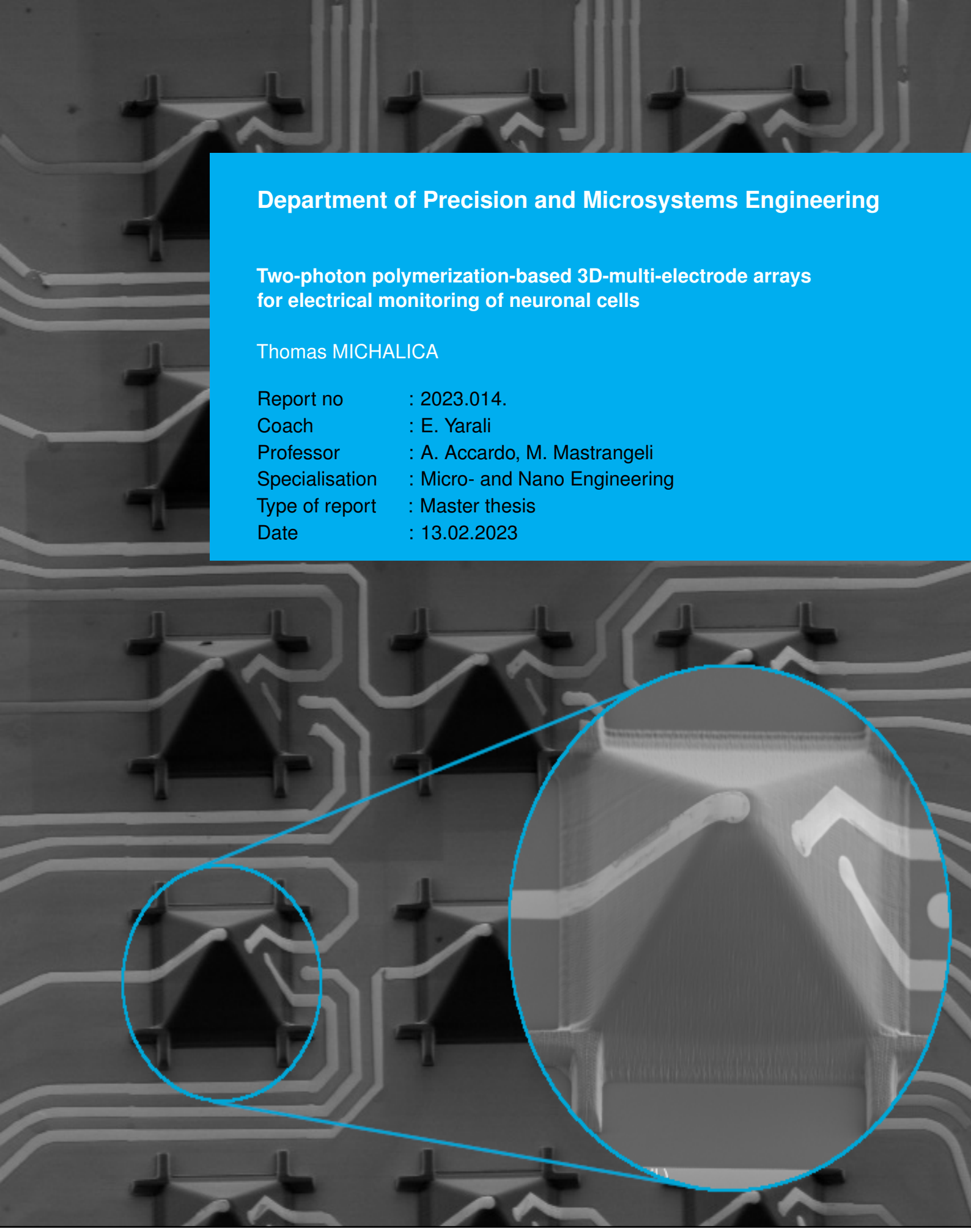

Department of Precision and Microsystems Engineering

Two-photon polymerization-based 3D-multi-electrode arrays for electrical monitoring of neuronal cells

Thomas MICHALICA

Report no	: 2023.014.
Coach	: E. Yarali
Professor	: A. Accardo, M. Mastrangeli
Specialisation	: Micro- and Nano Engineering
Type of report	: Master thesis
Date	: 13.02.2023

TU Delft Delft University of Technology

Challenge the future

Two-photon polymerization-based 3D-multi-electrode arrays for electrical monitoring of neuronal cells

MSc Candidate

Thomas Michalica 5377412

Daily Supervisor

E. Yarali, Msc.

Responsible Supervisor

Asst. Prof. A. Accardo

Asst. Prof.. M. Mastrangeli

Collaborator from the Leiden University Medical Center

Dr. J. P. Frimat

Department of Precision and Microsystems Engineering (PME)

Department of Microelectronics (EWI)

TU Delft Delft University of Technology

Acknowledgements

I would like to express my sincere gratitude to all those who have supported me to complete this thesis. It has been an incredible journey filled with challenges, learning experiences, and personal growth, and I could not have done it without their support and encouragement.

First and foremost, I would like to thank the Austrian taxpayers for providing me with a generous grant to pursue my education in the Netherlands.

I am deeply grateful to my supervisors, Angelo Accardo and Massimo Mastrangeli, for giving me the opportunity to work on this exciting project and for their guidance throughout the process. They allowed me to explore and experiment freely, and I always received valuable feedback and insights during our discussions. I also want to express my thanks to Jean-Philippe Frimat from LUMC for answering all my biological questions and giving valuable feedback, even though he still needs to wait for his 3D-multi-electrode arrays (3D-MEAs).

I am also thankful to all my colleagues from Angelo's and Massimo's groups for providing me with valuable tips and tricks about microfabrication tools and processes. Special thanks to Ebrahim Yarali, my daily supervisor, for supporting me throughout this journey. I would also like to acknowledge Ahmed Sharaf, the tool-owner of the *Nanoscribe* 3D-printer, for his invaluable help with various tool-related issues and experiments, as well as for sharing valuable process information. Finally, I want to thank Pieter van Altena for our intriguing geek conversations about two-photon polymerization (2PP), and for the free coffee!

My work would not have been possible without the endless support of all the lab engineers and technicians. Working at three different faculties of Delft Technical University (TUD) (3me, EWI, TNW) required a lot of coordination and organization. Therefore, I would like to thank the amazing technicians of the PME department for providing tool trainings and for keeping the workshop running. The staff of the Else Koi lab (EKL) cleanroom also deserves my deep gratitude for helping me with my microfabrication questions. I would like to specifically acknowledge Tom Scholtes for the valuable tool trainings and insights into the art of microfabrication. Furthermore, I want to express my gratitude to Henk van Zeijl and Johannes van Wingerden, two engineers whom I deeply admire. I enjoyed the fruitful discussions and their witty problem-solving skills, which ultimately led to solving various challenges faced during the development of the maskless photolithography process via 2PP on high-aspect ratio structures. I would also like to thank Martijn Tijssen from the PVMD-group for enabling the ITO-deposition experiments. I am very grateful for the assistance from the process engineers at the Kavli cleanroom. Roald van der Kolk taught me how to use the ICP-CVD deposition machine in a straightforward manner, and Bas van Asten supported me with the deposition of gold via evaporation.

I would also like to express my sincere gratitude towards my parents for raising me into the person I am today and for providing me with the opportunity and support to pursue my dreams. Finally, I want to thank my incredible girlfriend Nina for not only embarking on this adventure

with me to the Netherlands, but also for providing me with unwavering support throughout the journey. While the workload and deadlines did put some strain on our relationship, she stuck with me through it all. I am sorry for the sacrifices she had to make, but I am very grateful for her unwavering support. I could not have completed this thesis without her.

This work was supported by a Delft BioEngineering Institute (BEI) MSc grant and the "Moore4Medical" project funded by the ECSEL Joint Undertaking under grant agreement H2020-ECSEL-2019-IA-876190.

Their collective efforts and support have made this thesis a reality, and I am very grateful for their contributions to my personal and professional growth.

Abstract

3D-multi-electrode arrays (3D-MEAs) are needed to overcome the limitations of 2D-multi-electrode arrays (2D-MEAs) and enable the electrical characterization of 3D neuronal cultures in *in vitro* brain models, advancing the understanding of neurological disorders and paving the way to personalized medicine.

The aim of this thesis was to overcome some of the limitations of current 3D-MEA devices and develop structures approaching the stiffness of the brain microenvironment, by using materials softer than conventional Silicon. A polymeric 3D-MEA was designed and developed by means of an innovative combination of two-photon polymerization (2PP), a 3D printing technology with sub-micrometer resolution, and standard wafer-level microfabrication methods from the semiconductor industry. Two novel fabrication protocols were developed, the first being a combination of 2PP with high-aspect ratio photolithography, which, though feasible, proved to require an inconveniently laborious process flow. The second fabrication process employed instead 2PP to fabricate the polymeric structures, pattern the microelectrodes, and provide electrical insulation. The 2PP-based process flow was ultimately preferred due to its potential for fabrication of structures of higher aspect ratio and geometrical complexity for 3D-MEA, extending their measurement resolution. Furthermore, a wafer-level alignment routine was developed with an alignment repeatability of 2PP structures of $\pm 5\,\mu m$, which enabled the multi-step 2PP fabrication process. A novel maskless photolithography via 2PP process was also developed to pattern thin films over slanted surfaces, utilizing photoresist and glycerol-based immersion optics. The resulting 3D-MEA consisted of 15 printed polymeric pyramids featuring a total of 60 gold microelectrodes. The electrical insulation of the traces was partially successful, and will require further process development.

The results demonstrate the feasibility of merging, for the first time, the 2PP process with standard wafer-level microfabrication techniques, specifically for the fabrication of a 3D-MEA for *in vitro* studies of human induced pluripotent stem cell (hiPSC) neuronal cultures. The 2PP-based solutions provided in this thesis show a promising pathway for the development of more complex and biomimetic 3D-MEAs. More generally, the developed wafer-level alignment routine and maskless photolithography via 2PP process for high-aspect ratio structures contribute to advance the field of microfabrication, and may enable the development of other types of innovative microdevices.

Acronyms

2D-MEA 2D-multi-electrode array
2PP two-photon polymerization
3D-MEA 3D-multi-electrode array
AM additive manufacturing
BoC Brain-on-Chip
CAD computer aided design
CAM computer aided manufacturing
CMOS complementary metal-oxide-semiconductor
CNS central nervous system
CVD chemical vapor Deposition
CAR chemically amplified resist
DiLL dip-in laser lithography
DLW direct laser writing
dxf Drawing Interchange File Format
DOF depth of focus
ECM extracellular matrix
EU European Union
EKL Else Kooi lab
FDA Food and Drug Administration
GDSII Graphic Data System II
GWL General Writing Language
HD-MEA high-density multielectrode array
HMDS hexamethyldisilazane
hiPSC human induced pluripotent stem cell
iPSC induced pluripotent stem cell
ITO indium tin oxide
ICP-CVD inductively coupled plasma chemical vapor deposition
MEA multi-electrode array
MEMS micro-electro-mechanical systems
MFL multi-focal lithography
ORCHID Organ-on-Chip In Development
OoC Organ-on-Chip
PDMS poly-dimethylsiloxane
PNS peripheral nervous system
PVD physical vapor Deposition
SEM scanning electron microscope
SNR signal-to-noise ratio
SOI silicon-on-insulator

stl Standard Triangle Language
SAL special application lab
TUD Delft Technical University
WHO World Health Organisation

Contents

List of Figures

List of Tables

1. Introduction

Neurological disorders, such as dementia, epilepsy, stroke, and migraine, affect nearly one billion people worldwide, according to the World Health Organisation (WHO). These disorders are responsible for approximately 12 % of total global deaths. [1] In the European Union (EU), the cost of treating brain disorders was estimated to be €798 billion in 2010. [2] As the world population ages and the prevalence of age-related neurodegenerative diseases increases, the need for accurate models to study the brain and discover effective drugs becomes even more pressing. [3]

Traditionally, these models involve animal experimentation, which raises ethical concerns and is not always applicable to humans due to physiological differences. A report from Marx states that 11.5 million animals were used for scientific experiments within the EU in 2011. [4] Additionally, the results obtained from animal studies are often not applicable to humans. For example, 80 % of effective therapeutics in rodent models fail in human trials and less than 8 % of results from animal studies are reproducible in clinical cancer trials. [5, 6] Furthermore, the approval of drugs for the central nervous system (CNS) takes 39 % more time compared to non-CNS medication. [7]

An alternative approach is offered by *in vitro* brain models, often referred to as Brain-on-Chip (BoC) systems. These systems make use of microfabricated environments and engineered brain tissue to mimic key aspects of the brain. The potential of these systems was highlighted by the recent decision of the Congress of the United States of America, which issued the Food and Drug Administration (FDA) Modernization Act 2.0 in 2022, allowing for alternatives to animal testing for drug and biological product applications. [8] Therefore, in the near future BoC systems are expected to be used for preclinical trials.

A crucial methodology for analyzing the functional activity of neural cells models is electrophysiology, specifically via multi-electrode arrays (MEAs), which provide high temporal and spatial resolution of neuronal activity. While state-of-the-art 2D-multi-electrode array (2D-MEA) devices have all their measurement sites located on the same plane, emerging 3D-multi-electrode array (3D-MEA) devices provide measurement sites in all three spatial dimensions, enabling the measurement of the collective electric activity of 3D neuronal cell netwokrs.

This thesis aims to overcome the limitations of current silicon-based 3D-MEA by merging two-photon polymerization (2PP), a 3D printing technology with sub-micrometer resolution, and standard microfabrication methods from the semiconductor industry to enable the manufacturing of polymeric 3D-MEAs

The thesis begins with a literature review that provides a brief overview of the brain's cellular biology and introduces Organ-on-Chip (OoC) technology, with emphasis on BoC systems and electrophysiological measurement systems such as MEA. The state-of-the-art of emerging three-dimensional versions of MEAs is presented, highlighting achievements and limitations of current 3D-MEAs in terms of their commercial availability, biomimeticity, and design flexibility

are analysed.

develop structures approaching the stiffness of the brain microenvironment, by using materials softer than conventional Silicon.

As a result, the research question is defined, with the goal of overcoming some of limitations of current 3D-MEAs by utilizing structures approaching the stiffness of the brain microenvironment, by using materials softer than conventional Silicon in a wafer-level fabrication process. The proposed solution is merging 2PP and standard microfabrication methods to fabricate a polymeric 3D-MEA. An overview of the applied design and microfabrication methods is then provided.

The results are presented and discussed, starting with the digital design approach, which supported the development of the 2PP process by allowing for fast design iterations. After discussing the three main challenges of merging the 2PP process with standard microfabrication methods (*i.e.,* harsh environments, contamination, and wafer-level structure alignment), two fabrication process flows are presented. The first approach (Section 5.3) utilizes previous work performed at Delft Technical University (TUD), which was however not further pursued due to its complex fabrication requirements. A second approach was therefore developed, and makes use of a wafer-level multi-step 2PP process as well as of a novel maskless 2PP-based lithography process (Section 5.4). Both developed techniques are presented after introducing the process flow.

The results section concludes with the fabrication of the 3D-MEA and discusses the challenges and issues faced.

The thesis ends with a conclusion and recommendations for improvements in future work.

2. Literature review

2.1. Neuronal cells

The human nervous system consists of the central nervous system (CNS) and the peripheral nervous system (PNS). The CNS is made up of the brain and spinal cord, while the PNS connects the CNS to the receptors (sense organs) and effectors (muscles and glands). This system is composed of over 100 billion neurons and up to 50 times as many glial cells, which support and protect the neurons. A neuron's primary function is to receive and transmit information through chemical or electrical signals. In addition to neurons, the nervous system also contains glial cells, which come in four main types in the CNS (astrocytes, oligodendrocytes, microglia, and ependymal cells) and two main types in the PNS (satellite cells and Schwann cells). These neuroglia play important supportive roles for neurons, including providing scaffolding and nutrients, protecting against microorganisms, and insulating axons with myelin. Comprehensive explanations can be found in the literature, such as *The central nervous system* by Brodal. [9] A schematic illustration of a typical neuron is shown in Figure 2.1. A typical neuron has a

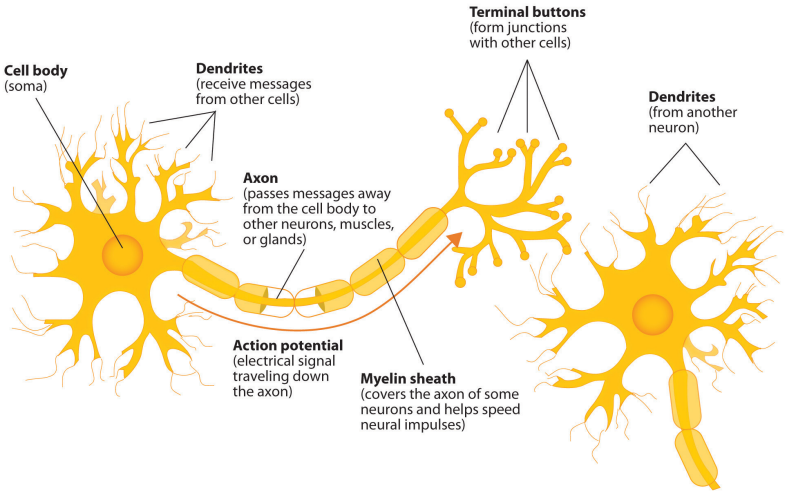

Figure 2.1.: Structure of a neuron. Retrieved and adapted from [10].

cell body called a soma, which is typically between5 µm and 140 µm in diameter and contains a nucleus and various organelles that are important for the basic functions of the cell. [11] The soma also has treelike appendices called neurites, which can be divided into two types: dendrites and axons. A neuron usually has multiple, short dendrites and one long axon, which is the longest branch of the cell. [12]

There are three main types of neurons: *multipolar* (which have many appendices and are the

most common type in the CNS), *bipolar* (which have two appendices), and *unipolar* (which have one central appendix). Dendrites are the main input site for incoming signals from other neurons and may be bristled with spines, small protrusions that increase the surface area and can form contact points with other neurons. These contact points are called synapses, and information is transferred from one neuron to another by the release of chemicals called neurotransmitters into the synapse, across a gap that is about 200 nm wide. [11]

The axon is usually a long extension from the cell body that may branch out into axon terminals at the end to connect with other neurons. When a neuron receives an incoming signal, it generates an electrical nerve impulse, also known as an action potential, which travels along the axon and causes the release of neurotransmitters at the axon terminals. These neurotransmitters can then influence the activity of other neurons, allowing information to be transmitted throughout the nervous system. Some axons are covered by a myelin sheath, which provides insulation and improves the speed of the nerve impulse.

2.2. Organ-on-Chip

The need for more accurate physiological models for drug discovery and screening has already been emphasized in the Introduction. Organ-on-Chip (OoC) devices attempt to solve this challenge and may pave the way to personalized treatments. Additionally, the high financial risk of drug development is well known: the total cost of an approved drug now averages $2.6 billion. [4] Especially in the R&D phase and preclinical trials, OoC are expected to enable significant savings, as experts estimate a reduction from 10 % to 26 %. [13]

In 2019, the European Organ-on-Chip In Development (ORCHID) project defined OoC as follows.[14]

> a fit-for-purpose microfluidic device, containing living engineered organ substructures in a controlled microenvironment, that recapitulates one or more aspects of the organ's dynamics, functionality and (patho)physiological response *in vitro* under real-time monitoring

Even though OoC technology is considered to be still in its infancy, considerable advances have been made in recent years. This multidisciplinary field is enabled by two core disciplines, cellular biology and microsystem technology. Several important cornerstones shall be briefly highlighted.

Cellular biology

From the biology point of view, the foundation of *in vitro* culturing was laid out with the so called *hanging drop* technique in 1907 by Harrison et al. [15] Since then, various cells have been cultured in open environments such as Petri dishes. Next, the discovery of stem cells led to the emergence of regenerative medicine and tissue engineering. [16] Stem cells are able to both differentiate into various types of cells and capable of indefinite proliferation, a process in which a cell grows and divides into two daughter cells. Although they were discussed already in the 19th century, their existence was demonstrated only in 1963. [17] Unfortunately, the extraction of human embryonic stem cells leads to the destruction of the embryo and therefore raises a moral issue. However, the remarkable discovery of induced pluripotent stem cells (iPSCs) in 2006

alleviated this problem by genetically engineering somatic, mature cells to be reprogrammed into pluripotent proliferating cells. [18] As human induced pluripotent stem cell (hiPSC) can be derived directly from the patient, personalized tissue engineering and drug testing is only a matter of time.

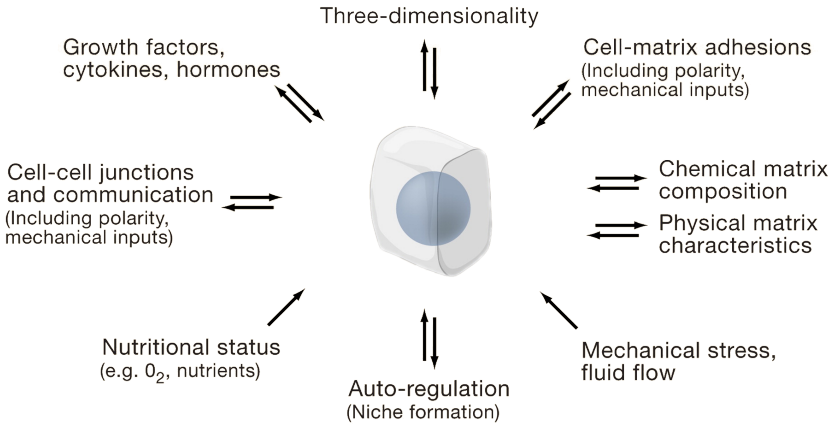

Figure 2.2.: Environmental factors influence cell behaviour. Retrieved and adapted from [19].

Achieving the successful cultivation and isolation of various cell types is an important step in the development of organ mimicking devices. However, understanding and manipulating the microenvironment surrounding these cells is also crucial, as it plays a key role in influencing cell behaviour. The extracellular matrix (ECM), a complex network of proteins and other molecules that make up the microenvironment, is responsible for providing structural support to cells and facilitating communication between cells. It is also involved in regulating various cellular processes, such as cell proliferation, differentiation, and migration. Therefore, to accurately mimic an organ *in vitro*, it is necessary to not only isolate and culture specific cell types, but also to recreate and control the ECM and other factors that influence cell behaviour. The key environmental factors influencing the cell's behaviour are summarized in Figure 2.2. [11, 16]

There has been much discussion in the scientific literature regarding the limitations of traditional two-dimensional (2D) culture models compared to more recent three-dimensional (3D) approaches. In particular, it has been noted that 2D models do not accurately reproduce the behaviour observed *in vivo* due to the lack of a third dimension in these cultures. This is expressed in differences in cell polarization, morphology, differentiation and interaction. [19, 20] Hence, the lack of depth limits the ability of 2D models to accurately mimic the physiological conditions found in the body. In contrast, 3D culture models more closely approximate the complex microenvironment and spatial organization found *in vivo*, leading to a more accurate representation of *in vivo* behaviour.

Microfabrication technology

Microfabrication technologies have fostered significant progress in the development of *in vitro* OoC devices. These technologies allow for the creation of artificial microenvironments around cells, including the production of scaffolds and compartmentalization for cells, micro channels for fluid transport, and artificial membranes. By enabling precise control over the microscale features of the artificial microenvironment, it is possible to create structures and conditions

that closely mimic those found *in vivo*. This has led to significant advancements in a variety of fields, including tissue engineering, drug discovery, and basic research. OoC enabled by microfabrication technologies have the potential to greatly facilitate the development of new therapies and treatments, as well as increase our understanding of fundamental biological processes. [21, 22]

The main technology driver is the semiconductor industry, which developed the photolithography process to manufacture and miniaturize integrated circuits. With this technique thin films can be patterned. The method will be discussed later in section 4.2.1. Based on this technology, micro-electro-mechanical systems (MEMS) were introduced and later combined with microfluidics to enable the first lab-on-chip gas chromatograph. [23] Furthermore, the development of poly-dimethylsiloxane (PDMS) and soft lithography enabled the fabrication of transparent, elastomeric microfluidic devices by replica molding. [24] Nowadays, plenty of microfabrication techniques with different use cases are available. The most commonly used techniques for the fabrication of OoC devices are summarized below. [22, 25]

- **Photolithography:** Pattern thin films by exposing a light-sensitive material to light.
- **Soft lithography:** Replica casts of elastomeric materials.
- **Reactive ion etching (RIE):** Removes material from a substrate using a reactive gas and an ion beam.
- **Two-photon polymerization (2PP):** Uses a focused laser beam to selectively polymerize a photosensitive material.
- **Stereolithography (SLA):** Uses a UV laser beam to selectively cure a photosensitive resin.
- **Ink-jet printing:** Deposits droplets of material onto a substrate.
- **Bioprinting:** Uses bioinks to create 3D structures for tissue engineering and regenerative medicine applications.
- **Electrospinning:** Produces nanofibers by electrostatically spinning a polymer solution.
- **Gas foaming:** Produces porous materials by injecting a gas into a liquid or a melt.

Huh et al. presented the first OoC device, a lung-on-chip in 2010. [26] In the following, advances in mimicking human's most complex organ, the brain, shall be explored briefly.

2.2.1. Brain on Chip

A short introduction about the brain has already been given in Section 2.1. The brain is the most complex organ in the human body, making it a significant challenge to create a physiologically accurate *in vitro* model. The complexity of the brain arises from its multi-scale nature, which includes the distinct microenvironment, various cell types and their organization, unique brain regions with subunits such as the blood-brain barrier (BBB), and interactions with other organs. These factors all contribute to the overall complexity of the brain and must be taken into consideration when attempting to mimic its function *in vitro*. [7] Despite these challenges, researchers have made significant progress in developing *in vitro* models of the brain using microfabrication techniques and other approaches. However, current Brain-on-Chip (BoC) designs only cover them partially. [7]

Figure 2.3 shows the common components of a BoC device and relates them to multi-electrode array (MEA).

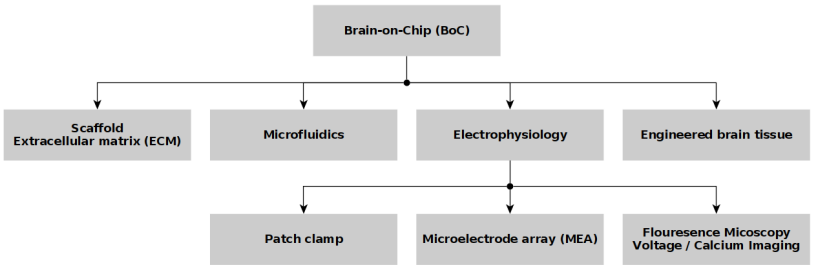

Figure 2.3.: The common components of a BoC device.

- **Extracellular matrix ECM or scaffolds:** These provide structural support and mimic the microenvironment of the brain, helping to maintain the function of brain cells.
- **Microfluidic components:** These allow for the manipulation and control of fluids at the microscale, which is important for maintaining the microenvironment of the brain tissue or add drugs.
- **Electrophysiological components:** These are used to measure the electrical activity of brain cells, providing insights into brain function.
- **Brain tissue:** This is the primary component of the brain-on-chip device and can be obtained from various sources, including primary cells, stem cells, or tissue explants. The brain tissue is cultured on or within the other components of the device to recreate the microenvironment and functional characteristics of the brain.

In addition to these core components, brain-on-chip devices may also include sensors and other monitoring systems to measure various parameters of the microenvironment, such as pH, oxygen levels, and temperature. In the following section electrophysiology will be introduced.

Electrophysiological analysis

Neuronal cells form complex networks to transmit and process information through the use of electrical and chemical signals. Within a neuron, the transmission of information occurs through electrical signaling along the axon, while communication between neurons occurs largely through chemical signaling via small gaps called synapses ($\approx 200\,\text{nm}$ in width). To study the function and activity of neurons and their networks, it is essential to be able to perform *in vitro* electrical characterization. This allows for the measurement and analysis of electrical activity in neurons and their networks, providing insight into their function and behavior. [16]

An overview of *in vitro* electrophysiological analysis methods is given in Table. 2.1. There are several techniques that can be employed to perform electrical characterization of neurons *in vitro*, including patch clamping, voltage-sensitive dye imaging, and multi-electrode arrays (MEAs). Patch clamping is a highly sensitive method that uses a micropipette to physically "patch" onto the cell membrane and record the ionic currents flowing through it. [16] However, is very limited in terms of throughput, since only a few needles can be used at the same time. Calcium- and voltage imaging involves the use of a fluorescent dye that changes intensity in response to changes in membrane potential. This techniques allows for the visualization of the electrical activity of a large population of neurons at once. The number of simultaneous measurable cells is limited by the field of view of the microscope and no absolute voltage measurements are possible. [16, 27] MEAs consist of an array of microelectrodes that can be used to measure the

electrical activity of a group of neurons simultaneously. This technique is often used to study the collective activity of neurons in a network. In the following Section 2.3, multi-electrode array (MEA) will be introduced and their advantages and disadvantages discussed.

Table 2.1.: Overview of *in vitro* electrophysiological analysis methods. [16, 27]

Technology	Characteristics		Resolution			Throughput*
	Advantage	Disadvantage	Cellular	Global	Temporal	
Patch clamping	Detailed analysis of certain neurons to specific perturbations	No information on network connectivity	Very high (single ion channel)	High	High (20 kHz)	Low (single cell)
Calcium imaging	Live imaging of cell groups	Limited global analysis in 3D, no information about absolute voltage, no long term measurements	High (single cell)	Medium (limited by imaging field)	Medium (≈ 1 kHz)	Medium (limited by imaging field)
Voltage imaging	Measurement of membrane potential	no information about absolute voltage, no long term measurements	Very high (single cell membrane)	Medium (limited by imaging field)	Medium (≈ 1 kHz)	Medium (limited by imaging field)
2D-MEA	High throughput measurement of global network connectivity and long-term studies	Limited global analysis in 3D	High	Medium (limited to plane)	High (≈ 10 kHz)	High
3D-MEA	High throughput measurement of global network connectivity and long-term studies in 3D	Limited spatial resolution	Low	High	High (≈ 10 kHz)	Very high
Mesh nanoelectronics	Long term measurement during development	Limited spatial resolution	Low	High	High (≈ 10 kHz)	high

* Throughput: Number of simultaneously measurable cells

2.3. Microelectrode arrays

Microelectrodes can detect the electrical signals produced by neurons due to their proximity to the cells. They can be fabricated in various sizes (diameter: 5 µm to 120 µm) and shapes using microfabrication techniques (see Section 4.2.1) borrowed from the semiconductor industry. [28] These electrodes are often arranged in a grid-like pattern, resulting in a multi-electrode array (MEA). If the probing sites of the array are located in a single plane, it is referred to as a 2D-multi-electrode array (2D-MEA). Current MEAs are capable of simultaneously recording the global neuronal activity with sub-millisecond temporal resolution and sub-cellular spatial resolution on a single plane. [29]

Since the development of the first prototypes of MEAs in 1970, there have been three major advancements in these devices. These include:

- **Material variety:** MEAs have been developed using a variety of materials, including metals, semiconductors, and polymers, each with their own unique properties and advantages.
- **Active devices with on-chip signal processing:** MEAs incorporating active devices, such as amplifiers and filters, onto the array itself, allowing for real-time signal processing and analysis.
- **3D-multi-electrode arrays (3D-MEAs):** These MEAs incorporate electrodes in the third dimension, allowing for the recording of more complex neural activity and the ability to study the function of three-dimensional neural networks.

In literature, 3D-MEAs are often referred to in two ways. One interpretation refers to MEAs with electrodes shaped like mushrooms (as shown in Figure 2.4A) or other 3D-shapes to increase

surface area and decrease impedance. These electrodes are still arranged in an array on a single plane. [16, 30] The other interpretation, which is used in this thesis, refers to MEAs that have multiple, distinct sampling points distributed in all three dimensions, as depicted in Figure 2.4B. [16, 31]

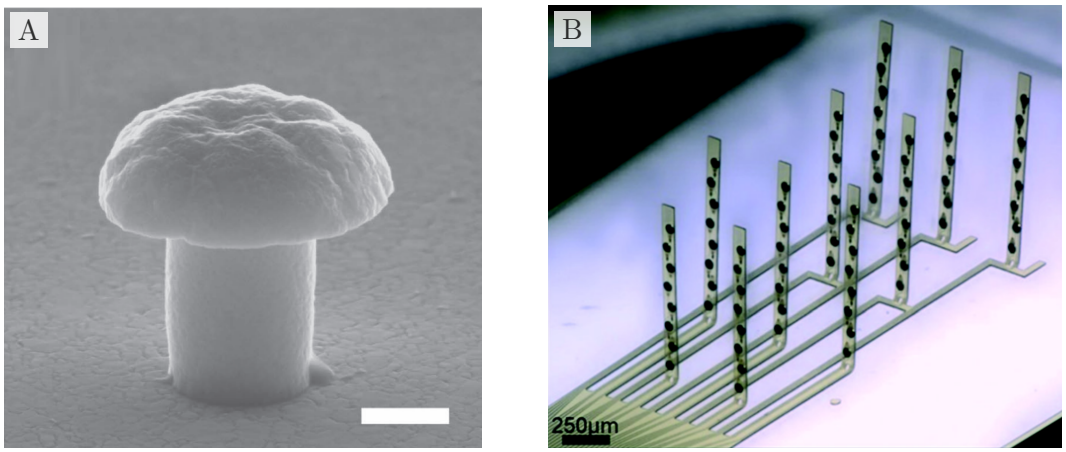

Figure 2.4.: Two interpretations of 3D-MEA: **(A)** 3D-shaped electrodes arranged on a plane (scalebar 500 nm). [30] **(B)** MEAs with multiple distinct sampling points distributed along all 3D directions. [31]

Electrode materials

There are many materials that can be used to fabricate microelectrodes, and different combinations of materials may be used to meet specific requirements. When selecting materials for microelectrodes, it is important to ensure that they are biocompatible and stable over long periods of time to avoid interference with the cell culture. Noble metals such as gold (Au) or platinum (Pt), as well as titanium nitride (TiN), are commonly used for this purpose. In addition, the signal-to-noise ratio (SNR) of the microelectrodes should be as high as possible to ensure accurate and reliable measurements. An acceptable ratio is reported to be 5:1. [32] Hence, a low electrode impedance is required, which is determined by the conductivity of the material.

Furthermore, size and shape of the microelectrodes impacts their performance, with smaller electrodes having a higher spatial resolution but lower SNR, while larger electrodes may have a lower spatial resolution but higher SNR. This issue of plain microelectrodes can be alleviated by increasing their effective surface area or modifying their surface properties. The interaction with cells and the quality of the recorded signals can be affected by increasing surface roughness or chemical functionalization. A technique is to coat them with porous conductive materials, such as Pt-black, metallic nanostructures, carbon nanotubes or conductive polymers. [16]

Finally, because inverted microscopes are preferred for real-time optical imaging of cell cultures, substrate, electrodes and their traces should be transparent. [16] Therefore, some commercially available MEAs use indium tin oxide (ITO) as a conductor with silicon nitride (SiN) as an insulator, although their signal-to-noise ratio (SNR) is worse than opaque, porous TiN microelectrodes. [33] The compromise is to coat ITO electrodes with a porous, but opaque conductor, such as TiN, to increase the signal-to-noise ratio. [34] Therefore, only the traces are

transparent and the microelectrodes are opaque. A possible solution could be nanoscale thin films, as 25 nm to 65 nm TiN electrodes offer reasonable optical transmission characteristics (≈18 % to 45 %) and better impedance ratings (590 kΩ to 1000 kΩ) than pure ITO electrodes (900 kΩ to 1200 kΩ) . [33]

In recent years, organic materials have also been explored for use in microelectrodes. Two of the most commonly used conductive polymers are polypyrrole (PPY) and poly(3,4-ethylen--edioxy-thiophene) (PEDOT:PSS). [16] These polymers have a flexible, polymeric structure that allows for the incorporation of bioactive molecules or growth factors on the surface of the electrodes. Additionally, organic microelectrodes (PEDOT:PSS: 2.8 GPa Young's modulus [35]) are softer than their metallic or ceramic counterparts (TiN: 395 GPa Young's modulus [36]), thus with a stiffness that approaches more the one of the brain tissue (kPa range Young's modulus [37]). This biomimetic property may make them more suitable for use in brain tissue recordings. However, it is worth noting that organic microelectrodes may have lower electrical conductivity and may be less stable over time compared to traditional materials. [35, 36]

The development of new materials and techniques for fabricating microelectrodes is an active area of research, with the goal of creating more advanced and efficient devices for measuring neuronal activity.

Passive micro electrode arrays

Microelectrode arrays (MEAs) can be divided into two categories: *passive* and *active*. *Passive* MEAs rely on external equipment for signal processing, such as filtering, amplifying, and analog-digital conversion, while *active* MEAs have an integrated electronic circuit on the device that performs at least some of these tasks. [16, 32]

Passive MEAs are the most common type and have been the focus of development for many years. State of the art 2D-MEAs typically have electrode diameters of 10 µm to 50 µm and a spacing of 100 µm to 500 µm Commercial devices may have 60, 128 or up to 256 electrodes arranged in a rectangular grid.

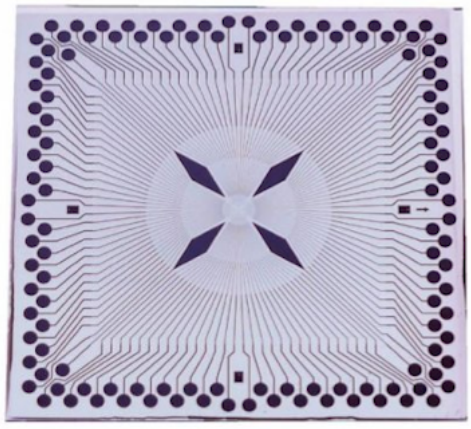

Figure 2.5.: Commercially available MEA-device with 120 electrodes for *in vitro* electrophysiology. [34]

An example of a 2D-MEA from*Multichannel Systems, Germany* is shown in Figure 2.5. The contact pads at the periphery of the device are used for off-site signal processing, and each

pad is individually wired to an electrode at the center of the device. This illustrates one of the limitations of passive MEAs: the density of electrodes that can be achieved is limited by the wiring and packing density. To increase the spatial resolution of the MEA, the size and spacing of the electrodes must be reduced, which can lead to challenges with wiring and signal-to-noise ratio (SNR) due to increased electrode impedance. In addition, the long lines connecting the electrodes to the signal processing units can introduce additional noise and parasitic capacitances that distort the signal. [16, 32]

Active micro electrode arrays

Active MEAs can address some of the limitations of *passive* MEAs. The use of complementary metal-oxide-semiconductor (CMOS) technology has allowed for the creation of monolithic 2D-MEA with integrated electronic circuits. These devices, called high-density multielectrode array (HD-MEA), have a significantly lower noise level due to local on-chip signal amplification and can have a much higher number of electrodes due to multiplexing at high speed, which resolves wiring restrictions. HD-MEAs can also have additional functionalities, such as on-chip spike detection, device calibration, electric stimulation sites, and temperature sensors. Different read-out architectures of HD-MEA are described by Obien et al. [32]

The state-of-the-art HD-MEA, created by Dragas et al., has a size of $4.48 \times 2.43\,\mathrm{mm}^2$ and contains59 760 electrodes with a spacing of 13.5 µm and an area of $3 \times 7.5\,\mu\mathrm{m}^2$, allowing for sub-cellular spatial and sub-millisecond time resolution in the measurement of electrical activity in a group of neurons.

HDMEAs also enable "electrical imaging" of neuronal cell cultures, allowing for the localization and characterization of individual cells based on their electric signals as shown in Figure 2.6. [39]

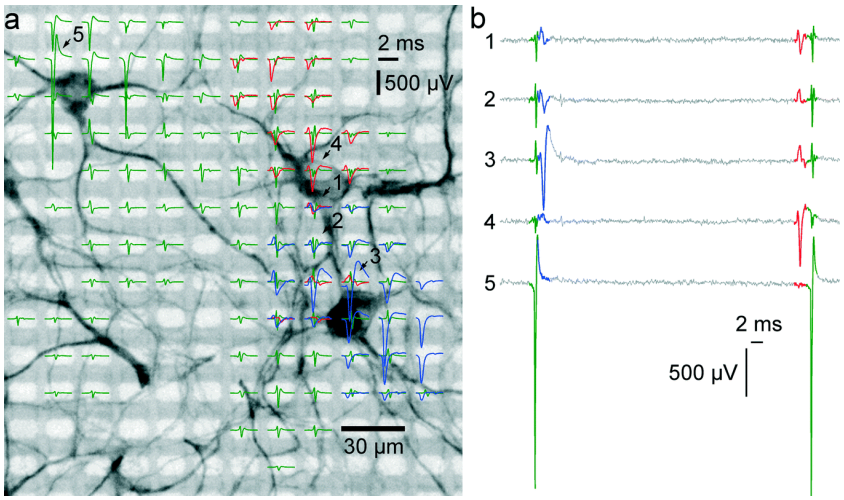

Figure 2.6.: Single cell localisation with HD-MEA. **(a)** Electrical signals of each electrode is superimposed to the corresponding fluorescence image. **(b)** Time signals of several electrodes. [39]

However, one major drawback of CMOS-based HD-MEAs is their opaque and stiff silicon substrate (169 GPa Young's modulus [40]), which can hamper live imaging methods for cell cultures and does not accurately reflect the stiffness of brain tissue. Additionally, CMOS based HD-MEAs require specialized fabrication facilities and are therefore more expensive to

produce compared to *passive* MEAs. However, the high resolution and on-chip signal processing capabilities make HD-MEAs a valuable tool for electrophysiology research.

2.3.1. 3D micro electrode arrays

The trend in *in vitro* brain models has shifted towards 3D cell cultures, and this shift has revealed the limitations of 2D-MEAs in capturing their global electrophysiological activity. The electrodes in 2D-MEAs are arranged in a single plane, which limits its measurement capabilities to only the signals at the surface of the cultures. This lack of measurement capability in three dimensions means that the full extent of the electrical activity of 3D neuronal cultures is not accurately captured.

To address this limitation, 3D-MEAs have been developed. These devices have independent measuring sites along all three spatial dimensions, enabling the electrical characterization of 3D neuronal cultures in *in vitro* brain models. Despite still being in its early stages, a few 3D-MEAs have been reported in the literature. [31, 41–44]. Three promising 3D-MEAs are presented below.

Flexible thin-film 3D microelectrode area

The 3D-MEA device described by Soscia et al. is shown inFigure 2.7. The device consists of a glass substrate with three separate cell culturing wells, each with its own independent 3D-MEA. This allows for the simultaneous monitoring of three cell cultures. The chip is compatible with the recording system MEA2100 from *Multichannel Systems GmbH (Germany)*. A close-up of the 3D-MEA (Figure 2.7C) shows that it consists of ten flexible polyimide pillars ($1100 \times 90 \times 15\,\mu m^3$) extending approximately perpendicular from the substrate, with a horizontal distance of 440 µm between the pillars. Each pillar contains eight electrodes with a diameter of 50 µm spaced 75 µm apart, for a total of 80 electrodes per array in a volume of $2.38\,mm^3$. Hence, the effective electrode density is approximately $33.6 \frac{\text{electrodes}}{mm^3}$.

The initial array is created using standard clean room processes as shown in (Figure 2.7D). Afterwards, the pillars are mechanically erected by plastically deforming a hinge at the lower end of the shank using a custom-made micro manipulator. A close up of the hinge is shown in Figure 2.7E. It has been reported that the actuation angle of the pillars decreases over time from $\approx 90°$ to down to $70°$ due to relaxation of the deformation.

The cross-section of a shank (pillar) is illustrated in Figure 2.7F. Each electrode is made of a 20 nm titanium (Ti) film with a 250 nm gold (Au) film and a porous platinum black (Pt black) layer to increase the signal-to-noise ratio. An average electrode impedance of 45 kΩ at 1 kHz was reported.

A co-culture of induced pluripotent stem cell (iPSC) derived neurons and astrocytes in a collagen-based hydrogel was seeded onto the described 3D-MEA for 45 days. Soscia et al. report electrophysiological recordings of neuronal activity throughout the 3D space. [31]

One advantage of the device is that it is made mostly of thin polyimide, which makes it less stiff (2.5 GPa Young's modulus [45]) and more biomimetic than other 3D-MEAs. Its transparency due to the glass substrate also allows for easy application of optical imaging techniques. Additionally, the design is compatible with commercial recording electronics, making it easy to use. However, the fabrication process involves manual actuation of the shanks with a

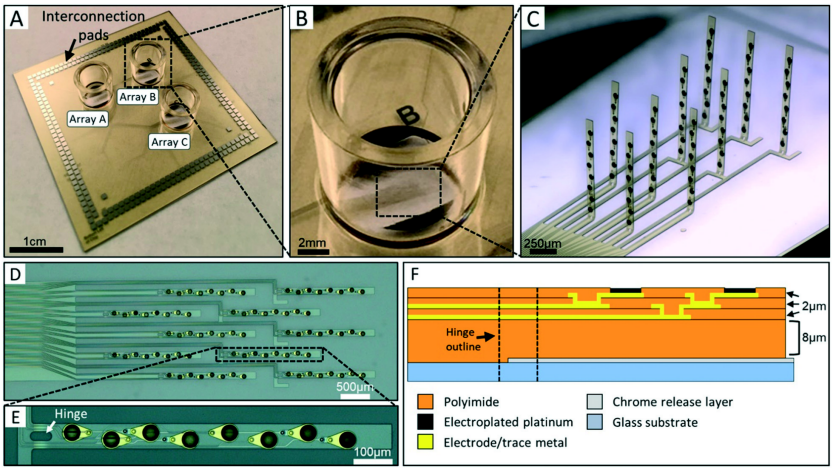

Figure 2.7.: **(A)** 3D-MEA device with three cell culture wells and corresponding arrays. **(B)** Single cell culture well. **(C)** Close-up of the actuated, transparent 3D-MEA. **(D)** The planar array prior actuation. **(E)** Close-up one shank with the deformable hinge design. **(F)** Cross-section of the shank. [31]

custom micro-manipulator, which limits mass production. Additionally, the plastically deformed hinges may relax over time, leading to changes in the positions of the microelectrodes and potential interference with long-term studies.

3D high-density microelectrode array with optical stimulation and drug delivery

Another 3D-MEA by Shin et al. is shown in Figure 2.8. It consists of 18 shanks with a total of 63 platinum black-plated microelectrodes, which are assembled by bonding three, fork-like, 2D-MEAs on top of each other. These were fabricated separately on a silicon-on-insulator (SOI) wafer with standard lithography microfabrication processes. The device includes five microfluidic channels and an optical fiber integrated into one of the 18 shanks, allowing for local chemical and optical stimulation of the cell culture. The multifunctional shank has four electrodes located on the periphery to record the electrophysiological response to the stimulation, and the 17 recording shanks ($6000 \times 63 \times 45\,\mu m^3$) allow for measurement of the propagation of this localized perturbation through the 3D neuronal network A scanning electron microscope (SEM) image of this so-called multifunctional shank ($6000 \times 145 \times 40\,\mu m^3$) is shown in Figure 2.8B. One of the 17 recording shanks is depicted in Figure 2.8C.

Each shank has three or four electrodes with a surface area of $20 \times 20\,\mu m^2$ and a spacing of 85 µm. An average electrode impedance of 15 kΩ at 1 kHz has been reported.

The shanks are arranged in a grid of three rows and six columns with a spacing of 500 µm and 360 µm, resulting in an observable volume of $0.555\,mm^3$ ($1850 \times 1000 \times 300\,\mu m^3$) and the effective electrode density is approximately $113 \frac{electrodes}{mm^3}$.

The device can be inserted into a culture well using a custom-made apparatus and has been used to measure the functional connectivity of primary rat cortical neurons in a collagen-based hydrogel.

The optical and chemical stimulation capabilities of this 3D-MEA enable various experiments. However, the device is not scalable due to manual assembly and requires custom read-out electronics, and its design is not biomimetic due to its high Young's modulus of 169 GPa. [40]

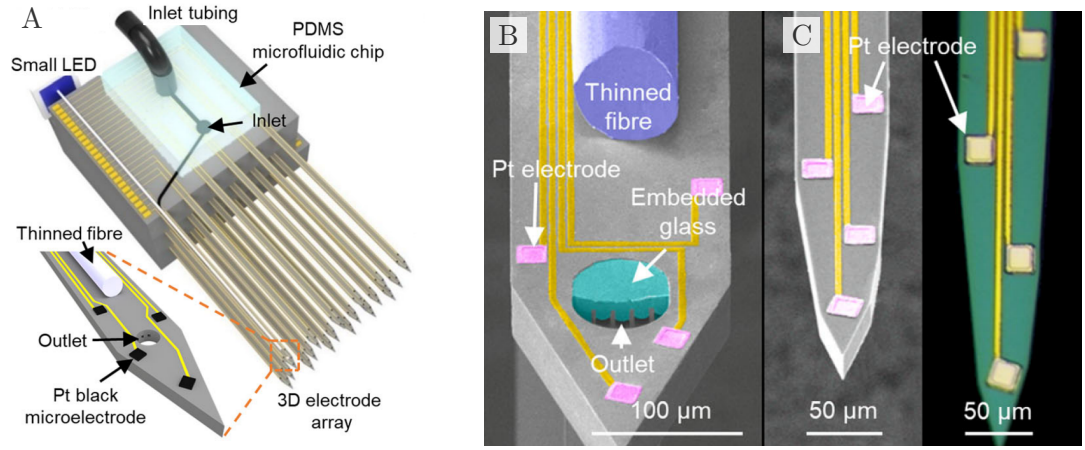

Figure 2.8.: 3D high-density microelectrode array with optical stimulation and drug delivery. [42]
(A) Assembled 3D-MEA with the integrated microfluidic device and optical fiber at the multifunctional shank. **(B)** Close-up image of the multifunctional shank. **(C)** Close-up image of the recording shank.

Silicon-based high throughput microelectrode array

This 3D-MEA was developed at the Delft Technical University. The assembled device, consisting of a custom made circuit board (Figure 2.9A) and a silicon chip ($18 \times 18\,\mathrm{mm}^2$), which is shown in Figure 2.9B. An SEM image of the 3D-MEA is shown in Figure 2.9C. It is made of 20 truncated silicon micropyramids arranged in a 5-by-4 grid. The pyramids have a base area of $200 \times 200\,\mu\mathrm{m}^2$, are approximately 90 µm height and the truncated plateau at the top is $20 \times 20\,\mu\mathrm{m}^2$ wide. The 3D-MEA features 60 microelectrodes ($20 \times 20\,\mu\mathrm{m}^2$), three per micro pyramid. Electrodes and traces are made of a 150 nm thick titanium nitride (TiN) layer on top of a 10 nm thick titanium layer. The electrode impedance was specified with $\approx 100\,\mathrm{k}\Omega$ at a frequency of 1 kHz. With a spacing of 200 µm between the micropyramids, the measurable volume ($1800 \times 1400 \times 90\,\mu\mathrm{m}^3$) is $0.292\,\mathrm{mm}^3$. Hence, the electrode density is approximately $205\frac{\mathrm{electrodes}}{\mathrm{mm}^3}$.

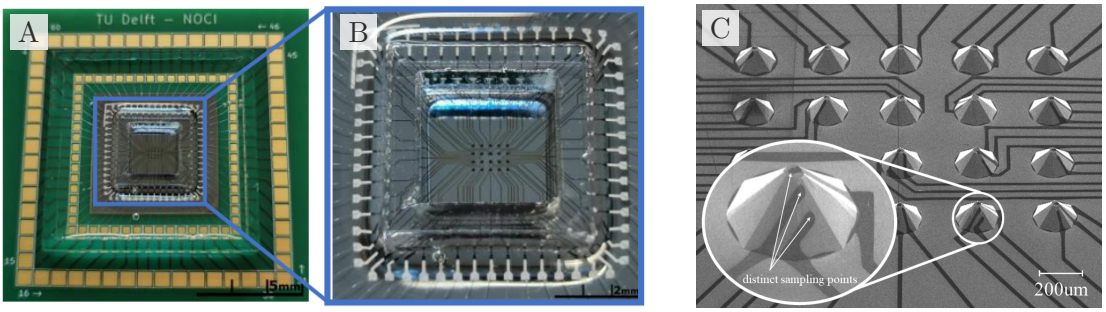

Figure 2.9.: Silicon-based 3D-MEA developed at Delft Technical University (TUD) [43]:
(A) 3D-MEA device with 60 readout pads at the periphery of the custom circuit board and the array in the center. **(B)** Close-up image of the silicon chip with the 3D-MEA. **(C)** SEM image of the pyramid structures with distinct sampling points.

The micropyramids are wet etched into the silicon substrate. Afterwards the traces and electrodes

are directly patterned onto the pyramids with a custom high aspect ratio photolithography process, which will be discussed in Section 4.2.2. By using only wafer-level microfabrication techniques, the production of the 3D-MEAs can be easily upscaled, unlike the previously mentioned designs.

However, this design also has some limitations. Since the device is made of silicon, its Young's modulus (169 GPa) is much higher than that of brain tissue. This may affect the behavior of the cells in culture and the measurements obtained. Additionally, the device is not transparent, so it cannot be used with optical imaging techniques. Overall, this 3D-MEA offers a unique manufacturing approach and a high electrode density, but may not be as biomimetic as some other designs.

3. Research design

3.1. Problem statement

As mentioned in the previous chapter, there are two types of multi-electrode arrays (MEAs): planar 2D-multi-electrode arrays (2D-MEAs), which have measurement sites located in one plane and are therefore limited to the outer surface of neuronal cell cultures, and 3D-multi-electrode arrays (3D-MEAs), which have additional measurement sites extended in the third spatial dimension and can therefore quantify the electrophysiological activity of 3D cell cultures. However, current 3D-MEAs have some limitations, which are listed below:

- Only a few 3D-MEAs have been developed and none are commercially available.
- Most of the MEA are not biomimetic as they are made out of silicon which features a Young's modulus of 169 GPa. [40]. This is eight orders of magnitudes higher than the one of brain tissue (kPa range [37]).
- Live imaging with common inverted microscopes is not possible due to non-transparent materials/structures (silicon).
- Limited flexibility in terms of the shape and size of the 3D-MEA
- Poor spatial resolution due to the large distance between measurement sites.

This thesis aims to address the limitations of current 3D-multi-electrode arrays by merging two-photon polymerization (2PP), a 3D printing technology with sub-micrometer resolution, and standard microfabrication methods from the semiconductor industry to enable a polymeric 3D-MEA and a more accurate and reliable method for measuring the electrophysiological activity of 3D neuronal cell cultures.

3.2. Research question

Building upon previous work performed on 3D-MEAs at the Delft Technical University (TUD), this project aims to explore the use of 2PP and photolithography techniques to create 3D-MEAs that are more accurate, reliable, and flexible in terms of design and materials. The initial research question of this project was:

> How can two-photon polymerization (2PP) and high aspect ratio photolithography enable the fabrication of polymer-metal 3D-multi-electrode arrays (3D-MEAs) for *in vitro* electrophysiology of neuronal cells

This was further split in the following sub-questions featuring a descending order of priority:

1. Which are the 2PP fabrication protocols enabling the high aspect ratio photolithography process?
2. How can structural design features such as rounded edges support the high aspect ratio photolithography process?

3. How does the topography of the structure, modified in terms of microstructural elements or changes in 2PP fabrication protocols, influence the electrical activity of the cell culture?
4. How can the 3D-MEA be manufactured to be optically transparent in order to be compatible with inverted microscopes?

The goal of this thesis was therefore to develop a polymeric 3D-MEA that utilizes a combination of two-photon polymerization, a 3D printing technology with sub-micrometer resolution, and standard microfabrication methods from the semiconductor industry to overcome the limitations of current 3D-MEAs.

The initial approach was to combine 2PP, which enables the fabrication of polymeric structures with arbitrary three-dimensional shape and sub-micro resolution, with high aspect ratio photolithography, which makes the patterning of thin-films over slanted surfaces possible. This combination of technologies had not been attempted before, and it was believed that it could provide a pathway to creating polymeric three-dimensional structures with patterned thin-films. The proposed fabrication protocol involved the use of 2PP to create a three-dimensional, polymeric structure, and high aspect ratio photolithography to fabricate microelectrodes on the surface of the structure.

However, during the research, it was found that the developed fabrication protocol was too complex, due to the constraints from harsh process environments that threatened the integrity of polymeric structures and the contamination risks from additional process steps. Therefore, a novel second fabrication process, not requiring the use of high-aspect ratio photolithography, was developed. Instead, the 2PP was utilized to fabricate the polymeric structures, and a photoresist mask was used to pattern the microelectrodes and the insulation of the latter. This resulted in the development of an aligned multi-step 2PP process to fabricate a first of its kind polymer-metal 3D-MEA on a wafer level.

4. Methodology

In this chapter the fabrication methods of the 3D-multi-electrode array (3D-MEA) are discussed. First the process considerations are presented, followed by the design approach. Afterwards, the used microfabrication tools are introduced while pointing out the physical limitations of various fabrication steps. Finally the applied verification methods are discussed.

4.1. Process development

Microdevices, such as micro-electro-mechanical systems (MEMS) or 3D-MEAs, are manufactured by combining several successive fabrication steps. A typical process template is shown in

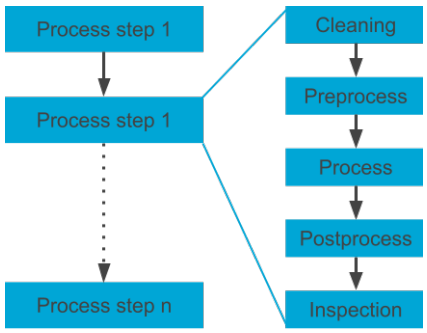

Figure 4.1.: Process flow template for fabricating a microdevice

Figure 4.1, illustrating the sequential manufacturing flow. Here, a standard fabrication step starts with a cleaning procedure to remove dust particles coming from the environment or residues from a previous process. Some techniques may require some preprocessing to prepare the substrate or improve surface adhesion. After execution of the microfabrication procedure postprocesses are often necessary. Such treatments may include chemical development or cleaning. Finally, the results are inspected in order to verify successful fabrication. Separate machines may be required for each of the processes. Utilized metrology tools are presented in section 4.3.

As depicted in Figure 4.2, process development is influenced by three mutually dependent factors: microfabrication, device design and device application.

Microfabrication Considerations

The selection and understanding of microfabrication tools is crucial for the successful development and fabrication of a novel microdevice. It is important to verify the compatibility of different microfabrication methods and machines during the process development. Factors such

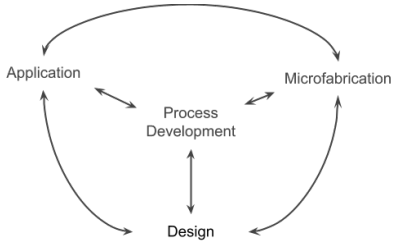

Figure 4.2.: Influencing factors of process development

as contamination, harsh environments, and constraints on available tools can limit the design freedom of the device.

Device Design Factors

The design of the device is closely tied to the chosen microfabrication process. The materials, resolution, and shape requirements of the device will influence the choice of process, and the device must be designed to be manufacturable within the limitations of the available microfabrication tools.

Device Application Factors

Manufacturing capabilities, including scalability, cost, and process time, can limit the scope of a device's potential applications. In the field of organ-on-chip technology, biocompatibility is an additional crucial consideration.

Substrate and Device Components

A 100 mm n-doped silicon wafer was chosen as substrate, as it is widely used and compatible with the employed microfabrication machinery. By using 20 mm × 20 mm wafer dies, 12 3D-MEA devices could be fabricated on a single wafer. The 3D-MEA devices are comprised of three main components:

- Polymeric structure: fabricated via additive manufacturing two-photon polymerization (2PP).
- Metallic electrodes: fabricated via maskless lithography and lift-off.
- Polymeric insulation: fabricated via aligned additive manufacturing.

The development of custom processes and their compatibility were assessed. Multiple iterations and trials were required to refine the process flow, which will be discussed in chapter 5.

4.1.1. Design of the digital twin

The digital twin of the 3D-MEA was designed using *CATIA V5*, a computer aided design (CAD) software from *Dassault Systèmes*. This software allowed for the creation of a detailed, accurate, and precise representation of the 3D-MEA device. It served as the design basis from which the inputs for various microfabrication processes were derived. By having all digital inputs

derived from one master design, possible compatibility errors were eliminated, and no further verification was needed. The digital twin provided a clear visual representation of the 3D-MEA and helped the understanding of the device's geometry and dimensions. A close-up rendering is shown in Figure 4.3. This was crucial in the development of the microfabrication processes and in the optimization of the final device's performance.

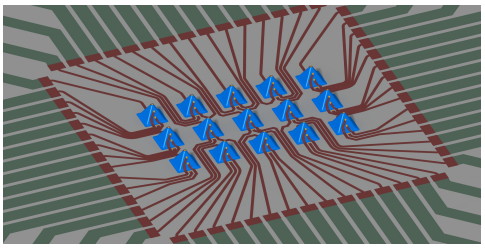

Figure 4.3.: The digital twin of the 3D-MEA.

Designing photomasks

Designing photomasks is a crucial step in the photolithography process, which will be discussed in section 4.2.1. These masks were directly derived by projecting the 3D digital structures from the digital twin onto an imaging plane. The results were exported as Drawing Interchange File Format (dxf) files and imported into the mask design software *Tanner L-Edit V16.3*. Hence, the full wafer mask layout only required arranging the imported 3D-MEA drawings onto a grid to fit the 12 dies. Finally, the layout was exported as a Graphic Data System II (GDSII) file and sent to the photomask supplier *JD Photo Data, (UK)*. By deriving the mask layouts directly from 3D models, complex designs are possible and the required software proficiency is reduced.

Additive Manufacturing

The digital twin also served as an input for the 2PP additive manufacturing system from *Nanoscribe, Germany*. The structures were exported as Standard Triangle Language (stl) files, which are an industry standard for additive manufacturing toolchains. With the parameterized design approach of the 3D structures, fast iterations and adaptations were possible during the process development. Manufacturing uncertainties, such as shrinkage or misalignment, were compensated within the digital model, allowing for precise and accurate fabrication of the 3D-MEA.

4.2. Fabrication methods

4.2.1. Fundamentals of photolithography

The photolithography process is the workhorse of the microelectronic fabrication industry. It enables to transfer patterns with features sizes down to few nanometers on a substrate surface. A schematic illustration of the most common process sequence is shown in Figure 4.4 and described below. First, a thin film of a photo-sensitive polymer (0.1 µm to 10 µm) is deposited on the substrate (step *a*). This process is commonly called coating, and it can be performed in several ways, typically by spinning (spin-coating) in case of small topography substrates

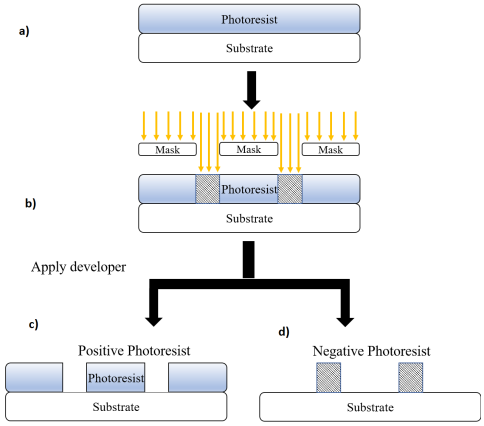

Figure 4.4.: Photolithographic pattern transfer

and spraying (spray-coating) for high-topography substrates. Prior treatment with adhesion promoters, such as hexamethyldisilazane (HMDS) (CAS 999-97-3), is recommended. In step (*b*), a photomask, which is a clear glass or quartz plate with a pattern of opaque and transparent areas, is used to locally expose the photo-sensitive resin, also called photoresist, to ultraviolet (UV) light. This induces a photo-chemical reaction which leads to changes in the chemical solubility of the photoresist. Finally, the substrate is placed in a developing solvent. If a so-called *positive* photoresist is used, the exposed regions are removed (step (*c*)). Therefore, the obtained pattern on the photoresist matches the opaque regions on the photomask . However, the inverted pattern can be achieved by applying a *negative* resist (step *d*). These polymers become insoluble upon UV light exposure, thus, the transparent areas of the photomask will be transferred to the photoresist. With the resulting polymeric mask, additional process steps can be used to add (deposit), remove (etch), or modify (implant) thin films of the exposed regions on the substrate. [46, 47] Afterwards, chemical solvents or oxygen plasma are used to strip the photoresist.

4.2.2. High-aspect ratio photolithography

The standard photolithography process is often referred to as a 2D fabrication method, since it is limited to pattern planar surfaces. This is due to optical constraints, as illustrated in Figure 4.5. Therefore, the design freedom is restricted and fabrication of three-dimensional structures is challenging.

Figure 4.5A shows a masked based pattern transfer over a surface with high topography (3D structures). Due to diffraction at the edges of the dark mask features, the imaging resolution and light intensity is reduced with an increasing gap between mask and photoresist. The smallest achievable line width $b_{\min}$ can be described according to Fresnel diffraction theory:

$$R = b_{\min} k \sqrt{\lambda \left(g + \frac{t}{2} \right)} \tag{4.1}$$

with λ as the light's wavelength, g as the gap between photoresist and mask and t as the resist thickness. The constant k is approximated with 1.5. [48]

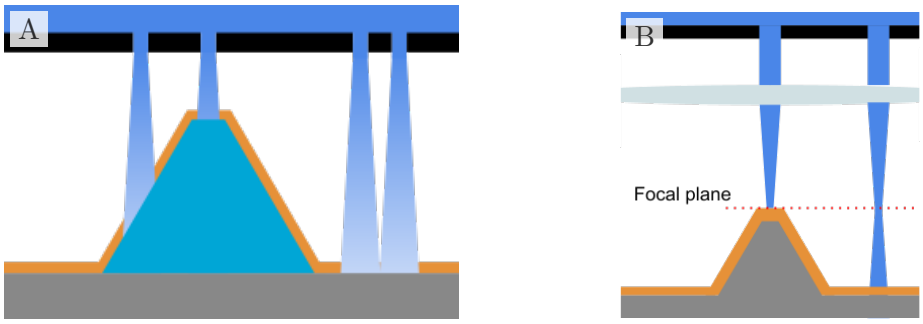

Figure 4.5.: Optical constraints of photolithogaphy systems when patterning tall structures: **(A)** Mask aligner based system. **(B)** Projection based system.

Projection based photolithography uses an optical system to expose the demagnified image of the mask into the photoresist. These systems are referred to as steppers, because they expose a large substrate area by stitching small exposure fields in a step-and-repeat method. This approach leads to smaller feature sizes b_{min} but is limited in transferring a pattern on a surface with high topography due to the small depth of focus (DOF). Figure 4.5B illustrates the issue of a small DOF on non-planar surfaces. The following equations describe this dependency:

$$R = b_{\text{min}} = k_1 \frac{\lambda}{NA} \tag{4.2}$$

$$DOF = k_2 \frac{\lambda}{NA^2} \tag{4.3}$$

The numerical aperture (NA) is a measure of the light-gathering ability of an optical system. It determines how much light can be focused into a small spot. A system with a high numerical aperture can focus light into a smaller spot and therefore can produce images with higher resolution. The factors k_1 and k_2 are machine and process depending constants. If the resolution is increased, the DOF is reduced.

PhD candidate Kolahdouz Esfahani explored the capabilities of these photolithography processes to pattern sidewalls of high topography structures during her PhD thesis at the Technical University Delft in 2017. [49] By utilizing the multi-focal lithography (MFL) function of the *ASML PAS5500/80* wafer stepper, a projection based photolithography machine, a 200 µm high sidewall (54.7°) was patterned with eight exposures and a resolution of 2 µm. For each exposure the focal plane of the mask projection system and the mask itself were changed. Furthermore, the EVG 420 mask aligner has been used at the Technical University Delft to pattern titanium nitride on a 100 µm high silicon pyramid (54.7°). [43, 50]

4.2.3. Spray-coating

A major challenge of substrates with high topography (3D structures) is the deposition of a conformal photoresist film, which is required to expose a pattern uniformly and error-free onto the resist. The industry standard to apply photoresist is spin coating, a technique for depositing thin, uniform films onto flat substrates. By adjusting the spin speed and viscosity of the coating material, the thickness of the deposited film is controlled. However, on non-flat substrates the spinning motion may cause the coating material to pool or accumulate in certain surface features such as bumps or valleys, leading to defects in the film.

With the spraycoater *EVG101, Austria*, a photoresist material is aerosolized by an ultrasonic atomizer and sprayed onto a slowly rotating substrate using a nozzle. The ultrasonic atomizer breaks the photoresist material into micrometer sized droplets, which are then directed by pressurized nitrogen towards the substrate and deposited as a thin film. This method allows to apply resist films to complex or irregularly shaped surfaces. Most important film properties are thickness, edge coverage and roughness. These are influenced by various process parameters, such as viscosity, solvent content, droplet size and flow rate of the photoresist material. Additionally, the atomization pressure, deposition rate and distance, as well as environmental factors such as humidity and temperature, all play a significant role. Air pockets may form due to solvent evaporation, which lead to defects in the transferred patterned after the photolithography process. By carefully controlling these factors, it is possible to achieve high-quality, reproducible coatings.

Protocol

A chemically amplified positive resist *AZ® 12XT-20PL-10, Merck KGaA, Germany*, was used for spray coating. [51] The photoresist was diluted with PGMEA (CAS 108-65-6) and Butanon (MEK, CAS 78-93-3) in a ratio of 1:6.3:8 by weight to decrease its viscosity. The following protocol was developed to coat substrates with tall features (up to 300 µm):

1. **Cleaning**: Remove organic residues
   - Submerge wafer in acetone (CAS 67-64-1) bath (2 min).
   - Rinse with isopropyl alcohol (IPA, CAS 67-63-0.) (30 s).
   - Rinse with deionized water (30 s).
2. **Drying:** Remove moisture from surface: 110 °C / 10 min.
3. **Surface treatment:** (*optional*): Improve resist adhesion with HMDS (CAS 999-97-3) treatment.
4. **Coating:**
   - *EVG101* spraycoater: recipe *HP 1000 mbar 2 mL 8 layers*: 8 coating steps (≈ 15 min).
   - Softbake: Remove solvents from resists: 110 °C / 3 min.
   - Repeat 2 - 3 times for proper edge coverage: depends on structure shape and size.
5. **Final Softbake:** Remove solvents: 110 °C / 6 min

Afterwards, the photoresist film is ready for exposure.

A hot plate was used to perform the heat treatments. Depending on the number of spray coating repetitions, the complete coating process, excluding exposure and development, takes 50 to 80 min. The achieved resist thickness is (6 ± 1) µm for two coating steps and (9 ± 1) µm for three.

4.2.4. 3D printing via two-photon polymerization

Two-photon polymerization (2PP), also known as two-photon absorption direct laser writing (DLW), is a light-assisted additive manufacturing (AM) technique (3D printing) that is notable for its high resolution, with feature sizes as small as 100 nm in all three dimensions. It can be used with a wide range of materials, including acrylate- and epoxy-based polymers, metal-polymer composites, biocompatible resins, and hydrogels. [52] This versatility allows for wide structural

design freedom and the ability to adjust properties such as material stiffness, refractive index, and thermal conductivity. Therefore, 2PP is a valuable tool in many microfabrication driven areas such as tissue engineering, MEMS, microfluidics or micro optics. [52–54] However, 2PP can be a time-consuming process, and the maximum build volume is relatively small, only a few cubic millimeters. [53]

Principle

The principle of 2PP is based on the non-linear optical process of multi-photon excitation, first proposed by Göppert-Mayer in 1931. [55] In this process, two near infrared photons are absorbed almost simultaneously by a molecule or atom, resulting in the excitation of an electron to a higher energy state. This is a much weaker process than single-photon absorption, and it requires the interaction of two photons with the same molecule or atom at the same time. The probability of two-photon absorption depends on the intensity of the light and the strength of the interaction between the light and the molecule or atom. A simplified absorption diagram is shown in Figure 4.6A. As the energy of a photon only depends on its frequency, the excited state can be reached by either absorbing one UV-light photon with the energy $h\nu$ or two photons of infrared-light, with an energy of $h\nu/2$. [53] This phenomenon occurs only within a nanometer sized volume (voxel, a 3D version of a 2D pixel) of the focal point of a high-energy femtosecond pulsed laser source, as Figure 4.6B illustrates the differences in terms of excitation volume. By comparison, a one-photon laser excites the sample along its light path, while a two-photon laser only excites a small volume at the focal plane. In addition to the 2PP fabrication method, this phenomenon is also applied in two-photon confocal imaging. [53]

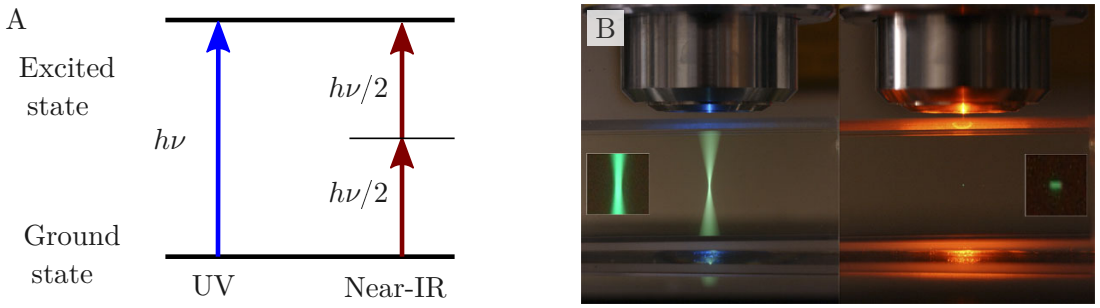

Figure 4.6.: Optical constraints of photolithogaphy systems when patterning tall structures:
(A) One- and two-photon absorption based on a simplified energy diagram. Adapted from [56].
(B) Excitation area of one- and two-photon absorption. Image by Steve Ruzin and Holly Aaron, UC Berkeley. [57]

Process

The 2PP process is based on photo-polymerization, similar to the photolithography process described in Section 4.2.1. A photoresist, which is a photo-sensitive resin, is used as the raw material. Negative photoresists solidify when they are exposed to light with sufficient energy, as the photo-initiators inside the resin gets activated and induce a polymerization reaction, forming and cross-linking the polymers. Non-polymerized material can then be dissolved after

the fabrication process. Positive photoresists, on the other hand, undergo cleavage of the polymer chains when exposed to light with sufficient energy, and these parts can be removed with a developer solution afterwards. [52]

In a 2PP machine, the focal spot of a femtosecond pulse laser needs to be precisely positioned in the build volume. This is archived by using galvo mirrors, small, fast-moving mirrors which deflect the laser beam in a desired direction, in combination with a focusing objective. Additionally a piezo-electric stage can be used to precisely manipulate the position of the substrate with respect to the objective. [54] The wavelength of the laser is typically in the near-infrared range, around 800 nm, such that single-photon absorption is not sufficient to initiate polymerization. As a result, the photoresist will only solidify in the focal voxel, where two-photon absorption occurs. The size and shape of the voxel depends on the magnification factor and numerical aperture of the focusing objective. By moving the laser beam through the resin, structures with feature sizes smaller than 100 nm can be fabricated. [52, 53]

Workflow

The fabrication of a structure using a *Nanoscribe* 3D printer involves a workflow that utilizes the General Writing Language (GWL) file as input. The GWL file describes the trajectories that the laser focus will follow within a 2PP resin and also configures the system parameters to be used during the printing process.

The general fabrication workflow is depicted in Figure 4.7, and includes the following steps:

1. The designed digital 3D model is loaded into Nanoscribe's computer aided manufacturing (CAM) software *DeScribe* to prepare the design for fabrication.
2. The digital model is then sliced into thin layers, typically ranging from 0.1-5 µm, along the z-axis.
3. Each layer is then divided into stripes, either along the x- or the y-axis, through a process called hatching. The typical distance between stripes is 0.2-1 µm.
4. The GWL file, which is the output of the CAM software, is then imported into Nanoscribe's printer control software *Nanowrite* to execute the 3D printing process. The laser is guided along the hatched lines of each layer to construct the model.

Post-processing steps are required after the fabrication, which include cleaning the sample with a developing fluid, typically propylene-glycol-methyl-ether-acetate (PGMEA, mr-Dev 600) and isopropanol. Additional steps may include post-curing with UV light or temperature to induce further cross-linking of the polymer. This processing can result in shrinkage, which can be accounted for by upscaling the digital model of the structure accordingly. [54, 58] It is important to note that, as non-polymerized photoresins are cytotoxic, post-processing steps are crucial if the fabricated structures are used in cell cultures.

As shown in Figure 4.8, there are three main configurations for the 2PP process. The oil immersion setup (Figure 4.8A) uses oil to 3D print structures made of materials which cannot be in direct contact with the objective lens and allow for the fabrication of objects through a transparent substrate. The other configuration is the dip-in laser lithography (DiLL) setup (Figure 4.8B), which involves immersing the objective into the resin to reduce the number of interfaces and enable the fabrication of tall structures up to a few millimeters. Additionally, the maskless lithography configuration (Figure 4.8C) can be used to pattern photoresist films,

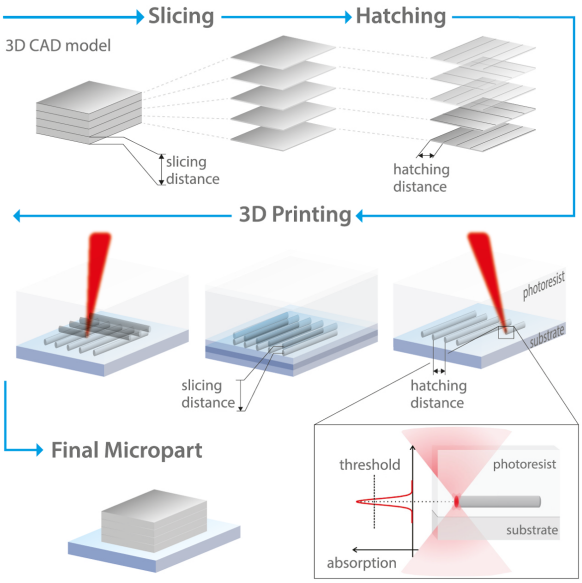

Figure 4.7.: The 2PP fabrication workflow. [58]

either in air mode with an air gap between the objective and photoresist film or in immersion mode with an immersion medium to improve the resolution of the objective.

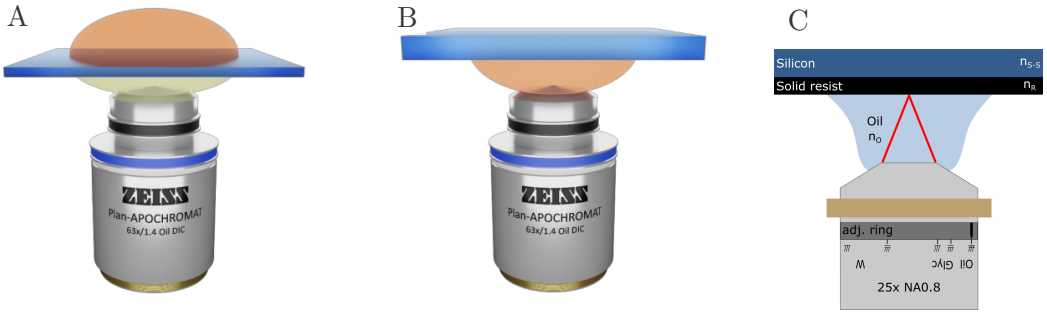

Figure 4.8.: chematic representation of the 2PP sample configurations: **(A)** Oil immersion configuration (oil in yellowish, resin in red).- [59] **(B)** dip-in laser lithography (DiLL) configuration (resin in red). [59] **(C)** Maskless lithography configuration (Oil can also be omitted). [54]

As previously discussed, the voxel size depends on the optical objective used in the 2PP process. To cater to various needs, *Nanoscribe*, a leading provider of 2PP machines, offers four objectives with different magnifications (10x, 20x, 25x and 63x) for their 3D printers. As a result, four different feature sizes can be achieved, with the 63x configuration offering the highest feature resolution but also the longest fabrication time. This trade-off between resolution and fabrication time is illustrated in Table. 4.1.

Table 4.1.: Four different configurations of the *Nanoscribe* systems.

Feature set	Small	Medium	Large	Maskless lithography
Objective	63x NA1.4	25x NA0.8	10x NA0.3	20x NA0.5
Min. Feature size	0.2 µm	0.6 µm	1.2 µm	1 µm
Print field	⌀200 µm	⌀400 µm	⌀1000 µm	⌀600 µm
Print time	0.4 mm^3/h	0.8 mm^3/h	6.8 mm^3/h	7.6 mm^2/h
Min. Slicing distance	0.2 µm	0.4 µm	2 µm	3-6 µm
Min. Hatching distance	0.2 µm	0.4 µm	1 µm	0.7-1.2 µm

Protocol

The polymeric structures of the 3D-MEA were fabricated with the 2PP system from *Photonic Professional GT+* from *Nanoscribe* according to the following protocol:

- **Cleaning**: Remove organic residues
  - Submerge wafer in acetone (CAS 67-64-1) bath (2 min).
  - Rinse with isopropyl alcohol (IPA, CAS 67-63-0) (30 s).
  - Air dry for 5 min. Verify that no visual residues remain.
- **Surface treatment**: Improve adhesion by making the surface more hydrophobic
  - Oxygen plasma, *Diener Femto*: 100 W / 15 min / 5-6 sccm O_2
  - Silanization: Submerge in bath for >2 h : 30 mL ethanol (CAS 64-17-5) mixed with 3 mL MAPTMS[1]
  - Rinse with acetone and deionized water
- **Deposit photoresin**: IP-Q, methacrylaty-based (*Nanoscribe, Germany*)
- **Fabrication:** *Photonic Professional GT+* Large feature set (10x objective) from *Nanoscribe*
- **Development:** Remove unpolymerized photoresin
  - Submerge in PGMEA[2] bath: 25 min
  - Submerge in IPA bath: 25 min
  - Air dry for 5 min

4.2.5. Photolithography via two-photon polymerization

In this thesis the 2PP system was also used to pattern a thin film of a photo-sensitive polymer. Since no mask is involved in this process like in conventional photolithogaphy processes, this method is also referred to as maskless photolithogaphy or direct laser (photoresist) writing. The following protocol was used to expose the spray-coated AZ® 12XT photoresist, which covered the 3D-MEA structures. Glycerol was utilized as an immersion media to decrease the parasitic reflection of the laser beam at the slanted sidewalls of high-aspect ratio structures. Further considerations will be discussed in detail in Section 5.6 as part of the results chapter.

[1] 3-(trimethoxysilyl)propyl methacrylate (CAS 21142-29-0)
[2] Propylene glycol methyl ether acetate (CAS 108-65-6)

- **Spray coating**: Cover structures with photoresist layer according to protocol in Section 4.2.3
- **Deposit Immersion media**: on the to be exposed areas: glycerol (CAS 56-81-5)
- **Exposure:** *Photonic Professional GT+* Medium feature set (25x objective) from *Nanoscribe* Pattern resist with suitable dose.
- **Cleaning:** Remove immersion media
  - Rinse with DI water
  - Blow dry the substrate
- **Post exposure bake (PEB):** 90 °C / 2 min
- **Development:** Remove exposed resist
  - Submerge wafer in AZ® 326 MIF / 3 min to 4 min
  - Rinse with deionized water 1 min,
  - Blow or spin dry the substrate

4.2.6. Thin film deposition

In this project, various methods were employed for the deposition of thin films, including inductively coupled plasma chemical vapor deposition (ICP-CVD) for the production of low temperature silicon oxide and silicon nitride films, sputter coating (physical vapor Deposition (PVD)) for the production of titanium nitride and ITO films, and evaporation (PVD) for the production of gold films. These methods will be discussed in more detail below, including their respective advantages and limitations as well as the specific procedures that were followed in their application.

Low-temperature silicon nitride and silicon oxide deposition

Thin films of silicon nitride and silicon oxide were used as protection layers for the polymeric structures to prevent damage from the plasma of other process steps. These films were deposited using an inductively coupled plasma chemical vapor deposition (ICP-CVD) system called the *PlasmaPro100* from *Oxford Instruments* at the *Kavli* cleanroom of the Delft Technical University (TUD). This system is capable of depositing high quality dielectric films at low temperatures, making it an ideal choice in presence of polymers which cannot stand extremely high temperatures. Standard machine recipes were used for the deposition of thin films. These recipes helped to ensure consistent and high quality.

Silicon nitride was deposited at a temperature of 40 °C, with a deposition rate of 45.6 nm/min. The thin film precursors were silane gas (SiH_4) as the primary reactant gas combined with nitrogen (N_2) as nitrogen source to convert the silicon atoms into silicon nitride. Argon (Ar) was used as carrier gas. The deposited thickness of the films was between 200 nmand500 nm.

Silicon oxide films were deposited using the ICP-CVD system at a temperature of 75 °C, with a deposition rate of 71 nm/min. The primary reactant gas was silane gas (SiH_4) with oxygen (O_2) as oxidizing agent and argon (Ar) as carrier gas. The deposited thickness of the films was between 200 nmand800 nm.

Titanium nitride deposition

In this study, titanium nitride (TiN) thin films with a thickness of 100 to 200 nm were deposited as electrode material. This material was chosen due to its high electrical conductivity, chemical stability, and biocompatibility, making it well suited for use in Organ-on-Chip (OoC) applications.

The *Sigma 204* sputter coater from *SPTS Trikon* at the *EKL* cleanroom of TUD was used to deposit the TiN film via reactive sputtering, where the target material titanium is sputtered (bombarded with ions from an argon plasma) in a vacuum chamber, while a reactive gas (nitrogen N_2) is introduced into the chamber. This causes the sputtered titanium atoms to react with the nitrogen gas, forming TiN on the substrate. Thickness, composition, and other properties of the TiN film can be controlled by adjusting the sputtering power, reactive gas flow rate, and other process parameters.

To minimize thermal stress on the polymeric structures of the 3D-MEAs, a standard recipe was used with a low plasma source power of 1000 W and the substrate was cooled to 25 °C during the deposition of the titanium nitride (TiN) film. To improve the adhesion of the TiN film, a 10 nm thin intermediate titanium (Ti) film was also deposited prior to introducing the reactive nitrogen gas. In order to avoid contamination of the tool, a carrier wafer had to be used.

ITO deposition

indium tin oxide (ITO) is a suitable material for OoC applications due to its transparency and biocompatibility. The material's transparency enables imaging of cells while its biocompatibility makes it safe to use in biological systems.

ITO deposition was performed using the *Zorro*-machine at EKL, which employs an RF-magnetron sputtering process. The deposition was performed using a tilted ITO target with a 100 mm diameter, with a composition of 90 wt% In_2O_3 and 10 wt% SnO_2. During the deposition, the substrate rotated and was subjected to a sputtering gas of Argon at a pressure of 20 µbar, with a RF-power of 130 W. The process was carried out at room temperature to not harm the polymeric structures.

Gold deposition

Gold (Au) is a material that has been used as an electrode in this project. Due to its high electrical conductivity, chemical stability, and biocompatibility, it is well-suited for use in microelectrode and organ-on-chip applications.

To deposit the gold film, the *FC-20349* system from *Temescal* at the Kavli Lab was used. The system employs electron beam evaporation to deposit the source material in a vacuum chamber onto the substrate, resulting in a thin film. The deposition process is highly directional, with the evaporated material primarily condensing onto the substrate from a single direction. This can result in weak edge coverage and shadowing, where protruding features on the substrate block the evaporated material from reaching certain areas, which is important to consider in the lift-off process that will be used later in the fabrication process.

Prior to depositing the gold film, a 10 nm thin intermediate titanium adhesion layer was also deposited using this system. This adhesion layer helps to improve the overall adhesion of the

gold film to the substrate.

4.3. Metrology

Microfabricated structures are too small to be measured or inspected with the naked eye. For comparison, they are typically smaller than a human hair, which has an average diameter of about 50 µm. [60] In order to measure and verify the fabricated devices in this project, several tools were used, including an optical microscope and a scanning electron microscope (SEM). A profilometer was also used to quickly measure the heights of thin films. These tools allowed for both qualitative and quantitative analysis of the microfabricated structures throughout the development process.

4.3.1. Scanning Electron Microscopy

The scanning electron microscope (SEM) *Regulus 8230* by *Hitachi* was the most frequently used metrology tool in this project. It was used both at the *EKL* and *Kavli* cleanrooms. A SEM produces images by scanning the sample with a focused beam of high-energy electrons and detecting the interactions of the electrons with the sample using various detectors. In this project, the SEM provided valuable qualitative information about the fabricated structures during the 2PP fabrication process development. The tool is capable of loading 100 mm wafers, but due to the use of processes and materials that are not compatible with the CMOS fabrication process, a dedicated contaminated wafer holder had to be used.

The SEM was mostly used to image non-conductive surfaces (photopolymers and dielectrics (SiN)), which can lead to charging of the substrate due to the interaction of the high-energy electrons with the sample. To reduce charging, low accelerating voltages of between 500 V to 1000 V were used and the Charge Suppression Scan (CSS) mode was employed. In this mode, each line scan is repeated multiple times at high frequency and averaged before scanning the next line. This fast scanning reduces the build-up of charge in the sample and results in better image quality when observing non-conductive samples.

The SEM is also capable of tilting the substrate holder, which is helpful for imaging 3D-MEAs. Typical tilting angles were 30° to 40°. The tool is equipped with multiple electron detectors, and the upper secondary electron (SE) detector was typically used, unless the sample was tilted, in which case the lower SE detector provided better images.

4.3.2. Optical microscopy

Throughout the fabrication process, various optical microscopes at different cleanroom locations were used to qualitatively verify the integrity of the 3D-MEAs. Magnifications up to 63x were employed, and images were recorded using a camera and related software. The software also allowed for the addition of scalebars and the measurement of the length of imaged structures. These optical microscopes provided a valuable tool for visualizing and verifying the microfabricated structures during the fabrication process.

5. Results and discussion

5.1. 3D-microelectrode array design

A rendering of the designed 3D-multi-electrode array (3D-MEA) is shown in Figure 5.1. This design was inspired by previous work carried out at Delft Technical University (TUD), which was discussed in Section 2.3.1. The 3D-MEA is fabricated on a 20 mm × 20 mm silicon die, hence, 12 3D-MEA devices could be fabricated on a 100 mm wafer. Around the perimiter of the die, 60 aluminium pads (1 mm × 0.750 mm) are arranged for wire bonding the device to a printed circuit board (PCB) with a read-out circuit, as shown in Figure 5.1A. Each of the pads connects to an independent electrode of the multi-electrode array (MEA).

The 3D-MEA is located in the center of a die and occupies an area of 1.8 mm^2. A close-up is depicted in Figure 5.1B. It is made up of 15 polymeric truncated pyramids, arranged in a 3 × 5 array and spaced 400 µm apart. Each pyramid has a footprint of 200 µm × 200 µm and a truncated top of 30 µm × 30 µm. The height of the pyramid can vary between 100 µmand250 µm, depending on the design. To enhance the manufacturability of the 3D-MEA, all edges and intersections have been rounded. The presence of sharp edges may result in a non-uniform photoresist film or create cracks during the deposition process of the electrode material due to edge-covering issues. Each pyramid is equipped with 4 microelectrodes with a diameter of 18 µm. One electrode is placed at the top, two at the sidewall, and one at the bottom of the pyramid.

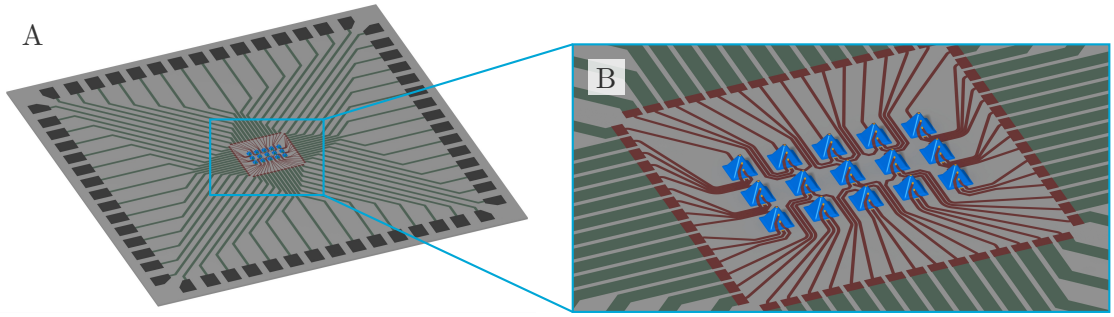

Figure 5.1.: Rendering of the 3D-MEA design: **(A)** 20 mm × 20 mm silicon die with the 3D-MEA. **(B)** Close-up view of the 3D-MEA.

In the center of the device, the electrodes and traces (15 µm wide) are made of gold and isolated with an acrylate-based proprietary polymer (IP-Q, *Nanoscribe*). However, the outer traces are 100 µm wide and not in contact with the cell culture, so they are made of titanium nitride and isolated with silicon nitride. This hybrid fabrication process, which will be discussed in Section 5.4, involves using different materials and insulation layers for the inner and outer traces due to limitations of the chosen fabrication methods and to improve fabrication time and design flexibility. Gold is well-suited for use in the inner traces due to its good electrical conductivity

and biocompatibility, while titanium nitride and silicon nitride are more suitable for the outer traces due to their fast and established standard fabrication processes at TUD.

5.1.1. Design strategy

The digital design of the 3D-multi-electrode array (3D-MEA) was split into three parts: the planar front-end traces, the planar back-end traces, and the 3D back-end structures, as shown in Figure 5.2. This separation was motivated by the fabrication strategy, which utilizes complementary metal-oxide-semiconductor (CMOS)-compatible, masked photolithography-based methods for the front-end traces, and a novel two-photon polymerization (2PP)-based process for the back-end structures. The approach allows for fast iteration of process parameters and custom designs of the 3D back-end structures, while the front-end traces, which connect the 3D-MEA with the outside world, can be fabricated in high volumes using a well-established photolithographic approach.

The front-end traces (Figure 5.2A) connect the outer aluminium pads with titanium nitride pads located at the center of the die, around the perimeter of a3 mm × 3 mm square, where it connects with the back-end traces. The back-end traces (Figure 5.2B) and 3D back-end structures (Figure 5.2C) are interconnected, with the latter consisting of identical polymeric truncated pyramids. To simplify the design process of electrodes and insulation, the pyramids were made identical, enabling easy 3D printing and design of the array.

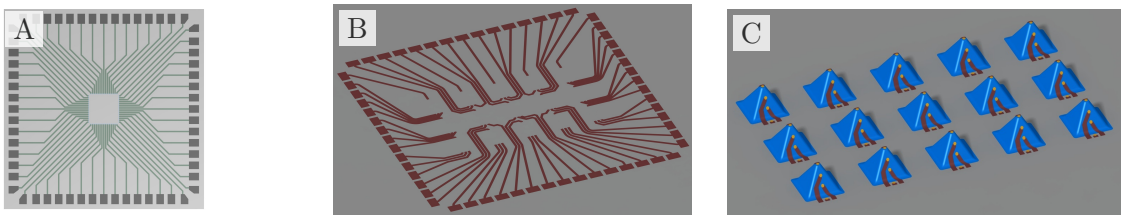

Figure 5.2.: Overview of the three parts of the digital 3D-MEA design: **(A) Front-end:** Connection between Al-pads and back-end. **(B) Back-end traces:** Planar structures fabricated with 2PP. **(C) Back-end structures:** 3D structures fabricated with 2PP.

Parameterized design

The digital twin of the 3D-MEA design allows for the modification of parameters of the complete 3D-MEA, which is made up of the 3D structure, electrodes, and insulation. By changing the height of the pyramid, the rest of the design adjusts accordingly, as shown in Figure 5.3. The footprint remains the same, resulting in a taller pyramid with steeper sidewalls. The electrodes and insulation are also modified to fit the new design of the pyramid. This flexibility is particularly useful for the development of the 2PP fabrication process, as it allows for fast iterations of different dimensions. Manufacturing uncertainties, such as shrinkage or misalignment, can also be compensated for within the digital model. Overall, the parametrization of the 3D-MEA design allows for efficient optimization and development of the fabrication process.

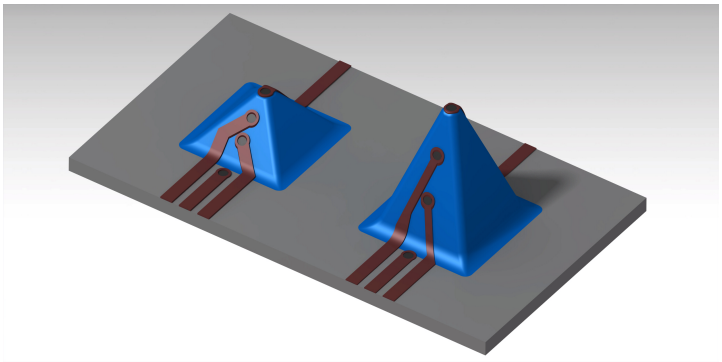

Figure 5.3.: Parameterized design enables fast iterations.

Advantages and limitations

The 2PP fabrication process used for the back-end structures of the 3D-MEA offers several advantages, including the ability to create custom designs and quickly iterate on process parameters to optimize fabrication time and yield. However, it should be noted that this method may have a slower fabrication speed compared to other techniques. Despite this limitation, the combination of 2PP and high-volume CMOS fabrication in the design of the 3D-MEA allows to exploit the benefits of both methods to be utilized. The front-end traces were designed for compatibility with high-volume CMOS fabrication, while the back-end structures were created using the flexible 2PP process, which offers high design freedom and the ability to quickly iterate on design changes. The high level of design freedom offered by 2PP can also be used to create more biomimetic structures for *in vitro* cell studies. Overall, the 2PP process enables the creation of a reliable and versatile 3D-MEA suitable for a wide range of *in vitro* cell studies, as will be discussed in the following sections.

5.2. Merging 2PP with cleanroom fabrication methods

The main goal of this research was to investigate the feasibility of using 2PP to fabricate a 3D-multi-electrode array (3D-MEA). In order to merge the 2PP process with standard microfabrication techniques at wafer-level, such as photolithography and thin film deposition methods like chemical vapor Deposition (CVD) and physical vapor Deposition (PVD), three major challenges had to be addressed. These challenges included the potentially harmful effects of classical microfabrication processes on polymers, the risk of contamination of tools, and the potential positional alignment issues in the sub-sequential process steps. To successfully integrate 2PP with cleanroom fabrication methods, it was necessary to carefully consider the compatibility of these processes with the printed structures, as well as the potential risks of contamination and the importance of accurate positional alignment in the fabrication process. In the following paragraphs, these constraints will be discussed.

Harmful process environments

One challenge in merging the 2PP process with standard microfabrication techniques was the potential harm that certain processes can cause to printed polymeric structures. While 2PP

structures are made of polymers, many standard microfabrication techniques were developed for use with silicon and other metals in the integrated circuit industry.

Thin film deposition processes often involve high temperatures, which can be harmful to the printed polymeric structures used in the 3D-MEA. The degradation (carbonization) temperature of the polymer used in this project is 282 °C, and exposing it to higher temperatures would cause damage. Elevated temperatures will cause additional crosslinking of the photopolymer, which leads to shrinking, deformation or even delamination of the substrate. [54] Similarly, etching processes that use aggressive solvents or plasma to remove materials may attack the polymeric structures of the 3D-MEA.

In addition, the standard cleaning process for silicon wafers is optimized to remove organic residues, which makes it incompatible with the polymeric structures of the 3D-MEA. Overall, care had to be taken to ensure that the employed microfabrication processes did not have harmful effects on the printed polymeric structures.

These prerequisites required to avoid high temperature processes and protecting the polymer structures. The maximum temperature the polymeric structures had to endure was therefore limited to 110 °C during softbaking of photoresist, which was necessary to dry the resist and remove solvents.

In order to protect the structures from potential harmful plasma or solvents, they were covered with a protective layer of a dielectric material after fabrication. As introduced in Section 4.2.6, a low temperate inductively coupled plasma chemical vapor deposition (ICP-CVD) machine was used to deposit such thin films. Experiments were conducted using 800 nm silicon oxide, deposited at the lowest possible temperature of 75 °C, as shown in Figure 5.4A. The quality of the deposited film decreases with decreased temperature, and cracks were observed at the edges of the pyramids. However, silicon nitride with acceptable quality was deposited at a temperature of 40 °C, as shown in Figure 5.4B. Therefore, silicon nitride was chosen as a protective layer for the polymeric structures.

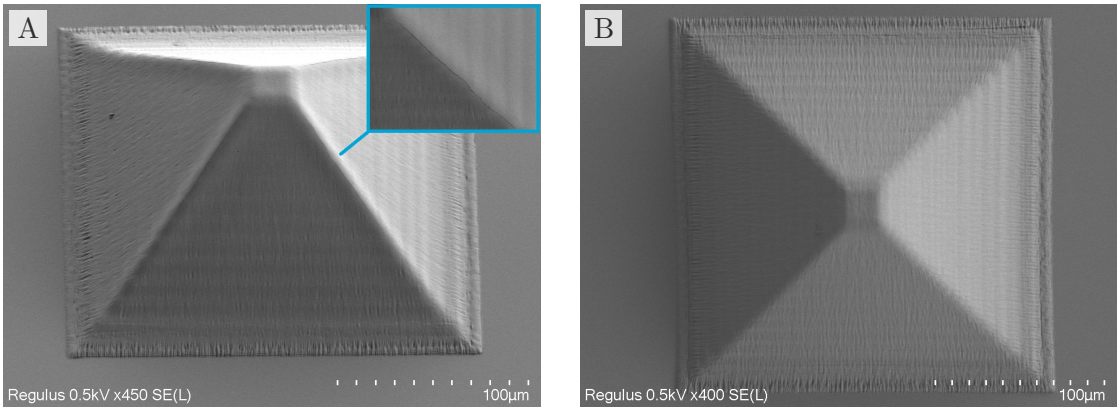

Figure 5.4.: Passivation layer deposited on polymeric pyramid structure:
(A) 800 nm silicon oxide deposited at 75 °C. Cracks occurred at edges of the pyramid. **(B)** 500 nm defect-free silicon nitrite deposited at 40 °C.

Contamination of tools

Contamination is a major concern in cleanroom environments, especially in semiconductor fabrication where even small amounts of impurities can cause defects in the finished product. Metals such as gold or copper can contaminate cleanroom tools, causing critical defects in the processed wafers of other users. The fabrication process was carried out in three different cleanrooms located in different university faculties, each with strict and different rules about cleanliness and contamination. The developed fabrication protocol had to be carefully designed to avoid interfering with established processes and tools used by other users. In this project, the risk of contamination was a significant challenge when merging the 2PP process with standard microfabrication techniques, since Organ-on-Chip (OoC) projects have different requirements about contamination and allowed materials.

There were two main sources of contamination risk: bringing processed wafers from one cleanroom into another, and the use of a proprietary acrylic polymer (IP-Q) that had not been processed in other tools before and had an unknown chemical composition. These risks could potentially contaminate the cleanroom tools and interfere with the established processes of other users.

The strict rules about cleanliness and contamination in the cleanrooms used for this project complicated the development of the process flow for the 3D-MEA and restricted the use of certain tools. For example, no plasma etching tools were allowed at the Else Koi lab (EKL) cleanroom, and any wet etching processes had to be carried out in self-filled baths. These constraints added time to the fabrication process and required special care when handling dangerous chemicals such as buffered hydrofluoric acid (BHF). BHF is a highly corrosive and toxic chemical that poses a serious danger to humans and the environment if not handled properly.

To further mitigate the risks of contamination, strict protocols were followed to ensure cleanliness during the fabrication process and when switching between cleanrooms.

Positional alignment of process steps

The final challenge in merging the 2PP process with standard microfabrication techniques was the need for precise positional alignment of the different process steps involved in fabricating a 3D-MEA. This was necessary because the fabrication of a 3D-MEA involves a sequential process, with the polymeric 3D structures being created first, followed by the electrodes and finally the insulation layers. It was important that these different layers were aligned in the correct positional arrangement in order for the 3D-MEA to function properly. To achieve this, the 2PP structures had to be precisely positioned on the wafer such that subsequent processes could be accurately applied to the correct locations. In addition, the positional alignment of the 2PP structures and the front-end structures was critical for the overall functionality of the 3D-MEA.

In the semiconductor industry, standard photolithography processes typically use alignment markers to ensure that subsequent patterns are correctly aligned with each other. To merge the 2PP process with cleanroom fabrication methods, a similar alignment process had to be developed. This is discussed in more detail in Section 5.5.2.

5.3. Method 1: Masked pattern transfer-based process flow

The presented process flow enables the fabrication of a polymeric 3D-MEA and merges the 2PP process with standard microfabrication techniques, such as photolithography and thin film deposition methods. The protocol from the previously developed 3D-MEA at TUD was used as a starting point for the development. [43, 50] It makes use of the high aspect ratio photolithography technique described in Section 4.2.2.

However, this process flow required major adaptations due to the constraints discussed in the previous section about merging 2PP with standard microfabrication techniques. The main issues were contamination risk and harmful process environments. As a result of the imposed restrictions, a rather complex fabrication process was needed to address them. First, and foremost, the contamination risk of tools limited the available tools and therefore required a wet etching-based approach. In order to wet etch the titanium nitrite (TiN) electrodes, a hard mask made of silicon nitrite (SiN) was needed, as the RCA-1 etchant would attack the photomask. To protect the polymeric structures from harmful environments encountered during the microfabrication processes, a protection was needed after 2PP fabrication, which also had to be removed at the end of the process chain, adding complexity.

The process required six pattern transfers via masks. Each pattern transfer needed a spray coating step which takes between 40-80 minutes, and the pattern had to be transferred via the proximity aligner *EVG 420*. The mask designs are shown in the Appendix A.1. Furthermore, the process required switching multiple times between cleanrooms, which increased contamination and fabrication time.

5.3.1. Process flow

An overview of the process flow will be given in the following, the detailed protocol can be found in the Appendix A.2.

1) Zero Layer:
Fabrication: alignment markers for subsequent photolithography steps

- Alignment markers for wafer stepper *PAS550* and mask aligner *EVG 420*
- Standard process @ EKL
- Plasma etched (120 nm) into silicon bulk
- Etcher: *Trikon Ωmega 201*

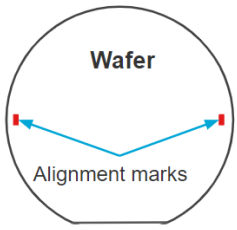

2) Base Layer:
Fabrication: dice grid and vernier scales into the bulk material of the wafer

- Marks die perimeter to aid 2PP fabrication
- Standard process @ EKL: Mask: Figure A.1a
- Plasma etched (120 nm) into silicon bulk
- Etcher: *Trikon Ωmega 201*

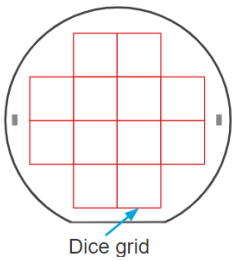

3) Structure fabrication:
Fabrication: Polymeric pyramid structures via 2PP

- Aligned wafer-scale 2PP fabrication
- Photoresin:IP-Q
- 15 Pyramids (200 µm × 200 µm × 100 µm)
- *Photonic Professional GT+* @ PME-lab

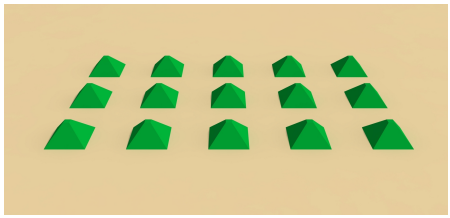

4) Passivation layer:
Deposition of SiN to protect polymeric structures

- Low temperature ICPCVD @ Kavli Lab
- 500 nm SiN @ 75 °C (10 min)

5) Electrode layer:
Fabricate TiN electrodes via wet etching and SiN hard-mask

- Sputter *Sigma 204*: 100 nm TiN (low power)
- Deposition: 200 nm SiN for hard mask
- Spray-coating
- Sidewall photolithography with *EVG 420*: Mask: Figure A.1b
- Etch hardmask with BHF[1]
- TiN etching with RCA-1[2]

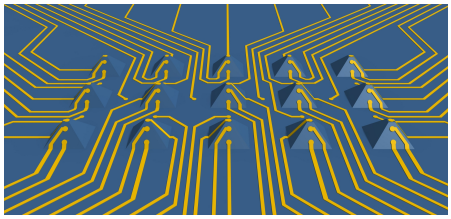

6) Passivation layer:
Passivation of electrodes with SiN

- Low temperature ICPCVD @ Kavli Lab
- 200 nm SiN @ 75 °C (10 min)

7) Openings for pads:
Etch openings into SiN for Al contact pads to connect with electrode traces

- Spray-coating
- Sidwall photolithography with *EVG 420*: Mask Figure A.1c
- Wet etch BHF @ special application lab (SAL)

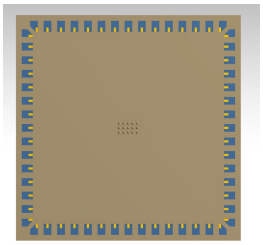

[1] buffered hydrofluoric acid (BHF)
[2] RCA-1: Ammonium hydroxide (NH_4OH, CAS 1336-21-6), hydrogen peroxide (H_2O_2, CAS 7722-84-1), DI water (H2O) (1:1:5)

8) Aluminum pads:
Fabricate Al-contact pads as interface to electrodes

- Sputter *Sigma 204*: 500 nm aluminium (Al) (low power)
- Spray-coating
- Sidwall photolithography with *EVG 420*: Mask Figure A.1d
- Wet etch Al @ SAL

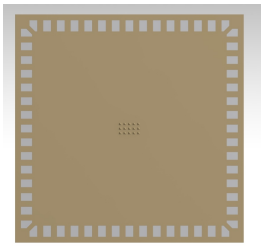

9) Openings for electrodes:
Etch openings into SiN insulation to expose electrodes

- Spray-coating
- Sidwall photolithography with *EVG 420*: Mask Figure A.1e
- Wet etch BHF @ SAL

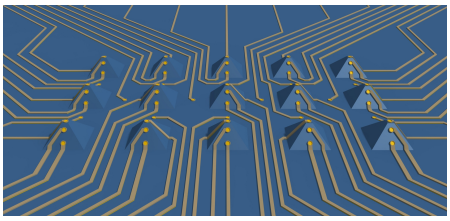

10) Openings for pyramids:
Etch openings into SiN insulation to expose polymeric pyramids

- Spray-coating
- Sidwall photolithography with *EVG 420*: Mask Figure A.1f
- Wet etch BHF @ SAL

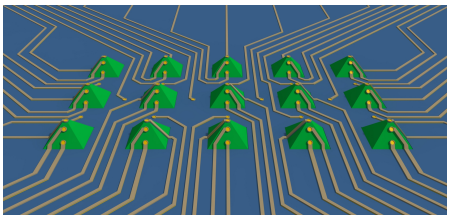

The presented process flow demonstrates the feasibility of merging the 2PP process with standard microfabrication techniques for the fabrication of a 3D-MEA for *in vitro* cell studies of neurons. However, it also highlights the challenges and complexities that arise when merging these techniques, particularly in regards to contamination and harmful process environments.

To address these challenges, the process flow required careful design to avoid interfering with established processes and tools used by other users. The risk of contamination was a significant challenge when merging the 2PP process with standard microfabrication techniques, since OoC projects have different requirements about contamination and allowed materials. The strict rules about cleanliness and contamination in the cleanrooms used for this project complicated the development of the process flow for the 3D-MEA and restricted the use of certain tools. To mitigate the risks of contamination, strict protocols were followed to ensure cleanliness during the fabrication process and when switching between cleanrooms.

Another challenge was the potential harm that certain processes can cause to printed polymeric structures, as thin film deposition processes often involve high temperatures, which can be harmful to the printed polymeric structures used in the 3D-MEA. To protect the structures from potential harmful plasma or solvents, they were covered with a protective layer of a robust dielectric material (SiN) after fabrication.

Hence, to improve the efficiency and effectiveness of this process flow, further research is needed to address these challenges and find solutions. For example the use of other microfabrication techniques could be investigated, such as nanoimprint lithography, that have the potential to

simplify the process flow and reduce the number of pattern transfers needed. Additionally, utilizing more flexible and experimental-friendly facilities, as opposed to the used cleanrooms, may also help to mitigate contamination issues and simplify the fabrication process.

Figure 5.5A shows a rendering of the 20 mm × 20 mm wafer die fabricated with the masked pattern transfer based process flow. In Figure 5.5B a close-up is depicted.

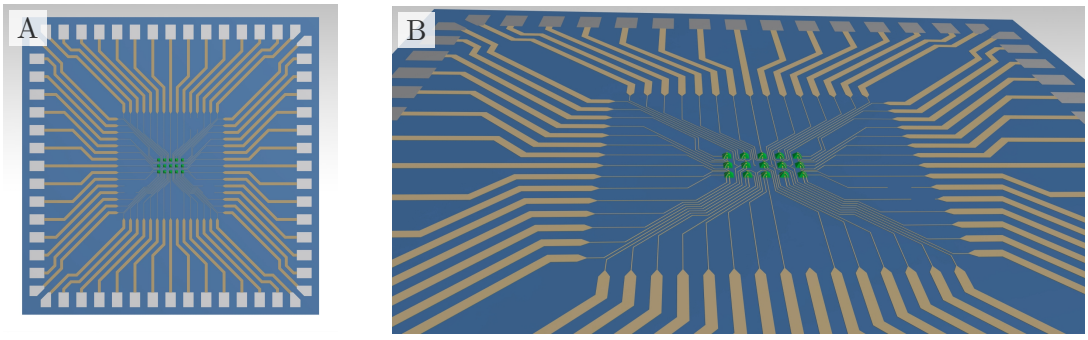

Figure 5.5.: Renderings of the 3D-MEA fabricated with the masked pattern transfer based process flow:
(A) Wafer die overview. **(B)** Close-up of the 3D-MEA.

A processed wafer is shown in Figure 5.6. An etch-test had been conducted on the SiN hard mask for wet etching the electrodes with RCA-1 (Step 5 of the protocol).

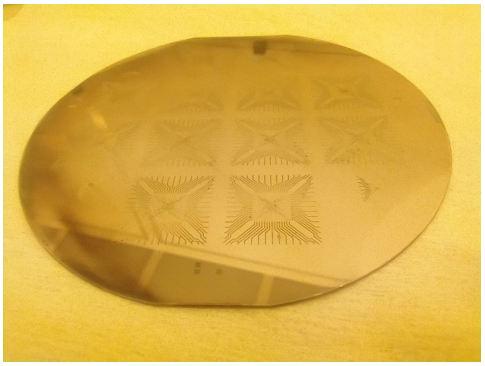

Figure 5.6.: Etched SiN hard mask for wet etching the electrodes.

5.4. Method 2: Two-photon polymerization-based process flow

The 2PP-based process flow was developed to address the challenges and complexities faced with the masked pattern transfer-based process flow discussed in Section 5.3. By using this approach, it was possible to reduce the number of switches between cleanrooms, making the fabrication process less time-consuming and easier to plan. Additionally, the use of a proximity aligner for photolithography in the mask-based process resulted in complex process development and limited the structure height to less than 100 µm due to diffraction and alignment issues. Furthermore, the process required many wet etching steps with dangerous chemicals, which were undesirable. The risk of possible contamination of microfabrication tools also required

extra care and limited the use of established, fast standard processes.

While the standard mask-based pattern transfer methods used in the semiconductor industry rely on one-photon absorption to expose a thin film of photoresist, an experiment was conducted with the two-photon absorption based 3D printer to see if pattern transfer was possible. The results of the experiment, a dose test, are shown in Figure 5.7. This test showed that patterns could be successfully written into both negative photoresist *AZ® nLOF 2000, Merck KGaA, Germany* (see Figure 5.7A) and positive photoresist *AZ® 12XT-20PL-10, Merck KGaA, Germany* (see Figure 5.7B). The development of the process using the 2PP 3D printer to pattern high-aspect ratio structures will be discussed later in Section 5.6: *Maskless photolithography via two-photon polymerization on high aspect ratio structures.*

It is worth mentioning that the 2PP-based process flow enabled the fabrication of 3D-MEA with higher aspect ratios and more complex geometries, which were not possible with the masked pattern transfer based process flow However, it also required the development of new process parameters and compatibility within the process chain, as discussed in Section 5.2.

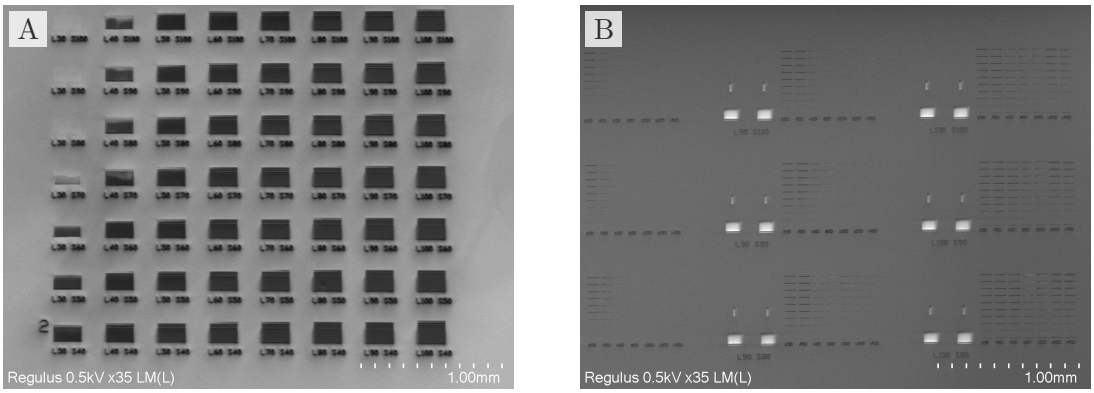

Figure 5.7.: 2D maskless lithography via 2PP test results: **(A)** Negative-tone photoresist AZ nLof 2000. **(B)** Positive-tone photoresist AZ 12XT.

5.4.1. Process flow

In order to reduce issues in terms of contamination, the fabrication process was split into two parts: the front-end and back-end process. The front-end process is a CMOS-compatible, fast, and mask-based fabrication to connect the 3D-MEA via titanium nitride traces and aluminum pads with a PCB with read-out circuit. It limits the required patterning space for the 2PP system to reduce fabrication time.

The back-end fabrication is fully based on 2PP and makes use of the developed wafer-level multi-step fabrication protocol. It includes the fabrication of the 3D-MEA structures, electrodes and insulation and is connected to the front-end structures. The first step was to fabricate polymeric pyramids with 2PP as the structural part of the 3D-MEA. In the second step, a spraycoated positive-tone photoresist was patterned with 2PP to fabricate gold electrodes via lift-off method. Finally, the last step was to print insulation traces on top of the electrode traces.

Front-end process

1) Zero Layer:
Fabrication: alignment markers for subsequent masks

- Alignment markers for wafer stepper *PAS550* and mask aligner *EVG 420*
- Standard process @ EKL
- Plasma etched (120 nm) into silicon bulk
- Etcher: *Trikon Ωmega 201*

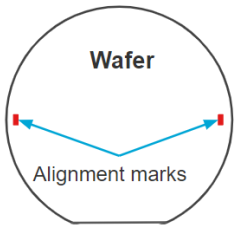

2) Base Layer:
Fabrication: die grid and vernier scales into bulk

- Marks die perimeter to aid 2PP fabrication
- Standard process @ EKL: Mask Figure B.1a
- Plasma etched (120 nm) into silicon bulk
- Etcher: *Trikon Ωmega 201*

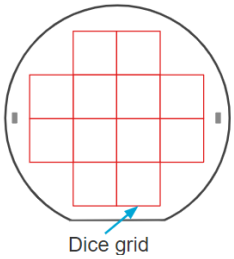

3) Oxide Layer:
Serves as insulation layer

- *Novellus Concept One*
- Standard process @ EKL
- PECVD 300 nm SiO_2

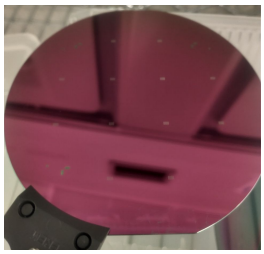

4) Metal trace layer:
Fabrication: TiN metal traces

- Standard processes @ EKL
- Sputter 200 nm TiN with *Trikon Sigma 204*
- Mask aligner EVG 420: Mask Figure B.1b
- Plasma etch TiN with *Trikon Sigma 201*

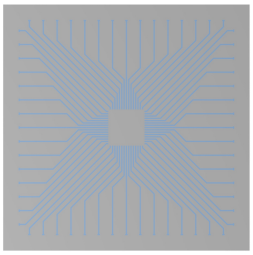

5) Insulation layer:
Fabrication: Insulate metal traces with SiO_2 and expose regions for Al pad contact and back-end.

- Standard process @ EKL
- Deposit 300 nm SiO_2 with Novellus Concept 1 (PECVD)
- Mask aligner EVG 420: Mask Figure B.1c
- Plasma etch SiO_2 with *Drytek Triode 384T*

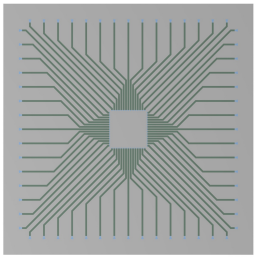

6) Aluminium layer:

Fabrication:Al-contact pads as interface to electrodes

- Standard process @ EKL
- Deposit 600 nm Al with Trikon Sigma 204 Dealer
- Mask aligner EVG 420: Mask Figure B.1d
- Wet etch Al with Transene A [61]

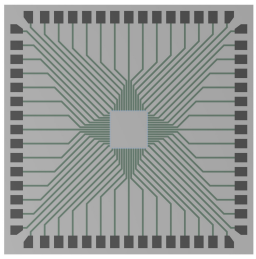

Back-end process

7) Structure fabrication:

Fabrication: Polymeric pyramid structures with 2PP

- Aligned wafer-scale 2PP fabrication
- *Photonic Professional GT+* @ PME-lab
- Large feature set: 10x objective
- Photoresin:IP-Q
- 12 × 15 Pyramids (200 µm × 200 µm × 100 µm)

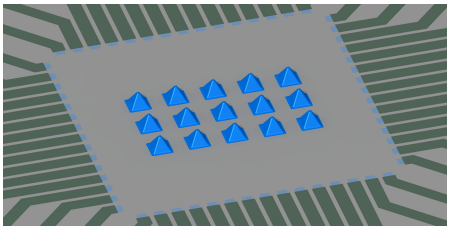

8) Passivation layer:

Deposition of SiO_2 to mitigate base poisoning of photoresist (see Section 5.6.1)

- Low temperature ICPCVD @ Kavli Lab
- 200 nm SiO_2 @ 40 °C (10 min)

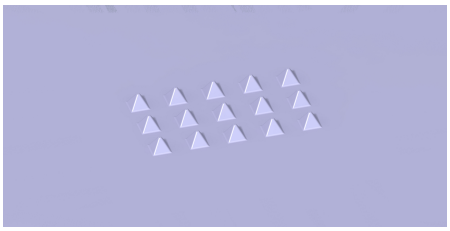

9) Pattern electrodes via 2PP:

Pattern positive photoresist layer with 2PP

- Spray coating of AZ 12XT (6 µm to 10 µm)
- *Photonic Professional GT+* @ PME-lab
- Medium feature set: 25x objective with glycerol immersion
- Expose electrode traces with aligned wafer-scale 2PP fabrication
- Development in AZ 322 MIF @ EKL

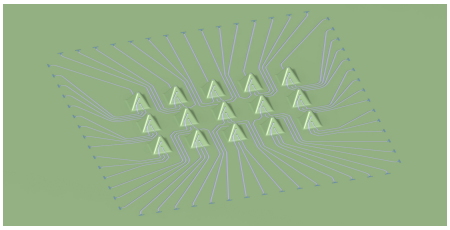

10) Deposit electrode material:

Deposition: Evaporation of gold as electrode material

- Electron beam evaporation: *Temescal FC-20349* @ Kavli
- Deposit 10 nm titanium and 100 nm gold

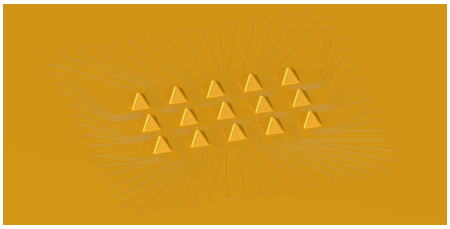

11) Lift-off:

Remove sacrificial photoresist layer to remove unwanted

material.

- Submerge reversed wafer for ≈ 20 min in acetone bath
- Dissolve sacrificial photoresist
- Remove SiO_2 passivation layer with BHF (30 s)

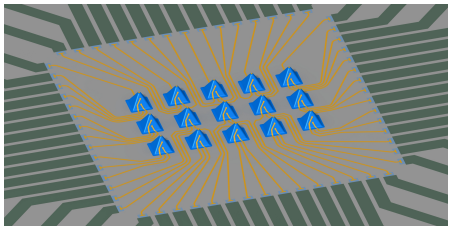

12) Insulation:
Fabrication: insulation of electrode traces with 2PP

- Aligned wafer-scale 2PP fabrication
- *Photonic Professional GT+* @ PME-lab
- Large feature set: 10x objective
- Photoresin:IP-Q

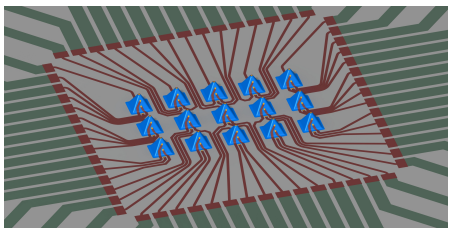

The presented process flow demonstrates another possibility for merging the 2PP process with standard microfabrication techniques in order to fabricate a 3D-MEA for *in vitro* cell studies of neurons. By splitting the process into a CMOS-compatible front-end and a multi-step 2PP-based back-end, a clear separation was achieved which mitigates the contamination issues. This approach allows for the utilization of the benefits from both methods and reduces their downsides. The front-end process was designed for compatibility with established, high-volume CMOS fabrication, providing a development platform for the 2PP-based back-end process.

The 2PP-based back-end process offers high design freedom and the ability to quickly iterate on design changes, including the ability to create custom designs and optimize fabrication time and yield. It is worth noting that this method may have a slower fabrication speed (lower throughput) compared to other techniques. However, the benefits such as higher design freedom and the ability to create more biomimetic structures may outweigh the slower fabrication speed for certain applications.

Compared to the mask-based protocol, the 2PP-based process flow enables the fabrication of higher and more complex structures for 3D-MEA, extending its measurement resolution, and requires only one spray coating step with minimal requirements for film conformity. Additionally, no use of the proximity aligner is required. However, it does require more complex 2PP processes.

It is worth noting that the process flow presented here is specific to the fabrication of 3D-MEA for *in vitro* cell studies of neurons, and may not be directly applicable to other types of organ-on-chip systems. However, the principle of splitting the fabrication process into front-end and back-end, and utilizing both mask-based and 2PP photolithography techniques, can be adapted to other microfabrication applications.

5.5. Wafer-scale multi-step two-photon polymerization process

The process flow for fabricating the 3D-MEA described in Section 5.4 relies on a wafer-scale multi-step two-photon polymerization process. This toolset enables precise alignment of 2PP-fabricated structures on a 100 mm wafer substrate, allowing for a multi-step fabrication protocol that can also incorporate different process steps such as thin film deposition. It also enables a multi-material approach, allowing for the fabrication of structures with one material and

the addition of features with another material. Additionally, this process flow allows for the change of feature sets by printing large, bulky structures with a small magnifying objective and switching to a different objective in the next fabrication step to add small features to the previously fabricated structures. All of these capabilities are made possible by the developed framework, which enables the alignment of multiple 2PP fabrication steps on a wafer-scale area. In the following text, the developed printer control routines are discussed, along with their limitations. The alignment method is then introduced, followed by a discussion of the challenges that occurred during successive aligned printing steps.

5.5.1. Printer control

A customizable print job in the form of a General Writing Language (GWL)-file was developed to fabricate the 3D-MEA according to the wafer-scale multi-step two-photon polymerization process. This print job is capable of fabricating 12 3D-MEA on a 100 mm wafer, with each MEA consisting of 15 pyramid structures. In addition to the MEAs, the print job may also include the fabrication of test structures, which can easily require the production of more than 180 structures in a single step of the process. The print job combines three steps: fabricating structures, patterning electrodes and traces, and finally printing insulation above the traces. It also allows for the addition of more fabrication steps to add design features to the 3D-MEA. Users can choose which part of the 3D-MEA to fabricate by setting a variable in the print job file accordingly. The most important code snippets are discussed in Appendix C.

Some highlights of the developed print job are:

Custom coordinate system and movement commands: Once the position stage has been referenced to the loaded wafer, the print job keeps track of the current position of the wafer stage. Using customized absolute and relative movement commands, it is able to reach any position on the wafer while updating its internal position state. To ensure the accuracy of the fabrication process, a backlash compensation has been implemented to account for the stage positioning mechanism, ensuring that every coordinate is approached from the same direction. Additionally, a local coordinate system can be used to position structures at the die level.

Unique fabrication settings for each fabrication step: Another feature of the developed print job is its ability to accommodate unique fabrication settings for each step of the process. Depending on the requirements of each fabrication step, the print job may use different configurations or materials, requiring changes to various fabrication parameters such as `laser dose`, `scanning speed`, or `interface position offset`. These changes are automatically implemented by the print job to ensure that the correct settings are used for each step of the process.

Global offsets for misalignment compensation: To compensate for misalignment errors, the print job includes the ability to set unique global coordinate offsets for each fabrication step. By applying these offsets, it is possible to correct for any misalignment that may occur during the process, improving the overall accuracy of the fabricated 3D-MEA.

Retract-and-approach movements: The print job also includes retract-and-approach movements to minimize the risk of damaging the objective during long distance movements, for example when moving from one die to the next. During these movements, the objective is retracted a safe distance of more than 4 mm and the movement speed is increased from from 200 µm s^{-1} to 1000 µm s^{-1}. Once the target position has been reached, the substrate is approached again. This not only minimizes the risk of damage to the objective, but also greatly increases the fabrication time and prevents smearing of the resin away from the printer's objective. Optionally, an automatic interface finding command can be issued to compensate for substrate tilt and positioning errors.

Wrapper for the interface finding routine: To facilitate the automatic process of finding the substrate interface, a wrapper for the interface finding routine was developed. This wrapper allows users to add an additional offset in the z-direction, which can be helpful when the substrate consists of multiple layers, such as a spraycoated photoresist film, and the interface is found within the substrate. If the current stage position is occupied by structures from a previous fabrication step, the interface finding routine may not work. To address this issue, users can define x- and y-offsets to move the stage to a nearby empty position, find the interface, and then move back to the previous position and start the fabrication.

Structure library: To keep the file structure of the print jobs lean and small, a large library with over 100 sliced structures was accumulated over the course of the project. These structures, which can be as large as 100 MB, can be referred to by a unique number inside the print job, allowing for fast switching of structures and designs without worrying about the location of the associated files. The structure library also makes it easy to associate structures that belong together, such as a 200 µm high pyramid fabricated in the first step that requires 200 µm electrodes fabricated on top in the second step. This approach is part of the digital twin toolchain, which aims to streamline the fabrication process and improve the accuracy and repeatability of the 3D-MEA.

5.5.2. Print structure alignment

Precisely positioning the 2PP fabricated structures on the wafer was the most crucial step to make the technique compatible with the vast microfabrication technologies for semiconductors. It employs alignment markers which are used for the PAS5500/80 wafer stepper from *ASML*. These are etched 120 nm into the silicon wafer. With the center of the wafer being the origin of a Cartesian coordinate system, their positions are `(−45 mm, 0)` and `(45 mm, 0)`, respectively. The goal is to use them as reference points and locate all other structures with respect to them.

The alignment method is composed of a two-step protocol. First the origin of the print field is correlated with the internal camera view. This allows for translational alignment. Second, the internal coordinate transformation tool from the printer control software is used to compensate rotational misalignment. In the following text the developed alignment protocol will be introduced.

Correlate origin of the print field with the internal camera view

The first step is to establish a correlation between the origin of the print field and the internal camera view of the *NanoWrite* software. This can be achieved by printing a simple cross, as shown in Figure 5.8A, at the origin of the print field, using the Describe CAM software, and then manually aligning the blue crosshair in the camera live-view with the printed cross. Figure 5.8B shows a magnified image of the printed cross, and Figure 5.8C shows the aligned blue crosshair on top of the printed cross. This correlation can be verified by moving the position stage to an empty area on the substrate and reprinting the cross, which should coincide with the crosshair in the camera view.

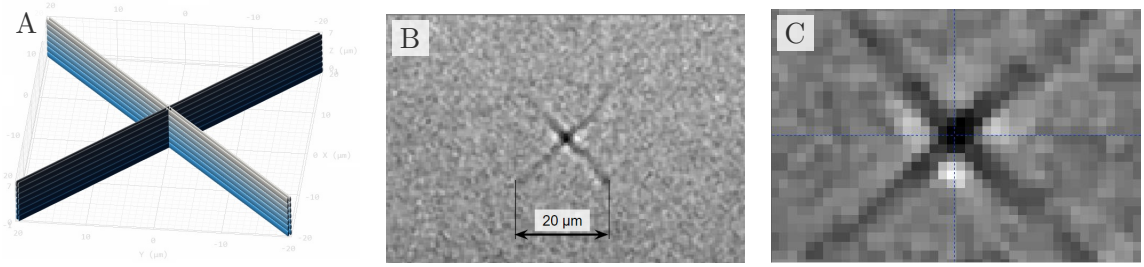

Figure 5.8.: Alignment process: **(A)** Cross in *Describe* CAM software: positioned at the origin. **(B)** Printed cross at the origin of the print field. **(C)** Crosshair of the camera view is manually dragged to align with the printed cross.

Once the correlation has been established, it is possible to align the origin of the print field with any other feature on the wafer by moving the position stage such that the crosshair coincides with the targeted feature. This approach allows for precise alignment of the 2PP structures with other features on the wafer substrate. However, the procedure only accounts for translational alignment and does not take into consideration its rotation. When inserting the wafer into the substrate holder of the 2PP machine it will have a varying rotational offset with respect to the holder. This leads to substantial misalignment when trying to combine multiple 2PP fabrication steps. To overcome this issue, the coordinate transformation tool within the *Nanowrite* printer control software was utilized to adjust the internal machine coordinate system according to the rotational offset of the wafer. This ensures precise alignment of the 2PP structures with other features on the wafer substrate. The workflow will be described in the following paragraphs.

Coordinate transformation

The first step for the coordinate transformation is to align the crosshair in the camera view with the alignment marker by moving the positioning stage of the 3D printer. A picture of the marker is shown in Figure 5.9A. Once crosshair coincides with the marker, the position coordinates have to be obtained within the software suite by clicking the `Get Position` button. The user interface with the camera view is shown in Figure 5.9B, were the crosshair coincides with the alignment marker. The same procedure has to be done with the second marker.

Next, the design coordinates are entered into the corresponding text fields. They define the desired rotated vector and were set to `(0, 0)` and `(1, 0)`. As a result, both alignment markers will be located at the rotated x-axis. Finally the `Transformation` switch is activated to rotate the internal coordinate system of the machine.

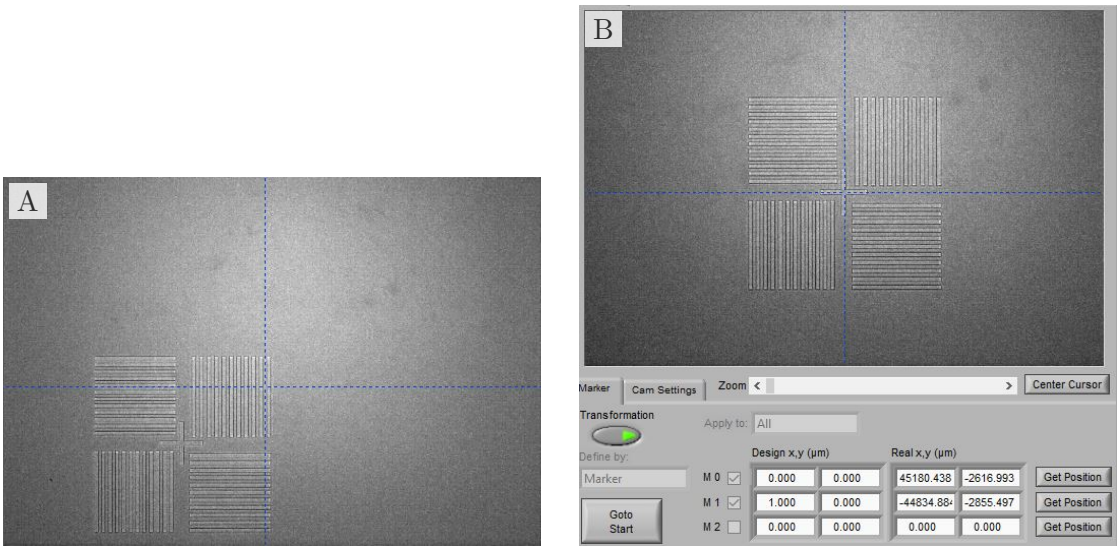

Figure 5.9.: Alignment procedure with coordinate transformation:
(A) Aligning the blue crosshair with the marker by moving the positioning stage. **(B)** User interface of the printer control software with aligned marker.

Nanowrite software bug

During the development of the alignment protocol, it was necessary to become familiar with the internal coordinate transformation tool of the printer control software *Nanowrite*. However, during this process, it was noted that when printing transformed structures in the DiLL configuration, they were mirrored around the y-axis. Initially, it was thought to be an error in the protocol, but it was later discovered to be an unknown bug in the software after consulting with a *Nanoscribe* support engineer.

With the current software version `(1.10.5)`, the bug has not been fixed. The proposed workaround is to mirror the 3D file before slicing. However, this is not a practical solution as it has to be taken into account when aligning to features or printing nonsymetrical features. Also, printed text will turn out mirrored and therefore unreadable.

The error is exemplified in Figure Figure 5.10, where a coordinate transformation has been conducted. The goal was to rotate the x-axis, such that it coincided with marker M0 and M1. As shown, the x-axis of the transformed structure T1 lies indeed on the reference points. However, the y-axis is inverted (e.g. mirrored around the x-axis). This non-intended behavior is clearly a bug of the coordinate transformation feature as it is actually performing a non-linear coordinate transformation. As of now, this issue has not been solved via software update, however, *Nanoscribe* suggest a workaround on their website. [54]

5.5.3. Challenges with successive printing steps

Misalignment

The main issue noticed during fabricating 3D-MEA with the multi-step 2PP fabrication process was the incorrect alignment of the successive fabricated structures. Multiple influencing factors have been identified and minimized as good as possible. The first factor is a global offset between

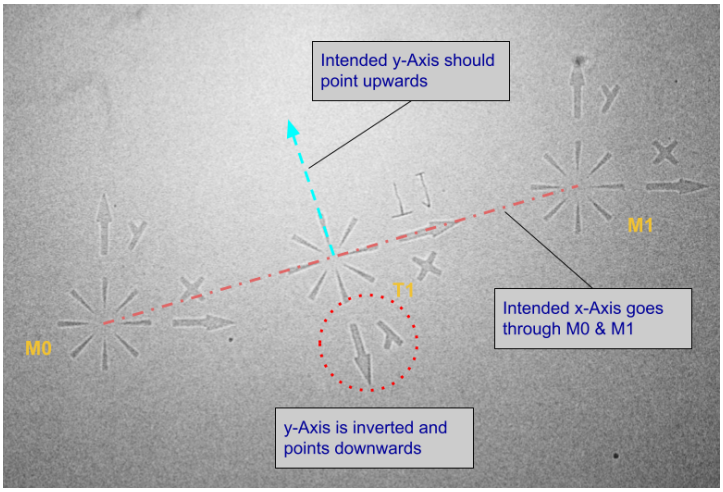

Figure 5.10.: Unintended inverted y-axis of the Nanowrite control software after the coordinate transformation.

two successive printing steps due to errors during the manual alignment procedure. Inaccuracies can occur during the correlation between print field origin and camera view or during referencing the alignment markers before starting the print job. These errors are bigger with larger feature sets (10x objective) compared to smaller feature sets (25x objective), which has to be taken into account when using different feature sets during the multi-step fabrication. Furthermore, the stage positioning repeatability is according to *Nanoscribe* specifications <1.5 µm. [54] This can cause misalignment of structures within a printing step.

An example of an early alignment test is shown in Figure 5.11. The test was conducted with the large feature set (10x objective) and IP-Q photoresin according to the protocol described in Section 4.2.4. This two-step printing test consists of a reference structure, which is printed first, and a cross printed aligned inside the reference structure. The dimensions of the test structure are given in Figure 5.11A. The printed structures were investigated and measured with an optical microscope (Figure 5.11B). Overall, the observed total misalignment of two consecutive printing steps was below ±5 µm. All these misalignment sources were accounted for in the design phase of the 3D-MEA by adding appropriate position tolerances.

Interface position finding

The interface position is where the substrate is located in relation to the focal plane of the 2PP objective. This position is critical for aligning the printed structures and serving as the starting point for the printing process. If the interface position is too high, the structure may detach from the substrate, but if it's too low, the structure may be missing features or have incorrect dimensions. In the case of maskless photolithography, the pattern may not be fully transferred if all parts of the photoresist are not exposed.

To help determine the interface position, the *Nanoscribe* 2PP machine has an automatic process. The machine projects a grid pattern (near-infrared: 850 nm) into the media (either resin or immersion oil) through the 2PP objective. At the optical interface, the refractive index changes abruptly, and part of the grid pattern is reflected back to a CCD-detector within the machine.

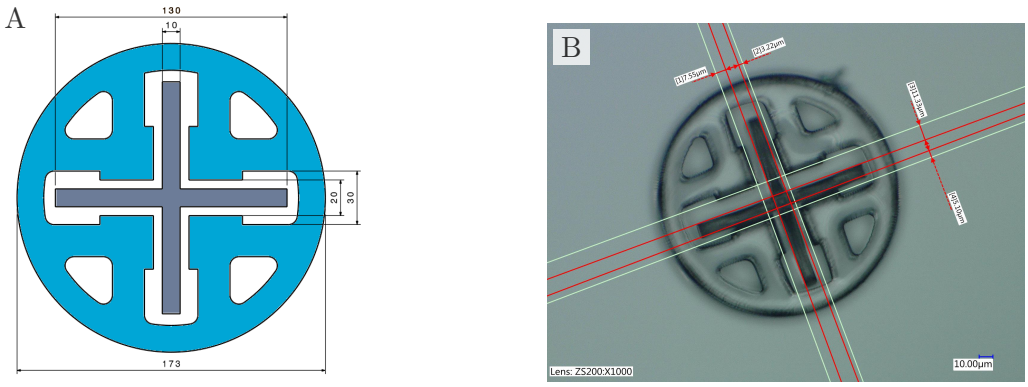

Figure 5.11.: Alignment test: Aligned cross printed inside a reference structure: **(A)** Dimensions (in µm) of the designed alignment test. **(B)** Optical microscope measurements of the alignment.

When the interface matches the focal plane of the 2PP objective, the reflected pattern can be detected. By adjusting the objective height, the interface position can be found.

The strength of the interface signal depends on the difference in refractive index between the substrate and medium ($\Delta n = n_{\text{substrate}} - n_{\text{medium}}$). The precision of the interface finding depends on the objective magnification, so a 63x objective will be more precise than a 10x objective. As a result, the automatic interface finder requires a smaller refractive index contrast for the 63x objective than the 10x objective. The minimum difference in refractive index required for each 2PP configuration is listed in Table. 5.1.

Table 5.1.: Minimum difference in refractive index Δn_{min} for automatic interface finding. [54]

	Small features 63x NA1.4	**Medium features** 25x NA0.8	**Large features** 10x NA0.3	**Maskless lithography** 20x NA0.5
Δn_{min}	0.04	0.1	0.5	-[1]

[1] not specified, ($\Delta n_{\text{air-resin}}$ typically sufficient)

One of the challenges with multi-step fabrication is that structures from previous steps impede the automatic interface finder. To address this issue, it is best practice to find the interface position at an empty area close to the target print area. A printer control routine was developed to find the interface at a defined position, as described in Section 5.5.1. This helps to ensure accurate alignment and overall success of the 2PP fabrication process.

Time and complexity

In this project, a process with three 2PP steps was developed to fabricate a 3D-MEA. However, each step in the process is different, making the overall fabrication time and complexity of the process more challenging. As a result, each step in the fabrication process requires its own process development to find the appropriate fabrication parameters and ensure compatibility within the process chain. The variety within the fabrication steps can be attributed to several factors.

- **CAD/CAM:**
  Process development starts with the design of the structure, as manufacturability and compatibility with the other process steps has to be ensured. Furthermore, CAM settings, such as slicing and hatching distance have to be chosen according to required resolution and fabrication time. These decisions will influence the process parameters, especially the required polymerization dose.
- **Material / photoresin:**
  The multi-step two-photon polymerization process enables sequential multi-material printing. Each material requires its own process parameters. In this project, theIP-Q photoresin was used for the pyramidal structures and for insulation, while the maskless photolithography process was used to pattern AZ 12XT and fabricate the electrodes.
- **Printer configuration**
  Depending on the required feature size, different objectives may be used to employ smaller voxels. Furthermore, the printing mode may change, as the 2PP system from *Nanoscribe* offers three different modes: Dip-in, oil, and maskless lithography (Air). Throughout the project, three objectives were used: 10x (DiLL), 20x (Air), and 25x (DiLL). The choice of objectives was based on their ability to achieve the required feature size and resolution. For example, the 10x objective was used for large features, such as the truncated pyramid structures, while the 20x and 25x objective were used for maskless lithography.
- **Substrate interface**
  The properties of the substrate can influence the 2PP process and may lead to print ac3DMEA artefacts. In this project, silicon was used as the initial substrate. However, silicon has a very high refractive index ($n = 3.71780\,\text{nm}$ [62]) which may reflect the incident beam, leading to printed artefacts. To address this issue, the polymerization dose was reduced when fabricating structures in close proximity to the interface. In addition to this, inhomogeneous interface properties, which can occur in a multi-step fabrication process, are an additional complication factor. For example, in this project, when printing the IP-Q-based insulation as the last fabrication step, the interfaces were silicon, gold, and polymerized IP-Q. This made the polymerization dose a function of position, which is difficult to implement with the current limited capabilities of the printer control software.

5.6. Maskless photolithography via two-photon polymerization on high aspect ratio structures

5.6.1. Base poisoning of chemically amplified resist

In this project, a chemically amplified positive resist, AZ® 12XT-20PL-10 from Merck KGaA, Germany, was employed. Chemically amplified resists (CARs) are a type of photoresist used in lithography that use a chemical amplification process to increase sensitivity to ultraviolet light. CARs consist of a polymer resin, a photoacid generator, a dissolution inhibitor, and an acid-labile protecting group. The acid-labile protecting group inhibits the dissolution of the photoresist in the developer before exposure. The photoacid generator generates acid after exposure to UV light which attacks the acid-labile protecting group, making the photoresist more soluble in a developer solution. CARs offer higher resolution compared to traditional photoresists, due to their high sensitivity to UV light resulting from the chemical amplification process that occurs in CARs.

The 2PP system was used in the 2D maskless lithography configuration with the 20x objective in air mode. Initial experiments in exposing electrode patterns onto the sidewalls of polymeric (IP-Q) pyramids yielded unexpected results, as illustrated in Figure 5.13. Only parts of the IP-Q structures were actually patterned and the underlying polymer was never fully exposed. A small layer of insoluble photoresist remained on top of the structures. Interestingly, the pattern transfer featuring underneath a silicon surface was successful. Figure 5.13A illustrates the observed results. The electrode traces at the bottom of the pyramid are fully exposed via the 2PP process, while the pattern on the top is only partially exposed into the photoresist. Furthermore, the close-up SEM image in Figure 5.13B reveals even the traces of the 2PP laser in the remaining photoresist. It can be observed that the perimeter of the pattern was exposed as a contour line while the inner area was rastered by the 2PP-laser. These effects occurred regardless of the used dose. Possible reasons for the unexpected results were thought to be due

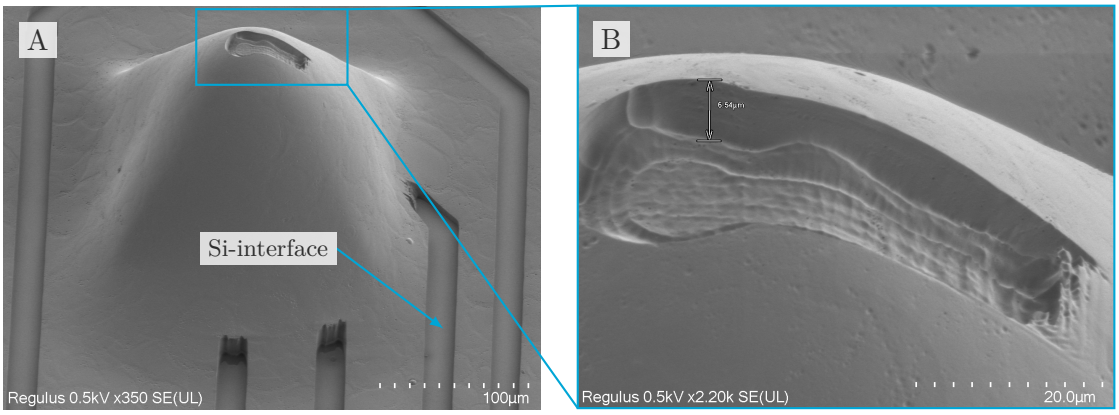

Figure 5.12.: Partially exposed resist pattern in AZ 12XT photoresist via 2PP: **(A)** Pyramid structure with partially exposed photoresist. **(B)** Close-up of the top elecrode pattern.

Figure 5.13.: Partially exposed pattern in AZ 12XT photoresist with 2PP

to shrinkage of the polymeric structure or an unindented z-offset in the fabrication process. Therefore, the digital model was modified to compensate for a measured shrinkage of 5 µm

and the thickness of the electrode pattern was increased to up to 40 µm, with the electrode structure extending 20 µm into the pyramid. Figure 5.14 shows a combined print job in the

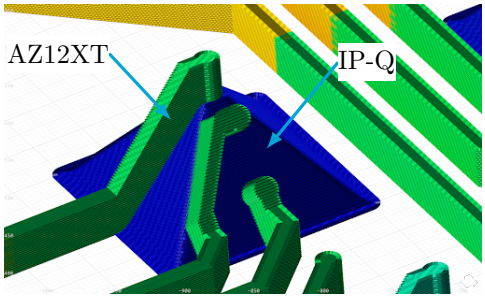

Figure 5.14.: CAM view of pyramid and electrode structures. Illustrating the increased thickness of the electrodes to pattern the AZ12XT photoresist

CAM software to illustrate the increased thickness of the electrodes compared to the 100 µm tall pyramid structures. However, these measures did not lead to substantial improvements in the partially exposed photoresist.

The phenomenon of base poisoning, which occurs in chemically amplified resists (CARs), was identified as the cause of the unexpected results observed in the patterning of the polymeric (IP-Q) pyramids. This issue, first observed in the 1980s and 1990s, occurs when traces of ammonia (NH_3) in the ambient atmosphere neutralize the acid generated after the exposure process, resulting in poor resolution or missing features in the final pattern. It was one of the challenges that needed to be addressed in the development and commercialization of CARs. [63]

The SEM image in Figure 5.15 illustrates the characteristic T-shaped sidewalls that result from base poisoning. The photoacids at the resist-air-interface are neutralized by diffusing ammonia from the ambient atmosphere, leading to a reduced acid concentration at the interface and, subsequently, a lower dissolution rate in the developer. This ultimately results in the formation of T-shaped sidewalls.

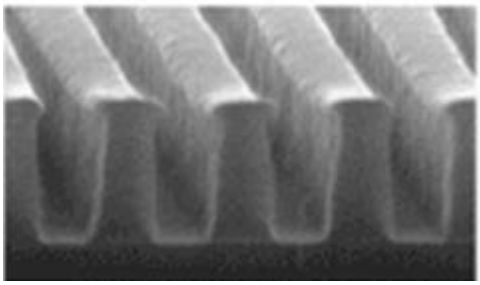

Figure 5.15.: Characteristic T-topping due base poisoning of the photoresist by the ambient atmosphere. [63]

The same effect occurred at the interface between the IP-Q polymer and the CAR photoresist. However, the precise mechanism by means of which the IP-Q reduces the amount of acids in the photoresist is not clear. It is not known whether it is due to base neutralization or if the acids diffuse into the IP-Q polymer. Additionally, the use of HMDS, which was used as an adhesion promoter for the photoresist, could also be a contributing factor. This is a topic that requires further research in future work. To address this issue, an inert intermediate layer of 200 nm of

silicon oxide (SiO_2) was deposited prior to spray-coating the photoresist. This measure created a barrier between the IP-Q substrate and the photoresist, preventing the neutralization of photoacid and eliminating the base poisoning effect. While this measure increased the overall process time and complexity, it was successful in allowing for successful pattern transfer onto the IP-Q structures.

5.6.2. Substrate interface effects

When using 2PP as a photolithography method to expose photoresist thin films, substrate interface effects play a significant role as the printing occurs in close proximity to the substrate. This is particularly true for highly reflective substrates, such as silicon, which has a refractive index of (n= 3.71) at the 2PP laser wavelength of 780 nm. [62] The reflected beam of the laser at the substrate interface can cause a change in light dose above the substrate, leading to print artefacts.

Figure 5.16 illustrates the two most prominent interface effects. If the focus of the 2PP optical system is located inside the substrate, the reflected beam will result in a voxel above the interface, as shown in Figure 5.16A. During the print process, this can cause over-exposure of the photoresist, as the focal point is gradually moved away from the substrate, eventually exposing the same region twice - once due to reflection at the substrate interface and once as intended. Overexposure results in larger voxel sizes and, therefore, reduced print resolution. In extreme cases, the local dose can be too high causing microbubbles in the resin due to rapid local temperature increase, leading to voids in the printed object. Bubble formation can be prevented by reducing the dose of the first few layers of the structure and choosing the correct interface offset to start the print job. This is a trade-off between good structure adhesion and risking overexposure.

The reflected beam can also interfere with the incoming beam, causing localized dose minima and maxima close to the interface. The interference results in wave-like patterns in the printed structures, as shown in Figure 5.16B. While at the maxima, the dose will be greater than anticipated, at the minima, it will be lower, even below the polymerization threshold. This can cause non-uniform patterns in the printed structures.

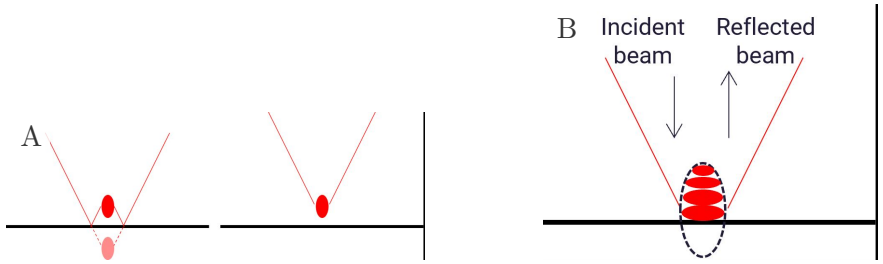

Figure 5.16.: The two main print artefacts due to highly reflective interface: **(A)** Reflection: The laser beam is reflected and exposes material above the interface. **(B)** Interference: The incident and reflected beam interfere resulting in wavelike patterns in the exposed voxel.

This highlights the importance of considering the substrate interface when conducting dose tests and optimizing the 2PP process for thin film patterning. The reflectivity of the substrate can greatly affect the amount of light that reaches the photoresist, resulting in variations in the dose

required for full exposure. This is demonstrated in the results shown in Figure 5.17, where two identical parameter sweeps were conducted on silicon andIP-Q substrates. Both interfaces were covered with a 200 nm thin film of silicon oxide (SiO_2) as an interlayer to ensure no chemical interaction between the substrate and photoresist (e.g. base poisoning). This consideration was discussed in Section 5.6.1. The test was conducted with the following print parameters:

- **Feature set:** 20x Objective - Air mode
- **Scanning Speed:** 100 mm s^{-1}
- **Laser Power:** Sweep: 10:3.75:100
- **Slicing Distance:** 2 µm
- **Hatching Distance:** 0.5 µm
- **Interface position offset:** 1 µm

The influence of the interface reflectivity is evident. The silicon substrate, with a refractive index of (n= 3.71) at a wavelength of 780 nm, was found to be highly reflective. A sufficient dose is delivered at a laser power setting of 73.75 (37 mW), as shown in Figure 5.17A. Compared to the IP-Q (see Figure 5.17B) with a refractive index of (n= 1.506) at the same wavelength, a laser power setting of 85 (42.5 mW) is needed to achieve a full exposure of the pattern. [54] The silicon oxide film has a refractive index of (n= 1.4537) at a wavelength of 780 nm.

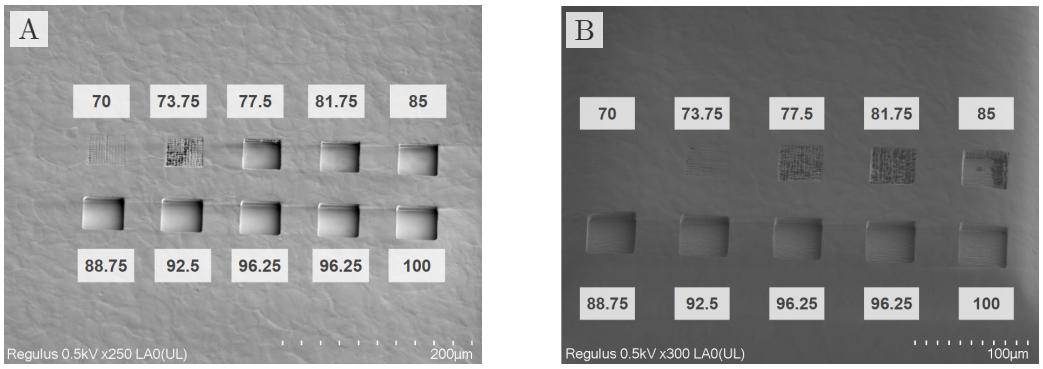

Figure 5.17.: Dose sweep on different interfaces (35° tilted view): **(A)** Si/SiO_2-interface. **(B)** IP-Q/SiO_2-interface.

In conclusion, the substrate interface effects play a significant role in the maskless 2PP photolithography process, particularly when using highly reflective substrates such as silicon. These effects can result in print artefacts such as over-exposure and wave-like patterns in the printed structures. It is recommended to use a low-reflection substrate, apply an anti-reflection coating on the substrate before printing and experimenting with different interface offsets and dose settings in order to achieve optimal results.

5.6.3. Pattern transfer on slanted surfaces

With the base poisoning effect being mitigated and interface effects considered, dose tests were conducted to determine the process window for the maskless photolithography via 2PP on high aspect ratio structures. To accomplish this, triangular prisms with changing slope angles from 50° to 75° (with 5° steps) were fabricated with IP-Q polymer via 2PP in an array of 3 by 10 (Figure 5.18A). Each prism has two sidewalls, providing the opportunity to check two

slopes with one structure, hence three prism designs were needed to conduct the test. After deposition of the inert silicon dioxide (SiO_2) thin film and spray-coating of the photoresist, arrays of electrode traces were patterned on the polymeric structures while varying process parameters to adjust the exposure dose.

- **Feature set:** 20x Objective - Air mode
- **Scanning Speed:** 100 mm s^{-1}
- **Laser Power:** Sweep per prism: 10:7.5:100
- **Power scaling:** Sweep: 0.1:0.1:1.1
- **Slicing Distance:** 1.5 µm
- **Hatching Distance:** 0.25 µm
- **Interface position offset:** 1 µm

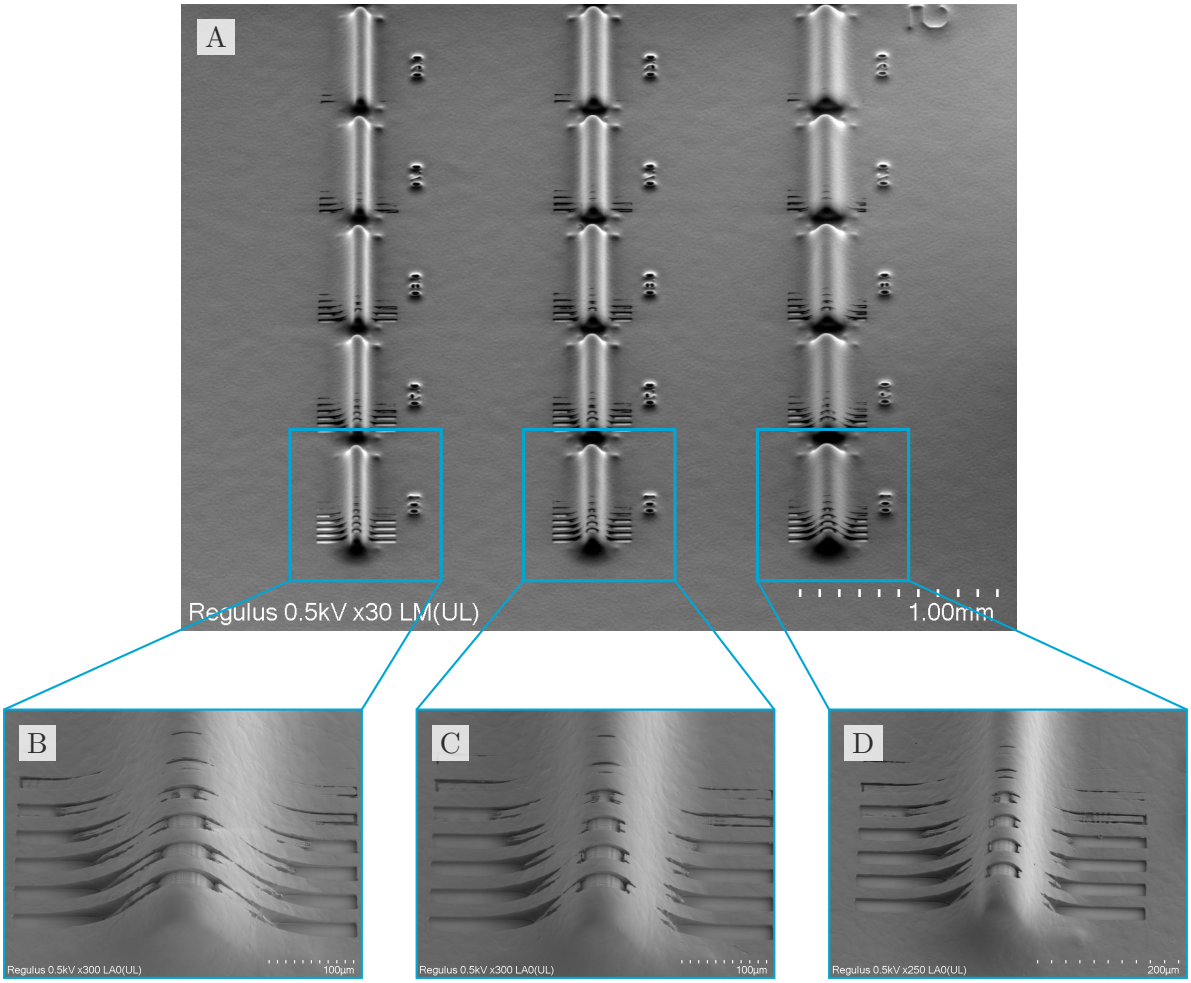

Figure 5.18.: **(A)** Dose test on triangular prisms. **(B)** Close-up: Prism with 50°/55°-slope. **(C)** Close-up: Prism with 60°/65°-slope. **(D)** Close-up: Prism with 70°/75°-slope.

Even at the highest laser power setting, the resist was not fully exposed at the sidewalls. In contrast to perpendicular surfaces, the top of the prism and the substrate, are exposed properly. The error pattern revealed a substantial sidewall angle dependency, where the steeper the sidewall angle, the less exposed photoresist. The prism with a slope of 50°/55° (Figure 5.18B)

shows the best results compared to the prism with a 60°/65° degree slope (Figure 5.18C) or the worst results at the prism with a 70°/75° slope (Figure 5.18D). This is due to reflection of the incident beam at the air-resist interface due to the high refractive index difference. Increasing the dose further by decreasing the scanning speed of the laser induced damage to the photoresist film, as shown by the burned resist and bubble formation in Figure 5.19.

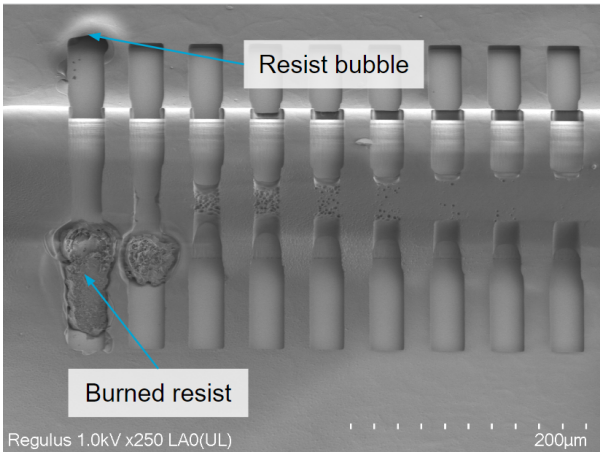

Figure 5.19.: Damage to the photoresist film was caused by high 2PP doses

The Fresnel equations, which describe the reflectance and transmittance of light at interfaces between different materials, can be used to describe the reflectance at the air-photoresist interface. The high refractive index difference between air and photoresist results in a high reflectance at this interface, which is a major contributor to the exposure errors at sidewalls observed with the maskless 2PP photolithography process. As such, the Fresnel equations provide insight into the underlying mechanism of the substrate interface effects and their impact on the process. The equations are dependent on the polarization of the light and are different for s-polarization (R_s, perpendicular to the plane of incidence) and p-polarization (R_p, parallel to the plane of incidence). [64]

$$R_s = \left| \frac{n_1 \cos\theta_\mathrm{i} - n_2 \cos\theta_\mathrm{t}}{n_1 \cos\theta_\mathrm{i} + n_2 \cos\theta_\mathrm{t}} \right|^2 \tag{5.1}$$

$$R_p = \left| \frac{n_1 \cos\theta_\mathrm{t} - n_2 \cos\theta_\mathrm{i}}{n_1 \cos\theta_\mathrm{t} + n_2 \cos\theta_\mathrm{i}} \right|^2 \tag{5.2}$$

$$\text{Snellś law:} \quad n_1 \sin\theta_\mathrm{i} = n_2 \sin\theta_\mathrm{t} \tag{5.3}$$

The equations describe a plane wave incident on a plane interface at an angle of θ_i in a media with refractive index n_1, which is transmitted through the interface at an angle θ_t with refractive index n_2. The refractive index of AZ® 12XT is $n = 1.564$ at 780 nm, while air can be approximated with $n = 1$. The reflectance of the air-photoresist interface with respect to the angle of incidence for the 2PP laser is shown in Figure 5.20. The graph was plotted with Python (Matplotlib [65]). As the sidewall slope increases, the dose delivered to the photoresist decreases due to the increased amount of light being reflected. While the p-polarized light has its minimum, known as the Brewster angle, at about 57°, the obtained results suggest that the laser light source of the 2PP system is circularly polarized (a combination of p- and s-polarization), as the pattern transfer capabilities decrease with increasing slope. This highlights the importance

of understanding the reflectance properties of the materials used in the microfabrication process in order to optimize them and achieve the desired results.

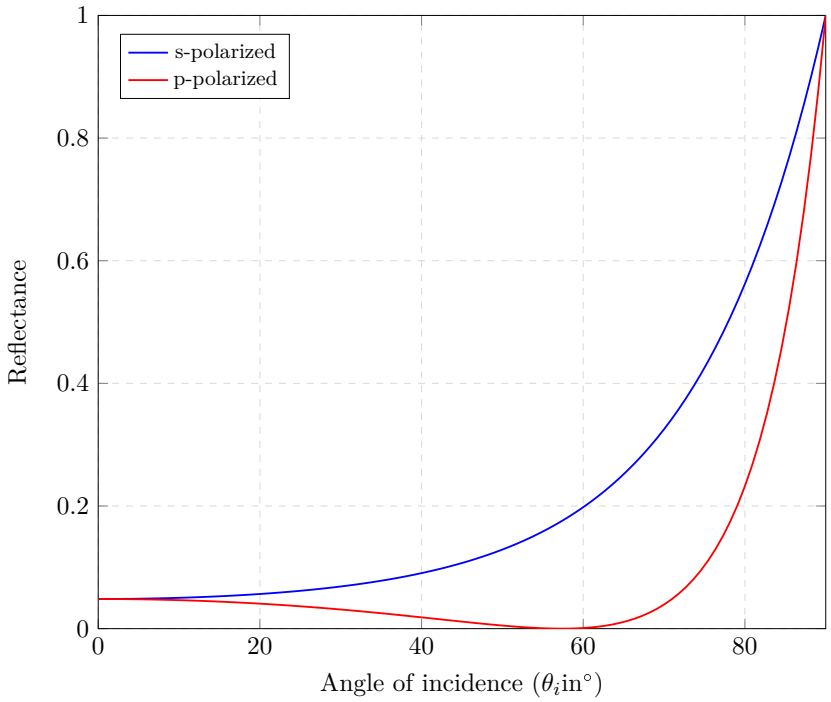

Figure 5.20.: Reflectance at the air/photoresist interface for the 2PP laser.

In order to reduce the reflection at the air-photoresist interface, an immersion medium with a refractive index closely matching that of the photoresist was used. This is illustrated in Figure 5.21, which compares the amount of light reflected at the interface in air versus an immersion medium. As observed in Figure 5.21A, a significant portion of the incident light is reflected away when in presence of an air environment. However, Figure 5.21B shows that when using an immersion medium with a closely matching refractive index, the amount of reflected light is greatly reduced. This demonstrates the effectiveness of refractive index matching in reducing reflectance and improving the 2PP photolithography process.

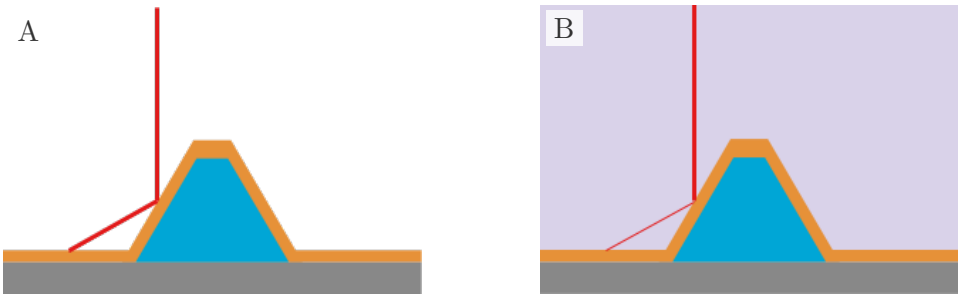

Figure 5.21.: Influence of the refractive index difference on the sidewall reflection: **(A)** High reflection at the air-resist interface. **(B)** Low reflection at the immersion media-resist interface.

Three immersion media were experimented with: glycerol (CAS 56-81-5), immersion oil (Im-

mersol 518 f, Carl Zeiss), and a hydrogel poly(ethylene glycol) diacrylate (PEGDA, CAS 26570-48-9).

Glycerol ($n = 1.4668$ for $\lambda = 780\,\text{nm}$) was initially discarded as a candidate immersion medium due to the formation of bubbles and cracks in the photoresist film during 2PP exposure, as shown in Figure 5.22. These issues could already be observed during the printing process, as shown in Figure 5.22A. The SEM images in Figure 5.22B revealed a damaged photoresist film, with pieces removed and other parts blistered.

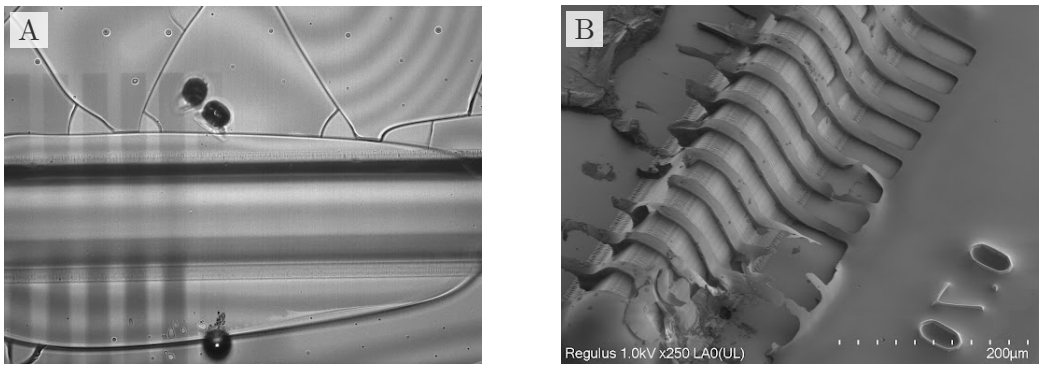

Figure 5.22.: Cracks develop in the photoresist film when exposing it via 2PP with glycerol as immersion media. **(A)** Internal camera view during 2PP exposure **(B)** SEM image after development. The bubbles and cracks made the photoresist film unusable.

The immersion oil *Immersol 518 f Carl Zeiss* had the best refractive index match to the photoresist, however, the oil dissolved the photoresist as shown in Figure 5.23A. The same result was found for PEGDA (see Figure 5.23B). As a result, these immersion media were not suitable for this application.

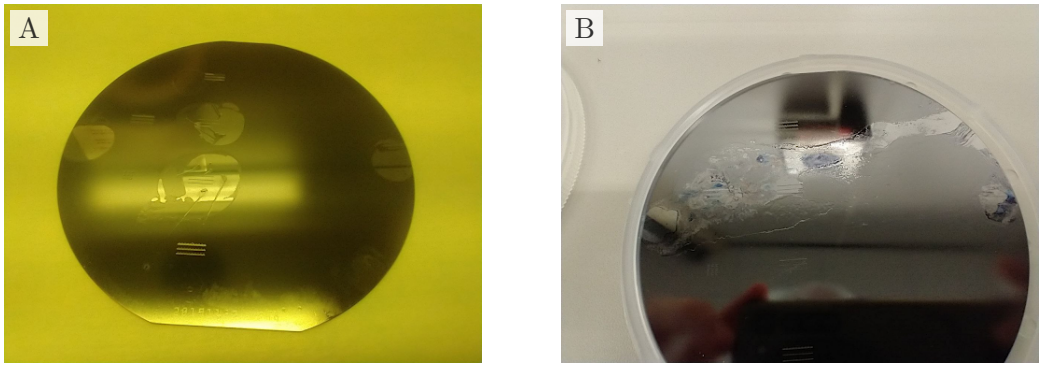

Figure 5.23.: Droplet tests on a AZ 12XT photoresist film: **(A)** Immersion oil Immersol 518 f dissolves photoresist. **(B)** PEGDA (Hydrogel) dissolves photoresist.

As no other appropriate immersion media were available, experiments continued with glycerol, which was the only one that did not dissolve the photoresist. Subsequently, more extensive dose tests were conducted and showed that it is feasible to transfer consistent patterns through 2PP on sidewalls with a slope angle of less than 60°. However, steeper angles demanded a higher dose of exposure, which caused an increase in the formation of bubbles and cracks in

the photoresist film. These bubbles disrupted correct exposure and resulted in pattern transfer errors. Further investigation is needed to fully understand the mechanism behind the formation of bubbles during the 2PP process, but it is believed to be a combination of multiple effects, such as outgassing of residual solvents in the photoresist and fast localized temperature peaks. Longer softbaking duration after spray-coating and immediate exposure afterwards reduced the bubble occurrence, but did not avert it completely.

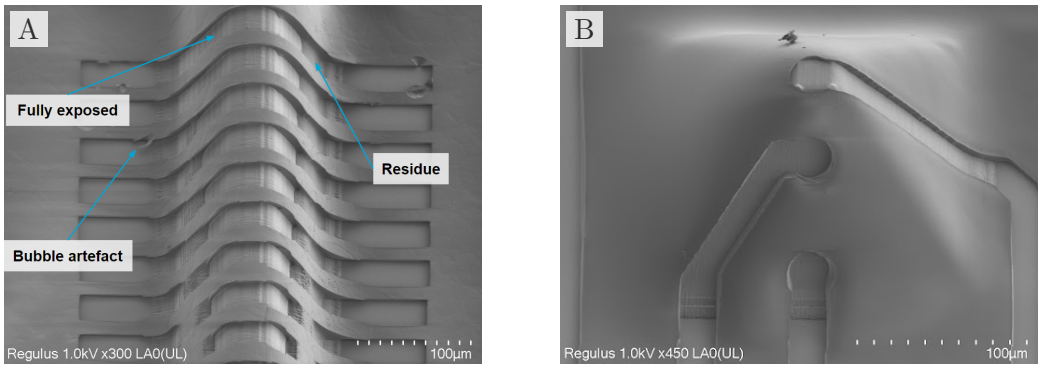

Figure 5.24.: Final 2PP exposure result with glycerol immersion media: **(A)** 60°/65°-prism with fully and partially exposed pattern. **(B)** Electrode pattern transfer on pyramid structure.

Figure 5.24 shows the results achieved with glycerol as immersion media. An electrode trace pattern on a 60°/65°-prism is depicted in Figure 5.24A, where the trace on the 60°-slope is fully exposed, however on a steeper slope of 65°, resist residues remain. Furthermore, artefacts due bubble formation could be identified. Despite the limitations, the successful transfer of a pyramid pattern on a 100 µm structure, as shown in Figure 5.24B, demonstrates the potential of 2PP for the fabrication of high aspect ratio structures in 3D-MEA applications. Following print parameters were used to archive these results.

- **Feature set:** 25x Objective - glycerol immersion mode
- **Scanning Speed:** $100\,\mathrm{mm\,s^{-1}}$
- **Laser Power:** 48
- **Power scaling:** 1.0
- **Slicing Distance:** 1.5 µm
- **Hatching Distance:** 0.25 µm
- **Interface position offset:** 1 µm

In conclusion, the development of the maskless photolithography via 2PP process was a challenging task, involving several obstacles such as base poisoning and interface effects, as well as reflection on slanted surfaces. One of the most significant challenges was the formation of bubbles and cracks when using glycerol as an immersion medium, which requires further investigation. The use of AZ 12XT photoresist may have contributed to these issues, and future research may explore the use of different photoresists to verify their chemical stability and reduce bubble and crack formation under 2PP exposure. However, it should be noted that the choice of AZ 12XT was made due to the availability of a pre-developed dilution and spray coating protocol, and a change in resist would require the development of a new process.

Despite these challenges, the maskless photolithography via 2PP process was successful in achieving repeatable pattern transfer on sidewalls with a slope of less than 60° and is therefore

suitable to fabricate 3D-MEAs. The use of an immersion medium with a refractive index matched to the photoresist was crucial in reducing reflectance at the air-photoresist interface. While glycerol was found to be the most suitable immersion medium, further research is needed to address the issues of bubble and crack formation. Additionally, future work may also explore the use of different photoresists to further optimize the process and improve the overall results. Overall, the maskless photolithography via 2PP process has the potential to contribute to the field of microfabrication, providing a cost-effective, flexible and efficient method for pattern transfer on high-aspect ratio structures.

5.7. 3D microelectrode array fabrication via two-photon polymerization

An overview of the two-photon polymerization-based process flow for the 3D-MEA was given in Section 5.4. Here, the details and challenges about relevant fabrication steps will be discussed.

5.7.1. Substrate preparation

Substrate preparation is an essential step in the fabrication of the 3D-MEA. The process starts by cleaning the silicon wafer with acetone and iso-propanol (IPA) to remove any contaminants. This is followed by plasma activation, where the wafer is exposed to oxygen plasma for 15 minutes. The activation diminishes over time, hence the wafer is immediately put into a silanisation solution. Silanization is a process that makes the substrate surface hydrophobic and leads to a chemical bond between the polymerized 2PP resin and the substrate. The silanization solution recommended by *Nanoscribe* is ethanol mixed with 0.5 vol% MAPTMS ([54]), but it was found that this concentration failed to provide enough adhesion for the 3D-MEA fabrication. A higher concentration of ethanol mixed with 10 vol% MAPTMS was used as it was found to be effective in the later stage of the experimental phase of this project. Finally, droplets of IP-Q resin were deposited at locations where the structures were going to be printed. Figure 5.25 shows the droplets placed at 12 dice locations for 3D-MEA fabrication. A 3D printed template was used to aid with locating the droplets.

5.7.2. Structure fabrication

The structural part of the 3D-MEA is made of 15 polymeric pyramids arranged in a 3 by 5 array (Step 7, Section 5.4). These were fabricated with the large feature set (10x objective) and IP-Q resin form *Nanoscribe*. The automatic interface position finder is executed before the fabrication of each pyramid, afterwards the thee stage is moved (400 µm) to the next pyramid location. Experiments have been conducted with pyramids with varying height, while the footprint of 200 mm × 200 mm and a truncated top of 30 mm × 30 mm remained unchanged. Table. 5.2 gives an overview of the simulated fabrication time, derived by using the DeScribe software, of these structures.

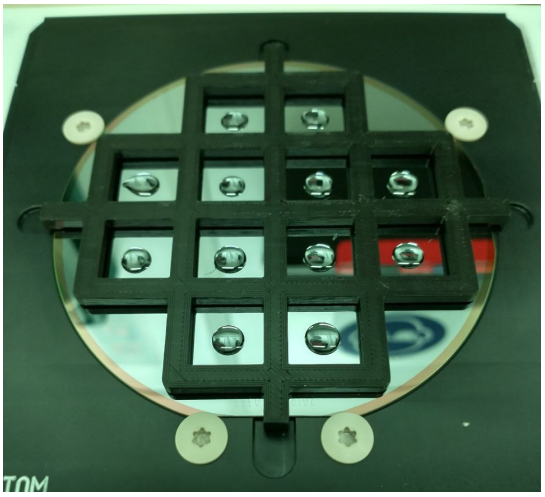

Figure 5.25.: Deposited photoresin droplets on a wafer with the aid of a locating template

Table 5.2.: Fabrication time [hh:ss] of various structures

	Pyramid height in µm			
	100	150	200	250
Pyramid	00:22	00:36	00:48	01:00
Pyramid array	06:39	09:57	12:58	16:02

Fabrication parameters

To optimize the process parameters for the IP-Q structures, a series of parameter tests were conducted. Pyramid structures were arranged in an array and a single process parameter was varied for each dimension of the array. Two examples of these parameter sweeps are illustrated in Figure 5.26. Figure 5.26A shows a large array in which the laser scanning speed was varied along the x-axis and the laser power was varied along the y-axis. In Figure 5.26B, the effects of varying slicing thickness (1 µm, 2 µm and 5 µm) and hatching distance (0.5 µm and 1 µm) were investigated. These tests were repeated for multiple laser scanning and laser power settings. It is worth noting that a printed pedestal structure was placed underneath the pyramids to decouple interface or delamination effects from the test results. The results were first qualitatively evaluated using a scanning electron microscope (SEM) to assess adhesion, feature reproduction, and surface quality. Finally, distance measurements were taken to monitor structure shrinkage.

Table. 5.3 shows the final process parameters to fabricate the the IP-Q based pyramids. A measurement (see Appendix D) of the pyramid's footprint (200 µm × 200 µm), showed that the actual values are (194.5 ± 1.9) µm in the x-direction and (194.8 ± 1.4) µm in the y-direction. This shrinkage of $\approx 3\,\%$ is due to shrinkage of the polymer. The first three layers of the structure are have a reduced exposure dose to improve adhesion (Base layer).

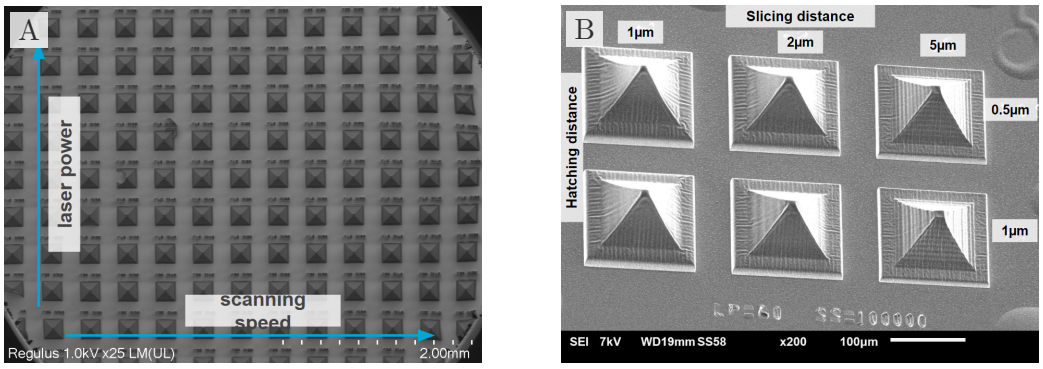

Figure 5.26.: P-Q process parameter sweeps: **(A)** Large dose test array. **(B)** Pyramids on pedestal with varying slicing and hatching distance.

Table 5.3.: Process parameter IP-Q

Large feature set: 10x Objective NA 0.3								
Distance			Laser Power	Power scale	Scanning speed	Base layer		
Slicing	Hatching	Interface				Count	Laser Power	Scanning Speed
[µm]	[µm]	[µm]	[%]	[-]	[mm s^{-1}]	[-]	[%]	[mm s^{-1}]
2	0.5	2	68[1]	1.0	100	3	68[1]	80

[1] ≙ 34 mW

Substrate adhesion throughout the fabrication process

During the fabrication of the polymeric structures of the 3D-MEA, an error pattern known as delamination was observed. This occurs when the structures detach from the substrate, as shown in the examples depicted in Figure 5.27.

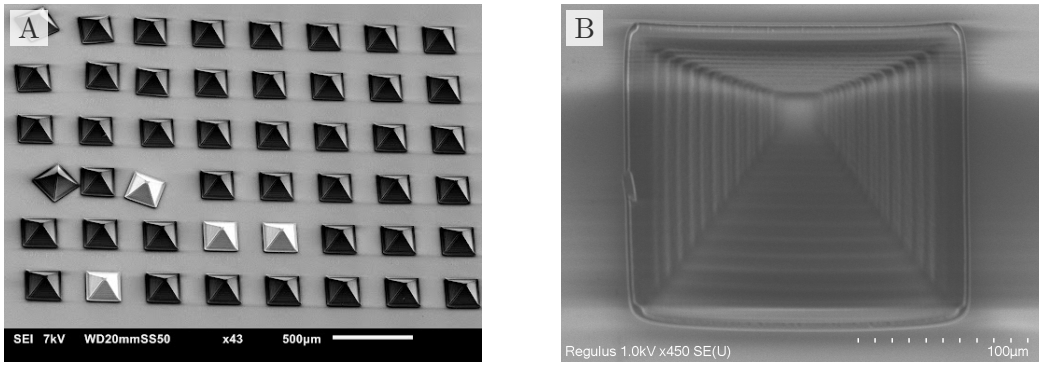

Figure 5.27.: Delamination of printed IP-Q structures: **(A)** Pyramid structures after a dose test, **(B)** Bulged up corners of a pyramid after 10 min in a 120 °C environment.

The polymerization dose has a strong influence on delamination behaviour, as shown in Figure 5.27A. This phenomenon was attributed to shrinkage of the polymerized structures,

which resulted in high stress at the structure-substrate interface. Thus, it is important to carefully control the fabrication parameters to prevent delamination.

Another factor that contribute to delamination is temperature exposure. During the fabrication process, structures with bulged up corners were noticed after the 3D-MEA went through multiple process steps. As illustrated in Figure 5.27B, exposure to a high temperature of 120 °C for 10 min resulted in deformation of the pyramid structure. It is hypothesized that this is due to temperature-induced cross-linking, which causes the polymer to shrink. [54]. Furthermore, the mismatch of the thermal expansion coefficient of the silicon substrate and the polymer structures may play a role in the delamination. Details are discussed in Section 5.7.4. To mitigate this issue, efforts were made to reduce temperature exposure as much as possible throughout the fabrication process.

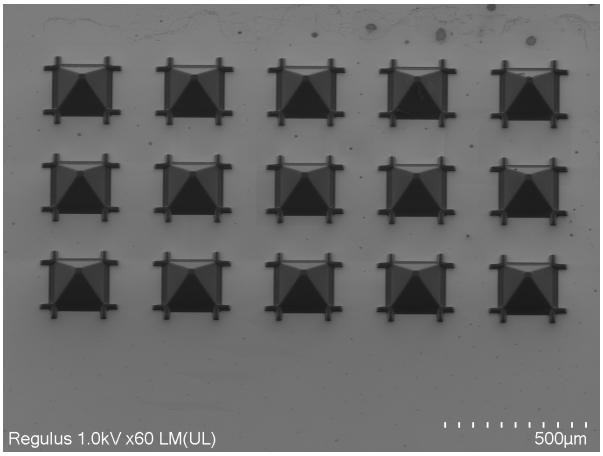

Figure 5.28.: Array with finned pyramids to reduce warping of structures.

To address the issue of delamination, design features were added to the structures to reduce warping. An example of this can be seen in Figure 5.28, where fins were added to the corners of the pyramid's footprint to prevent the edges from bulging up. This design variation was effective in preventing delamination. However, it did come with the downside of restricting the space between pyramids, which is needed for routing the electrode traces. In the final design, these features were omitted as the improved substrate preparation protocol (see Section 5.7.1) sufficiently prevented delamination.

In conclusion, delamination of the fabricated structures was an occasional issue that was encountered during the fabrication process of the 3D-MEA. The causes of delamination were found to be related to the polymerization dose, shrinkage and temperature exposure. To prevent delamination, the correct fabrication parameters were identified and implemented, and design features were added to reduce warping of structures. Additionally, improvements in the substrate preparation protocol were made to prevent delamination from occurring. It is worth noting that the delamination issue can have a significant impact on the overall yield of the 3D-MEA fabrication process. Therefore, further research is required to optimize the fabrication parameters and identify possible solutions to prevent delamination from occurring.

5.7.3. Electrode pattern transfer

High aspect ratio structure coating

In step 9 of the process flow (Section 5.4), a spray coating process was employed to cover the polymeric structures with photoresist in order to fabricate electrodes on them. However, it was observed that the thickness of the deposited thin film varied on the sidewalls. As depicted in Figure 5.29A, two adjacent pyramids of a 3D-MEA feature an inhomogeneous thickness of the photoresist film. The left pyramid (Figure 5.29B) has a much thicker ($\approx 6\,\mu m$)) photoresist film on its left sidewall compared to the right pyramid's (Figure 5.29C) right sidewall ($\approx 3\,\mu m$)). The reason for this inhomogeneous distribution has not been investigated yet, however, it is believed to be caused by the rotational forces acting on the still liquid film during the deposition process.

So far, this has not been a significant issue, since the 2PP-based lithography method does not rely on conformal coated photoresist films, unlike conventional mask-based methods. However, this might become an issue with coating taller or more complex structures as holes could occur in the film. Furthermore, an inhomogeneous photoresist film implies inhomogeneous development of the exposed regions, leading to discrepancies in the final patterned layer. Therefore, the developer solution dissolves unexposed areas of the photoresist (dark erosion) and distorts the final patterned layer.

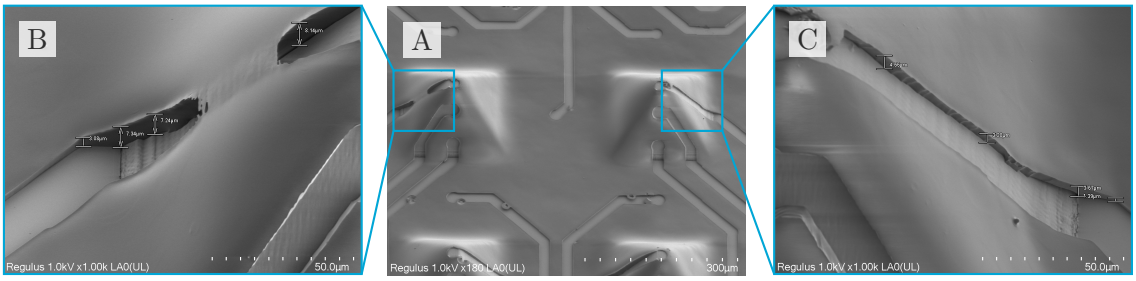

Figure 5.29.: (A) Inhomogeneous photoresist thickness on adjacent pyramid structures (35° tilted view).
(B) Close-up: Thick photoresist film **(C)** Close-up: Thin photoresist film

Fabrication parameters

The challenges to determine the process parameters for exposing the AZ 12XT photoresist with the 2PP system has been discussed in Section 5.6. Figure 5.30 shows the successful pattern transfer of electrode traces into the photoresist. An overview of the 3D-MEA is shown in Figure 5.30A, with a close up of a pyramid with four electrodes given in Figure 5.30B.

As previously discussed in Section 5.1, the 3D-MEA design involved splitting the 3D model of the electrode pattern into two parts: the planar electrode traces on the substrate and 3D traces on the pyramid structure. This was beneficial due to the different process conditions. The planar substrate has a high refractive index and therefore reflects the incident beam, leading to an increased light dose inside the photoresist. On the other hand, the sidewalls of the pyramid reflect the incident beam at the photoresist-interface, leading to a decreased light dose inside the resist. Therefore, different exposure doses were required.

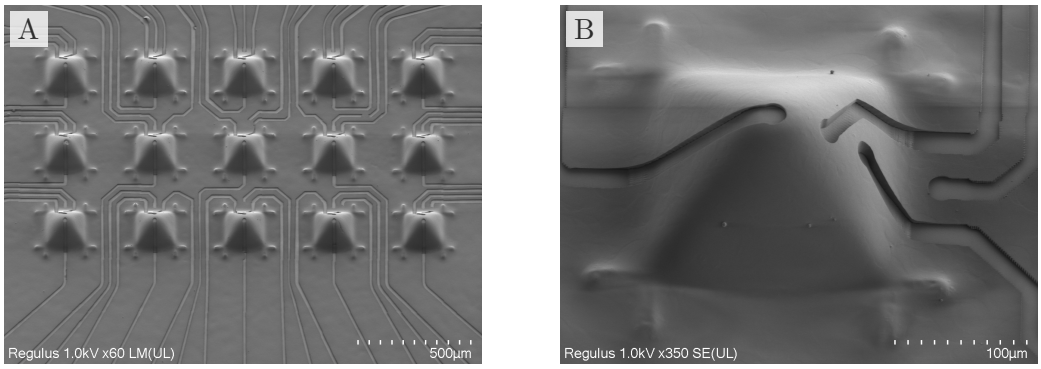

Figure 5.30.: Exposed electrode pattern in the photoresist: **(A)** Pattern transferred on the pyramid array.
(B) Four electrode pattern transfered on a pyramid.

Furthermore, the 3D electrode pattern required a higher printing resolution to correctly transfer them into the resist. However, higher printing resolution resulted in increased fabrication time as the slicing and hatching distances of the digital model had to be decreased. The advantage of splitting the electrode pattern into two parts also allows for faster printing of the planar parts with coarse resolution. However, the necessary process development became more complex as process parameters had to be determined for both printing cases and the print job-file had to be adapted accordingly.

Table. 5.4 summarizes the process parameters for the sidewall and substrate process conditions. The laser power for the substrate is lower than for the sidewalls, even though the slicing and hatching distance was increased. For further work it is recommended to resolve interface reflection, by using a less reflective substrate, e.g a glass wafer or a polymer film ($\approx 100\,\mu m$) on top of a silicon wafer. This would make the process development easier since less effects have to be considered.

Table 5.4.: 2PP process parameter AZ 12XT with glycerol immersion

Medium feature set: 25x Objective NA 0.8 with glycerol immersion									
	Distance			Laser Power	Power scale	Scan-ning speed	Base layer		
	Slicing	Hatching	Interface				Count	Laser Power	Scanning Speed
	[µm]	[µm]	[µm]	[%]	[-]	[mm s^{-1}]	[-]	[%]	[mm s^{-1}]
Sidewalls	1.5	0.25	1	48[1]	1.0	100	0	-	-
Substrate	2	0.75	1	44[2]	1.0	100	0	-	-

[1] ≙ 24 mW
[2] ≙ 22 mW

Resist development and failure modes

The most prominent issues encountered during the patterning of the positive photoresist AZ 12XT via 2PP over sidewalls with glycerol immersion are illustrated in Figure 5.31. Despite

extensive process development, the occurrence of microbubbles during the exposure process could not be completely prevented (Figure 5.31A). As a result, the photoresist underneath the bubble is not fully exposed, which in the worst case can disconnect the electrode trace, as can be observed in Figure 5.31B. Further process development is needed to mitigate these effects. However, given the other challenges faced with the used photoresist, it might be more beneficial to switch to a more suitable resist before instead.

Another issue encountered during the process development was over-development of the exposed resist, which occasionally led to dark erosion and delamination of resist parts. This was especially evident when varying the exposure dose to limit the microbubble formation, as it influenced the required development time. The best practice was to repeatedly develop the wafer for only 30 s and inspect the results after drying under the optical microscope. To limit delamination, the minimal width of resist structures may be increased to provide more adhesion surface.

In some instances, if the automatic interface finder fails to determine the substrate interface position, the electrode pattern is sometimes exposed in mid-air (see Figure 5.31A). As a result, it is not transferred into the photoresist, and parts of the electrode traces are missing. The *Nanoscribe* system offers parameters to change the sensitivity of the algorithm, which could be investigated to mitigate this error.

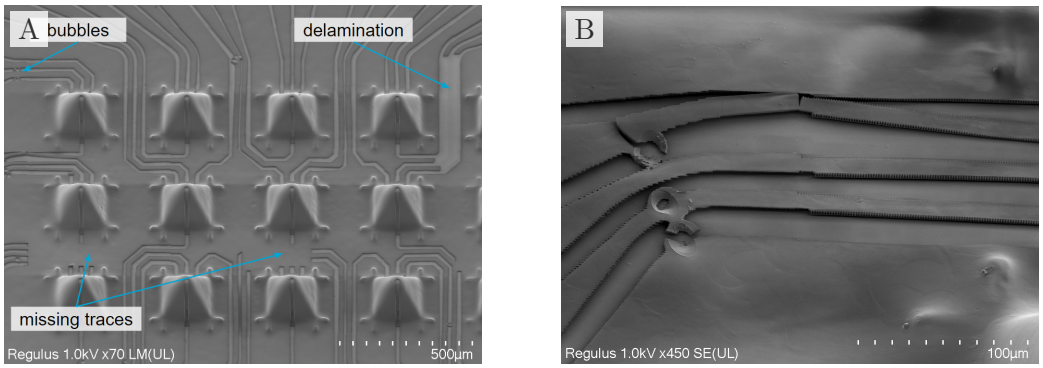

Figure 5.31.: Failure modes of 2PP maskless lithography with glycerol immersion: **(A)** 3D-MEA electrode pattern with microbubbles, delamination, and missing traces. **(B)** Close-up of the effects of microbubbles and delamination.

5.7.4. Electrode metallization

In this project, a lift-off process was employed to fabricate the electrodes (Step 10 and 11 in the process flow 5.4). The process involves the use photoresist as a sacrificial layer, which is applied over the substrate and patterned using photolithography techniques. The patterned photoresist film serves as a mask for the next step, in which a conductive layer is deposited on top of it. In the final step, the photoresist is removed by dissolving it in a solvent such as acetone, while the deposited material remains only on the exposed regions of the substrate. However, during the deposition process, material may cover the sidewalls of the photoresist, leading to challenges in the lift-off process. If the sacrificial layer is completely covered by material, the resist stripping solvent cannot dissolve it, resulting in unwanted material residues remaining on the substrate. The schematics of the process are illustrated here bellow.

Lift-off process

1) 2PP maskless lithography:
Pattern is exposed into positive photoresist which serves as a sacrificial layer

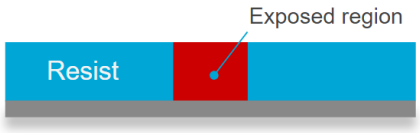

2) Development:
Exposed regions are dissolved in a developer solution.

3) Deposition:
Conductive electrode material is deposited on the sacrificial layer. Sidewalls may be covered by material.

4) Lift-off:
Remaining resist (sacrificial layer) removed, unwanted material may remain due to sidewall coverage.

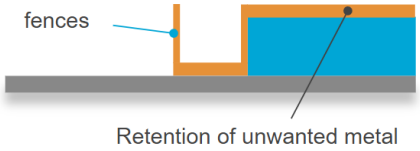

As illustrated, the sidewall coverage of material is a major issue for a successful lift-off process. To mitigate this issue, either deposition methods with low step coverage, such as evaporation, need to be used or the photoresist sidewalls need to be have negative slopes (undercut).

In this project, a method was proposed to improve the lift-off process by utilizing the design freedom of the 2PP-based maskless lithography process. Specifically, an undercut feature was added to the cross-section of the resist electrode pattern, which creates a shadowing effect and reduces sidewall deposition. This improved lift-off process is schematically illustrated in the following figures.

Lift-off process with improved cross-section

1) 2PP maskless lithography:
2PP enables exposure of undercuts, which are designed via CAD

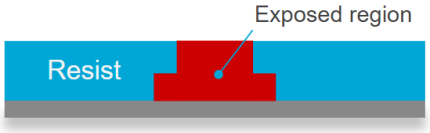

2) Development:
Exposed regions are dissolved in a developer solution.

3) Deposition:
Undercuts create shadow effect and mitigate sidewall deposition.

4) Lift-off:
Remaining resist removed, solvent can access sacrificial layer.

Implementation

In Figure 5.32, the implementation of this feature is shown. Figure 5.32A depicts the 3D model where the yellow electrode pattern with an undercut cross-section is covering the blue pyramid structure. This is the structure which will be exposed into the positive-tone photoresist, hence, it will be dissolved in the developer solution. An SEM image of the resulting resist pattern is shown in Figure 5.32B. The imaging was made at a 30° angle, however, the sidewall is not visible. On a side note, the saw tooth pattern in the resist is a result of the laser-based exposure, with each tooth being a voxel. While a higher dose would increase the voxel size and smoothen out the resist contour, the formation of microbubbles would be increased as well.

While the undercut feature can be successfully transferred into the planar photoresist films, initial attempts failed to achieve the same results on the pyramid sidewalls. It is hypothesized that this was due to the varying resist thickness. Additionally the actual pyramid dimensions might be different than the assumed dimensions in the digital model caused by shrinkage of the polymer. Therefore, a thicker photoresist film and an optimized shrinkage compensation in the digital model are needed to transfer the complete electrode pattern with the undercut feature.

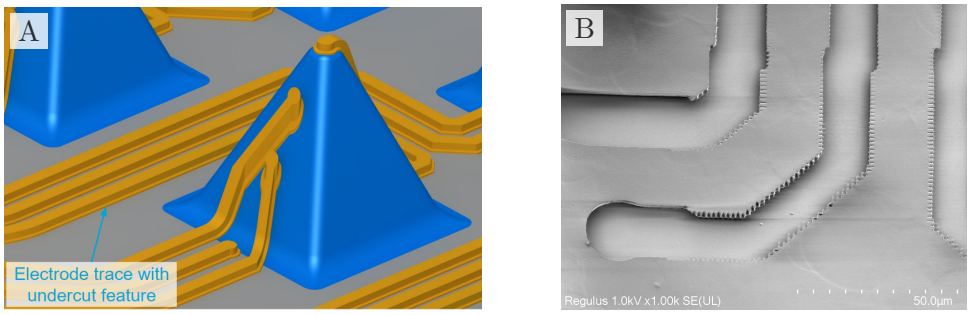

Figure 5.32.: Implementation of the undercut feature: **(A)** CAD-model of the pyramid structure with the electrode pattern enhanced with undercuts. **(B)** No sidewall visible in the exposed resist (30° tilted view).

Lift-Off: sputtered titanium nitride

The first lift-off attempts were conducted with sputtered titanium nitride (100 nm). The results show the successful fabrication of titanium nitride electrodes on top of polymeric pyramid structures, as shown in Figure 5.33A. However, the first lift-off process was conducted in an ultrasonic cleaner, which caused some of the structures to delaminate from the substrate

(see Figure 5.33B). Subsequent lift-off steps were conducted with acetone without ultrasound assistance. Additionally, parts of the electrode perimeter were covered with fences due to sidewall deposition, and titanium nitride flakes adhered to the substrate.

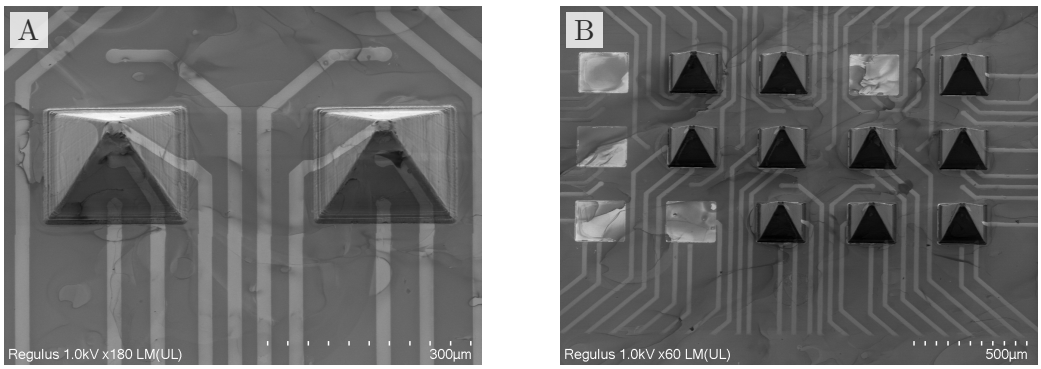

Figure 5.33.: Lift-off results of sputtered titanium nitride electrodes: **(A)** Patterned pyramids. **(B)** Pyramid structures delaminated due to the lift-off process.

Additionally, during the printing of IP-Q based insulation on top of the titanium nitride electrodes, microbubbles were observed, as shown in Figure 5.34. When printing on a silicon substrate (with a 200 nm SiO_2 layer), the IP-Q resin is polymerized properly. However, as soon as the interface changes to TiN, the resin is not polymerized due to microbubbles. It is believed that TiN absorbs the incoming light from the 2PP printer, resulting in local temperature peaks which cause microbubbles due to evaporation of chemicals in the photoresin.

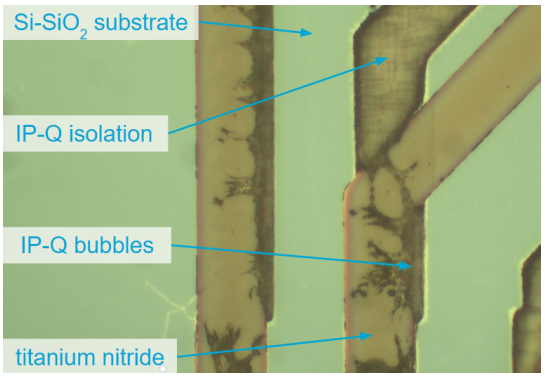

Figure 5.34.: IP-Q insulation printed on top of TiN electrodes.

These challenges encountered during the lift-off and subsequent insulation print led to the decision to abandon the use of TiN as an electrode material. Instead, experiments with indium tin oxide (ITO) and gold were conducted.

Lift-Off: sputtered indium tin oxide (ITO)

Indium tin oxide (ITO) was selected as a possible electrode material for the 3D-MEA due to its high conductivity, transparency, and biocompatibility. A layer of 100 nm of ITO was sputtered at room temperature on top of the patterned photoresist film. However, the results of the lift-off process, as shown in Figure 5.35, were not satisfactory. The lift-off process was

hindered due to strong sidewall coverage from the ITO sputter process. This resulted in material being deposited on the sidewalls of the photoresist pattern, making it inaccessible to the resist stripping solvent. As a result, unwanted material residues were left on the substrate. As shown in Figure 5.35A, large areas of the ITO film were not removed, resulting in short circuits between distinct electrodes thus making rendering the 3D-MEA unusable. Figure 5.35B shows a close-up of a pyramid with four ITO electrodes, where the fallen over fences stemming from the sidewall deposition can be clearly seen.

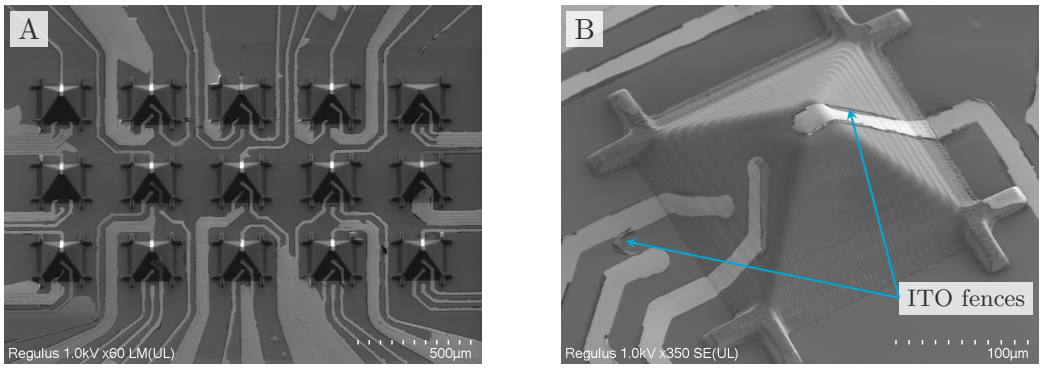

Figure 5.35.: Lift-off results of sputtered ITO electrodes: **(A)** Patterned 3D-MEA-structures. **(B)** Close-up of patterned pyramid.

The limiting issue of the lift-off process due to the sidewall coverage made the use of ITO for the current version of the 3D-MEA not feasible. However, future work might employ an improved undercut feature in the photoresist to mitigate sidewall deposition. A transparent 3D-MEA would enable optical monitoring of the cells grown on the chip, making ITO an ideal electrode material for this application. Therefore, it is recommended to explore other ways of patterning ITO, such as the use of diluted halogen acid HCl or oxalic acid for wet etching, as reported in the literature [66, 67]. These pathways might be worthwhile to explore to enable a fully transparent 3D-MEA.

Lift-Off: evaporated gold

The final electrode material that was used in this project was gold, which was deposited via electron beam evaporation. This process has limited step coverage, making it more suitable for the lift-off process. To improve adhesion, a 10 nm titanium layer was evaporated before switching the material to gold and depositing a 100 nmthick layer. The results of this process can be observed in Figure 5.36, where the 3D-MEA with gold electrodes is shown in Figure 5.36A and a close-up of a pyramid structure is shown in Figure 5.36B.

The evaporation deposition process proved to be the most suitable method for depositing the gold electrodes in combination with the lift-off process. This is due to the directionality and hence limited step coverage of the evaporation process, which prevented unwanted material from covering the sidewalls of the photoresist during the lift-off process.

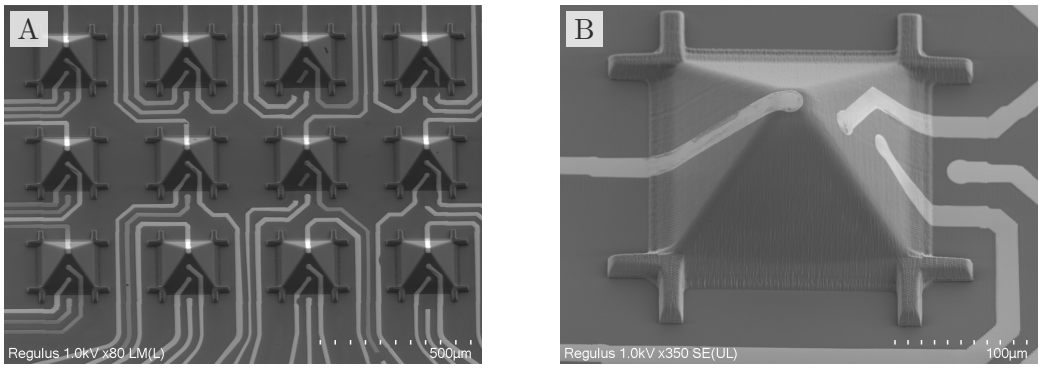

Figure 5.36.: Lift-off results of evaporated gold electrodes: **(A)** Patterned 3D-MEA-structures. **(B)** Close-up of patterned pyramid.

Removal of the protective SiO_2 layer

The following step was to remove the protective SiO_2 layer (Step 11 in the process flow 5.4), which was deposited to mitigate base poisoning of the chemically amplified photoresist (see Section 5.6.1). This was performed to uncover the polymeric (IP-Q) pyramid structures. Since the following step was to fabricate the insulation of the electrodes with the 2PP method and the same material as the pyramids, it was anticipated that this would provide a better adhesion between these structures.

The wafer was immersed for 20 s into buffered hydrofluoric acid (BHF) to remove the SiO_2 layer. An image of the pyramid with four electrodes is illustrated in Figure 5.37A. As indicated by the arrows and shown in the close-up image Figure 5.37B, cracks developed at the interface between IP-Q pyramid and silicon substrate.

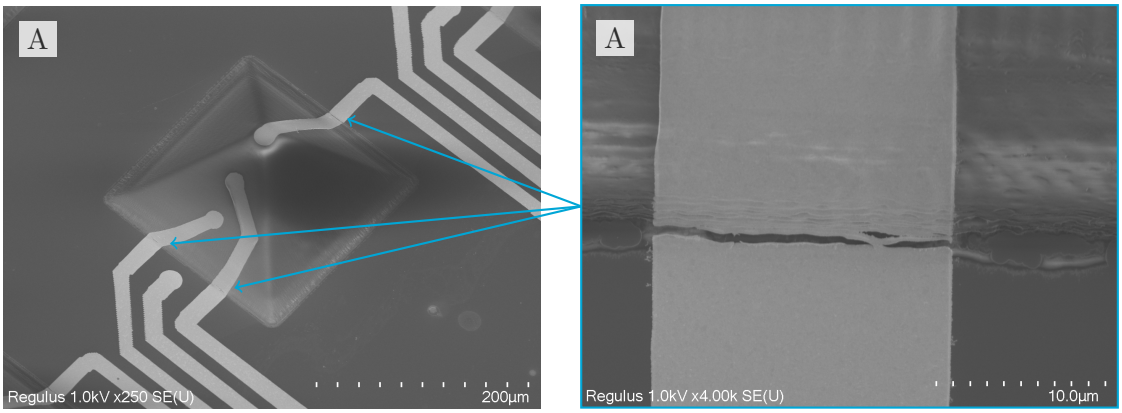

Figure 5.37.: Gold electrodes after removal of SiO_2 protective layer: **(A)** Pyramid with gold electrodes. **(B)** Close-up: Cracks in gold layer at the IP-Q-substrate interface.

The interface at the bottom of the pyramid structures proofed to be the source of failure modes throughout the process chain. The thermal expansion coefficient of IP-Q has not been reported yet, but based on the coefficient for IP-Dip, an acrylate based 2PP resin, it can be assumed that IP-Q has a similar coefficient of $8.0 \pm 0.4 \times 10^{-6}\,\mathrm{K}^{-1}$.[68]. However, the thermal expansion coefficient of silicon is significantly different, measuring at $2.45 \pm 0.04 \times 10^{-6}\,\mathrm{K}^{-1}$.[69].

These difference caused thermal stresses during the various fabrication steps, which resulted in occasional delamination of the structure or formation of cracks in the protective SiO_2 layer or gold electrode layer. Future work on the 3D-MEA should focus on resolving this issue. One solution could be to fabricate the 3D-MEA on a polymeric layer with similar thermal expansion properties. A suitable option could be polymethylmethacrylat (PMMA, CAS 9011-14-7) given IP-Q's methacrylate nature or polydimethylsiloxan (PDMS, CAS 63148-62-9) due to its low Young's modulus and and its ability to mimic the mechanical properties of biological tissues.

5.7.5. Insulation fabrication

The final step (12 of the protocol in Section 5.4) of the 3D-MEA fabrication involves insulating the electrode traces by printing a layer of IP-Q on top of them. The best results of this process can be seen in figure Figure 5.38A, which provides an overview of the 3D-MEA. However, it is observed that most of the electrode traces on the pyramids are not covered with the insulation material. This can be seen in the close-up image of a pyramid with a successfully printed insulation in Figure 5.38B.

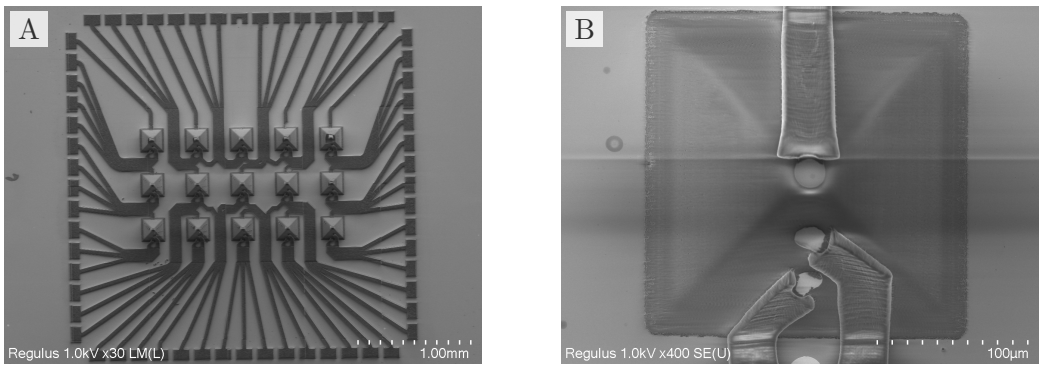

Figure 5.38.: Isolation printed on the electrode traces of the 3D-MEA.: **(A)** 3D-MEA with partially printed insulation. **(B)** Polymeric pyramid with gold electrodes and polymeric insulation.

Printing IP-Q on gold

An issue encountered during the fabrication of the 3D-MEA insulation was the uneven polymerization of the IP-Q layer on the gold and silicon interfaces. This was highlighted in a dose test (Figure 5.39A), where it was observed that the effective light dose changes at the interface, leading to varying polymerization rates. As shown in Figure 5.39B, the IP-Q layer is thicker on the gold interface compared to the silicon interface, despite using constant process parameters. This difference in polymerization rates caused warping due to different shrinkage rates in the structures, leading to delamination (Figure 5.39C). This phenomenon highlights again the importance of interface effects in 2PP-based polymerization processes.

To address the issue of interface effects during IP-Q polymerization with 2PP, a groove was implemented along the insulation structure. This design allows for printing to occur only on the silicon substrate, avoiding close proximity to the gold interface. The groove acts as a bridge above the gold interface, as can be seen in Figure 5.40.

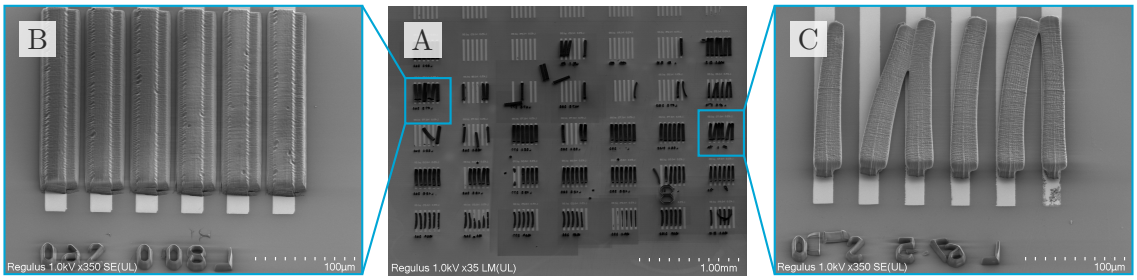

Figure 5.39.: (A) Dose test on gold and silicon (+ 200 nm SiO_2) interface results in inhomogeneous polymerization. **(B)** Thicker IP-Q on gold compared to Si/SiO_2-interface. **(A)** Stress due to different polymerization grade leads to warping.

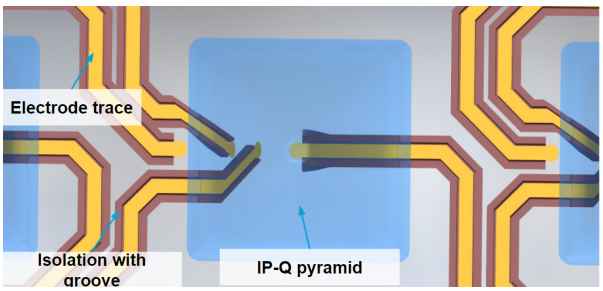

Figure 5.40.: Isolation groove to avoid printing on the gold interface. The 3D-MEA is shown from the backside.

Fabrication parameters

To ensure the successful fabrication of the insulation layer, the same process parameters were used as for the pyramid structure. These parameters are detailed in Table. 5.3. Despite the surface activation protocol, which included a 30 s oxygen plasma treatment (100 W, 5-6 sccm O_2) and 2 h immersion in an ethanol-MAPTMS solution (10 vol%), delamination and warping issues were still observed. These issues were particularly prevalent on the sidewalls of the

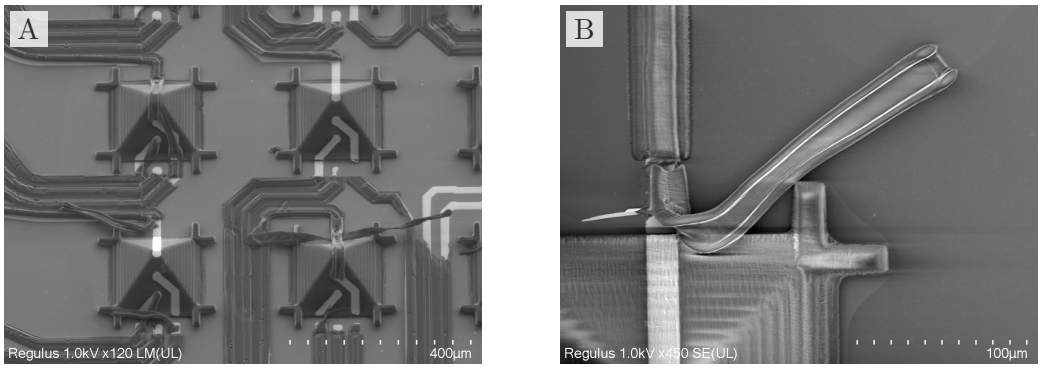

Figure 5.41.: Delamination issues of the fabricated electrode insulation: **(A)** 3D-MEA with delaminated insulation. **(B)** Close-up of a warped insulation structure with groove.

pyramids, as shown in Figure 5.41A. This suggests a similar reflection effect as encountered during the maskless photolithography process (Section 5.6). A close-up image of a warped

insulation structure (Figure 5.41B) shows the designed groove pattern intended to prevent printing on the gold interface. It is therefore necessary to further work on this issue and develop new process parameters. However, due to time constraints, it was not further investigated and will be a focus of future research.

In summary, the 12 arrays of polymeric structures were successfully fabricated via 2PP on the wafer. The spraycoated photoresist was exposed with the elctrode pattern in the second 2PP-based fabrication step. The developed alignment routine enabled to precisely and repeatedly position the 2PP structures a on a wafer level. Gold electrodes were fabricated via lift-off process onto the pyramid structures. However, two main challenges remain work for future work: cracks occurred at the substrate interface and the insulation structures is not adhering properly to the sidewalls of the pyramid structures.

In conclusion, the 12 arrays of polymeric structures were successfully fabricated on a wafer using 2PP. A precise alignment routine was developed, which enabled the accurate and repeatable positioning of the 2PP structures on the wafer level. The spray-coated photoresist was exposed with the electrode pattern in the second step of the 2PP-based fabrication process. Gold electrodes were then fabricated onto the pyramid structures through a lift-off process. However, two challenges still need to be addressed in future work: cracks formed at the substrate interface, and the insulation structures are not properly adhering to the sidewalls of the pyramid structures.

6. Conclusions and Future recommendations

The goal of this thesis was to develop a polymeric 3D-multi-electrode array (3D-MEA) that employed a combination of two-photon polymerization (2PP), a 3D printing technology with sub-micrometer resolution, and standard microfabrication methods from the semiconductor industry to overcome the limitations of current 3D-MEA devices.

Two fabrication protocols for polymeric 3D-MEAs were developed. The initial approach was to combine 2PP with high aspect ratio photolithography, however, this process flow proved too complex due to constraints from harsh process environments and contamination risks of microfabrication tools. Therefore, a novel hybrid fabrication process was developed which uses standard wafer-level microfabrication processes to fabricate a plattform (front-end process) which can be utilized by the 2PP-based process (back-end) to fabricate the polymeric structures, pattern the microelectrodes, and provide insulation, resulting in an aligned multi-step 2PP process.

The 2PP-based process flow was chosen as it enables the fabrication of higher and more complex structures for 3D-MEA compared to the initial mask-based process (method 1 in Section 5.3), which is limited by the diffraction occurring in the gap between structures and mask of the proximity aligner (Section 4.2.2). Therefore, higher structures with electrodes enable the electrical characterization of thicker 3D neuronal cultures. Additionally, 2PP-based process flow the requires only one spray coating step with minimal requirements for film conformity. Furthermore, a wafer level alignment routine was developed with repeatability alignment of 2PP structures of $\pm 5\,\mu m$, which enabled the multi-step 2PP fabrication process. A maskless photolithography via 2PP process was also developed to pattern high aspect ratio structures, utilizing AZ12XT photoresist with glycerol immersion. However, several challenges had to be solved, including base poisoning, interface effects, and reflection on slanted surfaces.

The fabricated 3D-MEA consisted of 15 printed (IP-Q) pyramids occupying an area of $1.8\,mm^2$, featuring 60 gold electrodes. Each pyramid had four electrodes at different heights, with the best fabrication results obtained using gold as the electrode material, as the deposition process was the most compatible one with the used lift-off method. The insulation of the traces was partially successful and requires further process development. Due to time limitations, no solution to the issue of cracks in gold electrodes caused by the transition between the hard silicon substrate and soft polymeric structure (IP-Q) could be implemented. Therefore, no electrical characterization or cell culturing were performed on the 3D-MEA.

The work was carried out in three different cleanrooms at three faculties of Delft Technical University (TUD) (3me, EWI, TNW), providing access to a wide range of microfabrication machines. However, coordinating processes, training on tools, reserving tools, and dealing with tool downtime all presented challenges. The biggest challenges faced during the project were process development due to the constraints discussed, patterning the sidewalls with 2PP, and dealing with interface effects during the 2PP process development.

The results presented in this thesis demonstrate the feasibility of combining the 2PP process with standard microfabrication techniques to manufacture a 3D-MEA for *in vitro* cell studies of neurons. However, it also highlights the challenges and complexities that arise when merging these techniques, particularly in regards to contamination and harsh process environments. The 2PP-based solutions presented in this thesis offer a pathway for the development of more complex and biomimetic (softer) 3D-MEA. Additionally, it has been shown that 2PP can replace the high aspect ratio photolithography process, while providing even more flexibility and design freedom. Finally, the developed wafer level alignment routine and the 2PP-based maskless photolithography process for high aspect ratio structures contribute to the field of microfabrication and may enable the development of other microdevices.

Change of 2PP substrate

The use of a silicon substrate in the 2PP process led to several issues, including delamination of the printed polymeric structures and cracks in the electrode material at the transition between substrate and structure. To address these issues, it is recommended that the 3D-MEA be fabricated on a polymeric substrate with similar thermal and mechanical properties. A polymeric layer, such as PMMA or PDMS, can be spin casted on top of a silicon wafer. A film thickness of at least 100 µm would mitigate reflective interface effects and simplify future 2PP process development by aligning the properties of substrate and structure. Additionally, the use of a polymer substrate would provide better adhesion for the printed structures, a more biomimetic environment and potentially additional functions such as microfluidic delivery of nutrients or drugs at the electrode sites. One possible challenge may be determining the correct interface position of the polymer layer, but this can be addressed by detecting the highly reflective silicon wafer underneath and programming an offset in the 2PP print job accordingly.

Transparency of 3D-MEA

The transparency of the 3D-MEA is important for live cell imaging and other applications that require visual access to the cells. While the polymeric structures of the 3D-MEA are transparent, the silicon substrate is not. Future work could explore the use of glass wafers instead of silicon as a substrate. Alternatively, a process step can be added to open the wafer from the backside, or the 3D-MEA can be removed from the wafer after fabrication, if it is fabricated on a polymer film. This would enable better visual access to the cells and potentially improve the functionality of the 3D-MEA.

3D-MEA Design Improvements

In this thesis, a simple pyramid design with a height of 100 µm was utilized to demonstrate the feasibility of fabricating 3D-MEA using 2PP. However, there is potential to further improve the design of the 3D-MEA to better mimic the native neural environment.

One approach could be to utilize the multi-step 2PP process to add a fourth step after fabricating the structure, electrodes, and insulation. This step could involve printing nanopillars on the 3D-MEA using different materials. The use of nanopillars could better mimic the natural neural environment and provide a more realistic niche for *in vitro* studies.

Additionally, higher 3D-MEA designs could be developed. The 2PP-based maskless photolithography process for high aspect ratio structures allows for the patterning of sidewalls with slopes up to 60°. Therefore, pyramids with a footprint of 200 µm × 200 µm could potentially be up to 170 µm high. This would enable the fabrication of more complex and biomimetic structures, increasing the resolution of the measurements and providing a more realistic environment for *in vitro* studies.

Maskless photolithography via two-photon polymerization on high aspect ratio structures

One of the biggest challenges faced during the project was the development of the 2PP-based maskless photolithography for high aspect ratio structures. The main issues encountered were base poisoning, interface effects, and reflection at the photoresist interface of slanted surfaces, as well as the occurrence of microbubbles.

The reflections are a physical phenomenon and can only be reduced by matching the refractive index of the immersion media with the photoresist. However, the base poisoning and microbubbles are properties of the photoresist itself. Therefore, future research should focus on finding alternatives to the photoresist AZ 12XT, which is a chemically amplified resist (CAR). CARs have the tendency to cause base poisoning, and also require an additional heating step (PEB) which can damage the 3D-MEA through delamination or cracks in the electrode layer due to stresses.

When looking for photoresists, it is important to ensure that they do not produce microbubbles during 2PP exposure, and also have good chemical stability against immersion media. An example of a suitable alternative is the photoresist AZ-IPS 6090 which was used to fabricate molds via 2PP with the use of immersion oil (Immersol 518 f). [70]

Furthermore, it would be interesting to develop the process for negative resist. This would require to adapt the multi-step 2PP-based fabrication protocol for the 3D-MEA, since the lift-off process would require to expose large regions of negative photoresist via 2PP, which is not feasible due to the fabrication time. However, it would enable the etching of other materials, such as Indium Tin Oxide (ITO), which is transparent. ITO can be etched using diluted halogen acid (HCl) or oxalic acid for wet etching, as reported in the literature. [66, 67]. The use of transparent electrodes would be beneficial for the goal of fabricating transparent 3D-MEAs for live cell imaging.

7. Self-reflection

My thesis was a perfect combination of two of my interests: the fascinating high-tech field of micro- and nanofabrication, and the complexities of the brain. I was thrilled to embark on this 1.5-year-long journey of exploration and learning.

My introduction to the impressive world of microfabrication occurred in three different cleanrooms, where I had the opportunity to utilize an array of formidable high-tech equipment. Being a mechanical engineer, I had limited knowledge of cell biology and Organ-on-Chip (OoC) technologies. However, the few insights I gained during this thesis into these fields, for example the intricacies of cellular machinery were truly inspiring and eye-opening.

I was somewhat disappointed that I could not deliver the final 3D-multi-electrode array (3D-MEA) devices, to see the results of the cell culturing and electrical characterization of neuronal cells. Nevertheless, I take solace in the fact that this treat might be reserved for the next master student who has the privilege of pursuing this endeavour.

At the beginning of my thesis, I was overwhelmed by the multitude of new things I faced. I had limited prior knowledge of microfabrication tools or measurement equipment, how to use them, or the correct sequence for manufacturing a 3D-MEA device. The cleanroom environment was exciting but intimidating, with strict rules about safety, contamination, and material handling. Using expensive and sensitive high-tech equipment or hazardous chemicals, such as BHF, for the first time was sometimes nerve-racking. However, as the thesis progressed, I learned how to navigate these environments and became more confident in handling the various tools and chemicals. Moreover, I discovered that the cleanroom is a social environment, with engineers responsible for the tools (tool-owners) and colleagues working on their own projects. I realized that it was essential to know whom to approach when developing a new process or facing any issues. Therefore, I proactively approached various tool-owners in different cleanrooms to learn about the machines and processes that would fit my fabrication goals. This approach resulted in many fruitful conversations, helping me to solve numerous challenges that I encountered during the course of my research.

I am grateful for the opportunity and freedom that my supervisors provided, enabling me to explore my ideas and experiments. Without this support, the novel two-photon polymerization-based process flow that I developed would not exist. However, this freedom also meant that I occasionally focused on optimizing a particular process step, losing sight of the bigger picture of fabricating the 3D-MEAs. This perfectionism, coupled with the project's complexity and the pivot to the 2PP-based process flow, resulted in extending the length of my thesis. Additionally, tool downtimes and sicknesses added to the delays. Looking back, a more rigorous organization of my research and a well-structured time plan could have streamlined my efforts. I acknowledge that my time management and planning skills require improvement to achieve better results in future projects.

The strict cleanroom contamination protocols of the EKL cleanroom were a significant challenge,

particularly at the start of the thesis. The initial masked pattern transfer-based process flow had to be repeatedly iterated to comply with these stringent guidelines. At times, I felt overwhelmed and unsure of my direction, which was demotivating, tedious, and time-consuming. However, these challenges sparked my creativity and led me to develop the novel two-photon polymerization-based process flow.

Developing the process for maskless photolithography via two-photon polymerization on high aspect ratio structures presented an exciting challenge that required constant problem-solving. Just as I resolved one issue, a new obstacle emerged. For instance, the base poisoning of the resist hindered proper pattern transfer. Once I overcame this by implementing an intermediate layer, I encountered reflections on the sidewalls that limited the exposure dose. Using an immersion media helped to reduce the reflections at the interface, but various media attacked the photoresist and had to be tested. Despite these drawbacks, I enjoyed this research and problem-solving activity. Ultimately, finding a suitable solution was extremely rewarding.

The many interesting, fun, and helpful conversations with colleagues, engineers, and professors were valuable during my thesis. However, I conducted all experiments on my own, and was the only one working on the 3D-MEA project. While this might be the idea of a master's thesis, it made me realize that I do not want to pursue a career in academia or a PhD. I enjoy experimental work and research, but I would prefer to work in a team.

The opportunity to delve deeply into this exciting topic was very inspiring and taught me a great deal. Due to the COVID-19 pandemic, my first year of studies at Delft Technical University (TUD) was mostly remote from home. Therefore, I am grateful for the chance to undertake such a practical and experimental thesis. Throughout the project, I was consistently supported by my supervisors and colleagues. In conclusion, I thoroughly enjoyed this journey and gained a wealth of knowledge.

References

[1] World Health Organization. *Neurological disorders: public health challenges*. World Health Organization, 2006.

[2] Jes Olesen et al. "The economic cost of brain disorders in Europe". In: *European journal of neurology* 19.1 (2012), pp. 155–162.

[3] Kunlin Jin et al. "The critical need to promote research of aging and aging-related diseases to improve health and longevity of the elderly population". In: *Aging and disease* 6.1 (2015), p. 1.

[4] Uwe Marx. "Biology-inspired microphysiological system approaches to solve the prediction dilemma of substance testing". In: *ALTEX* (2016). DOI: 10.14573/altex.1603161.

[5] Steve Perrin. "Preclinical research: Make mouse studies work". In: *Nature News* 507.7493 (2014), p. 423.

[6] Isabella WY Mak, Nathan Evaniew, and Michelle Ghert. "Lost in translation: animal models and clinical trials in cancer treatment". In: *American journal of translational research* 6.2 (2014), p. 114.

[7] Ben M. Maoz. "Brain-on-a-Chip: Characterizing the next generation of advanced in vitro platforms for modeling the central nervous system". In: *APL Bioengineering* 5.3 (Sept. 2021), p. 030902. DOI: 10.1063/5.0055812.

[8] U.S 117th Congress. "HR7667 - Food and Drug Amendments of 2022". In: (2022). URL: https://www.congress.gov/bill/117th-congress/house-bill/7667/text..

[9] Per Brodal. *The central nervous system*. en. 4th ed. New York, NY: Oxford University Press, Mar. 2010.

[10] Stangor Charles and Jennifer Walinga. *Introduction to Psychology – 1st Canadian Edition*. Victoria, B.C.: BCcampus, 2014. ISBN: 978-1-77420-005-6. URL: https://opentextbc.ca/introductiontopsychology/.

[11] Elaine N Marieb and Katja N Hoehn. *Human Anatomy & Physiology, Global Edition*. 10th ed. London, England: Pearson Education, June 2015.

[12] Casey Henley. *Foundations of Neuroscience*. Michigan State University, 2021. URL: https://openbooks.lib.msu.edu/neuroscience/front-matter/introduction/.

[13] Nora Franzen et al. "Impact of organ-on-a-chip technology on pharmaceutical R&D costs". In: *Drug Discovery Today* 24.9 (Sept. 2019), pp. 1720–1724. DOI: 10.1016/j.drudis.2019.06.003.

[14] Massimo Mastrangeli, Sylvie Millet, and Janny van den Eijnden-van Raaij. "Organ-on-chip in development: Towards a roadmap for organs-on-chip". In: *ALTEX* (2019), pp. 650–668. DOI: 10.14573/altex.1908271.

[15] Rose G. Harrison et al. "Observations of the living developing nerve fiber". In: *The Anatomical Record* 1.5 (June 1907), pp. 116–128. DOI: https://doi.org/10.1002/ar.1090010503.

[16] Csaba Forro et al. "Electrophysiology Read-Out Tools for Brain-on-Chip Biotechnology". In: *Micromachines* 12.2 (2021), p. 124.

[17] Miguel Ramalho-Santos and Holger Willenbring. "On the Origin of the Term "Stem Cell"". In: *Cell Stem Cell* 1.1 (June 2007), pp. 35–38. DOI: 10.1016/j.stem.2007.05.013.

[18] Kazutoshi Takahashi and Shinya Yamanaka. "Induction of Pluripotent Stem Cells from Mouse Embryonic and Adult Fibroblast Cultures by Defined Factors". In: *Cell* 126.4 (Aug. 2006), pp. 663–676. DOI: 10.1016/j.cell.2006.07.024.

[19] Kenneth M. Yamada and Edna Cukierman. "Modeling Tissue Morphogenesis and Cancer in 3D". In: *Cell* 130.4 (2007), pp. 601–610. DOI: 10.1016/j.cell.2007.08.006.

[20] Linda G. Griffith and Melody A. Swartz. “Capturing complex 3D tissue physiology in vitro”. In: *Nature Reviews Molecular Cell Biology* 7.3 (2006), pp. 211–224. DOI: 10.1038/nrm1858.

[21] Joseph R. Puryear III, Jeong-Kee Yoon, and YongTae Kim. “Advanced Fabrication Techniques of Microengineered Physiological Systems”. In: *Micromachines* 11.8 (2020). ISSN: 2072-666X. URL: https://www.mdpi.com/2072-666X/11/8/730.

[22] Zichen Qian et al. “Bioengineering Scaffolds for Regenerative Engineering”. In: (2019), pp. 444–461. DOI: 10.1016/b978-0-12-801238-3.99891-x.

[23] S.C. Terry, J.H. Jerman, and J.B. Angell. “A gas chromatographic air analyzer fabricated on a silicon wafer”. In: *IEEE Transactions on Electron Devices* 26.12 (Dec. 1979), pp. 1880–1886. DOI: 10.1109/t-ed.1979.19791.

[24] David C. Duffy et al. “Rapid Prototyping of Microfluidic Systems in Poly(dimethylsiloxane)”. In: *Analytical Chemistry* 70.23 (Oct. 1998), pp. 4974–4984. DOI: 10.1021/ac980656z.

[25] Alexandra M. Greiner, Benjamin Richter, and Martin Bastmeyer. “Micro-Engineered 3D Scaffolds for Cell Culture Studies”. In: *Macromolecular Bioscience* 12.10 (2012), pp. 1301–1314. DOI: 10.1002/mabi.201200132.

[26] Dongeun Huh et al. “Reconstituting Organ-Level Lung Functions on a Chip”. In: *Science* 328.5986 (June 2010), pp. 1662–1668. DOI: 10.1126/science.1188302.

[27] Austin P. Passaro and Steven L. Stice. “Electrophysiological Analysis of Brain Organoids: Current Approaches and Advancements”. In: *Frontiers in Neuroscience* 14 (Jan. 2021). DOI: 10.3389/fnins.2020.622137.

[28] Vijay Viswam et al. “Optimal Electrode Size for Multi-Scale Extracellular-Potential Recording From Neuronal Assemblies”. In: *Frontiers in Neuroscience* 13 (Apr. 2019). DOI: 10.3389/fnins.2019.00385.

[29] Marie Engelene J. Obien and Urs Frey. “Large-Scale, High-Resolution Microelectrode Arrays for Interrogation of Neurons and Networks”. In: *Advances in Neurobiology*. Springer International Publishing, 2019, pp. 83–123. DOI: 10.1007/978-3-030-11135-9_4.

[30] Sabrina Weidlich et al. “MEAs and 3D nanoelectrodes: electrodeposition as tool for a precisely controlled nanofabrication”. In: *Nanotechnology* 28.9 (Jan. 2017), p. 095302. DOI: 10.1088/1361-6528/aa57b5. URL: https://dx.doi.org/10.1088/1361-6528/aa57b5.

[31] David A Soscia et al. “A flexible 3-dimensional microelectrode array for in vitro brain models”. In: *Lab on a Chip* 20.5 (2020), pp. 901–911.

[32] Marie Engelene J. Obien et al. “Revealing neuronal function through microelectrode array recordings”. In: *Frontiers in Neuroscience* 8 (Jan. 2015). DOI: 10.3389/fnins.2014.00423.

[33] Tomi Ryynänen et al. “Microelectrode Array With Transparent ALD TiN Electrodes”. In: *Frontiers in Neuroscience* 13 (Mar. 2019). DOI: 10.3389/fnins.2019.00226.

[34] Multi Channel Systems MCS GmbH. *Multi Channel Systems*. Dec. 2021. URL: https://www.multichannelsystems.com/.

[35] Udo Lang, Nicola Naujoks, and Jurg Dual. “Mechanical characterization of PEDOT:PSS thin films”. In: *Synthetic Metals* 159.5-6 (Mar. 2009), pp. 473–479. DOI: 10.1016/j.synthmet.2008.11.005.

[36] B.A. Latella et al. “Titanium nitride/vanadium nitride alloy coatings: mechanical properties and adhesion characteristics”. In: *Surface and Coatings Technology* 200.11 (Mar. 2006), pp. 3605–3611. DOI: 10.1016/j.surfcoat.2004.09.008.

[37] S. Budday et al. “Mechanical characterization of human brain tissue”. In: *Acta Biomaterialia* 48 (2017), pp. 319–340. ISSN: 1742-7061. DOI: https://doi.org/10.1016/j.actbio.2016.10.036. URL: https://www.sciencedirect.com/science/article/pii/S1742706116305633.

[38] Jelena Dragas et al. “In Vitro Multi-Functional Microelectrode Array Featuring 59 760 Electrodes, 2048 Electrophysiology Channels, Stimulation, Impedance Measurement, and Neurotransmitter Detection Channels”. In: *IEEE Journal of Solid-State Circuits* 52.6 (June 2017), pp. 1576–1590. DOI: 10.1109/jssc.2017.2686580.

[39] Jan Müller et al. “High-resolution CMOS MEA platform to study neurons at subcellular, cellular, and network levels”. In: vol. 15. 13. Royal Society of Chemistry (RSC), 2015, pp. 2767–2780. DOI: 10.1039/c5lc00133a.

[40] Matthew A. Hopcroft, William D. Nix, and Thomas W. Kenny. “What is the Young’s Modulus of Silicon?” In: *Journal of Microelectromechanical Systems* 19.2 (Apr. 2010), pp. 229–238. DOI: 10.1109/jmems.2009.2039697.

[41] Heike Bartsch et al. “LTCC-based multi-electrode arrays for 3D in vitro cell cultures”. In: *Journal of Ceramic Science and Technology* 6.4 (2015), pp. 315–324.

[42] Hyogeun Shin et al. “3D high-density microelectrode array with optical stimulation and drug delivery for investigating neural circuit dynamics”. In: *Nature communications* 12.1 (2021), pp. 1–18.

[43] T. M. de Rijk. “A 3D microelectrode array to record neural activity at different tissue depths”. MA thesis. Delft University of Technology, 2020.

[44] Dmitry Kireev et al. “N3-MEA Probes: Scooping Neuronal Networks”. In: *Frontiers in neuroscience* 13 (Apr. 2019), p. 320. DOI: 10.3389/fnins.2019.00320.

[45] Birthe Rubehn and Thomas Stieglitz. “In vitro evaluation of the long-term stability of polyimide as a material for neural implants”. In: *Biomaterials* 31.13 (2010), pp. 3449–3458. ISSN: 0142-9612. DOI: https://doi.org/10.1016/j.biomaterials.2010.01.053. URL: https://www.sciencedirect.com/science/article/pii/S0142961210000852.

[46] Chang Liu. *Foundations of MEMS*. 2nd ed. Upper Saddle River, NJ: Pearson, Feb. 2011.

[47] Bharat Bhushan, ed. *Springer Handbook of Nanotechnology*. Springer Berlin Heidelberg, 2017. DOI: 10.1007/978-3-662-54357-3.

[48] Marc J. Madou. *Manufacturing Techniques for Microfabrication and Nanotechnology* -. Boca Raton, Fla: CRC Press, 2011. ISBN: 978-1-420-05519-1.

[49] Zahra Kolahdouz Esfahani. “Monolithic 3D Wafer Level Integration Applied for Smart LED Wafer Level Packaging”. PhD thesis. Delft University of Technology, 2017.

[50] Nele Revyn et al. “Recording Neuronal Activity On Chip with Segmented 3D Microelectrode Arrays”. In: *2022 IEEE 35th International Conference on Micro Electro Mechanical Systems Conference (MEMS)*. 2022, pp. 102–105. DOI: 10.1109/MEMS51670.2022.9699597.

[51] *Technical datasheet AZ 12XT-20PL Series*. Rev. 03/21. Merck KGaA. Mar. 2021.

[52] Jasper Van Hoorick et al., eds. *Polymer and Photonic Materials Towards Biomedical Breakthroughs*. Springer International Publishing, 2018. DOI: 10.1007/978-3-319-75801-5.

[53] Jürgen Stampfl, Robert Liska, and Aleksandr Ovsianikov, eds. *Multiphoton Lithography: Techniques, Materials and Applications*. Wiley-VCH Verlag GmbH & Co. KGaA, Nov. 2016. DOI: 10.1002/9783527682676.

[54] Nanoscribe GmbH & Co. KG. *Nanoguide*. 2021. DOI: https://doi.org/10.1007/978-3-319-75801-5. URL: https://support.nanoscribe.com/hc/en-gb.

[55] Maria Göppert-Mayer. “Über Elementarakte mit zwei Quantensprüngen”. In: *Annalen der Physik* 401.3 (1931), pp. 273–294. DOI: https://doi.org/10.1002/andp.19314010303. eprint: https://onlinelibrary.wiley.com/doi/pdf/10.1002/andp.19314010303. URL: https://onlinelibrary.wiley.com/doi/abs/10.1002/andp.19314010303.

[56] Peter R. Ogilby. “Singlet oxygen: there is indeed something new under the sun.” In: *Chemical Society reviews* 39 8 (2010), pp. 3181–209.

[57] Steve Ruzin and Holly Aaron. *1P vs 2P fluorescence imaging*. 2021. URL: http://microscopy.berkeley.edu/courses/TLM/2P/index.html.

[58] Nanoscribe GmbH & Co. KG. *Nanoscribe*. 2021. URL: https://www.nanoscribe.com/.

[59] Ada-Ioana Bunea et al. “Micro 3D Printing by Two-Photon Polymerization: Configurations and Parameters for the Nanoscribe System”. In: *Micro* 1.2 (Sept. 2021), pp. 164–180. DOI: 10.3390/micro1020013.

[60] Carmen LaTorre and Bharat Bhushan. “Nanotribological characterization of human hair and skin using atomic force microscopy”. In: *Ultramicroscopy* 105.1 (2005). Proceedings of the Sixth

International Conference on Scanning Probe Microscopy, Sensors and Nanostructures, pp. 155–175. ISSN: 0304-3991. DOI: https://doi.org/10.1016/j.ultramic.2005.06.032. URL: https://www.sciencedirect.com/science/article/pii/S030439910500135X.

[61] Transene Company Inc. *Aluminum Etchants*. 2023. URL: https://transene.com/aluminum/.

[62] D. E. Aspnes and A. A. Studna. "Dielectric functions and optical parameters of Si, Ge, GaP, GaAs, GaSb, InP, InAs, and InSb from 1.5 to 6.0 eV". In: *Phys. Rev. B* 27 (2 Jan. 1983), pp. 985–1009. DOI: 10.1103/PhysRevB.27.985. URL: https://link.aps.org/doi/10.1103/PhysRevB.27.985.

[63] Clifford Henderson. *Introduction to Chemically Amplified Photoresists*. 2023. URL: https://sites.google.com/site/hendersonresearchgroup/helpful-primers-introductions/introduction-to-chemically-amplified-photoresists.

[64] E. Hecht. *Optics*. Pearson education. Addison-Wesley, 2002. ISBN: 9780321188786.

[65] J. D. Hunter. "Matplotlib: A 2D graphics environment". In: *Computing in Science & Engineering* 9.3 (2007), pp. 90–95. DOI: 10.1109/MCSE.2007.55.

[66] M. Scholten and J. E. A. M. van den Meerakker. "On the Mechanism of ITO Etching: The Specificity of Halogen Acids". In: *Journal of The Electrochemical Society* 140.2 (Feb. 1993), p. 471. DOI: 10.1149/1.2221071. URL: https://dx.doi.org/10.1149/1.2221071.

[67] Tzu-Hsuan Tsai and Yung-Fu Wu. "Wet etching mechanisms of ITO films in oxalic acid". In: *Microelectronic Engineering* 83.3 (2006), pp. 536–541. ISSN: 0167-9317. DOI: https://doi.org/10.1016/j.mee.2005.12.003. URL: https://www.sciencedirect.com/science/article/pii/S0167931705005599.

[68] Jingyuan Qu et al. "Micro-Structured Two-Component 3D Metamaterials with Negative Thermal-Expansion Coefficient from Positive Constituents". In: *Scientific Reports* 7.1 (Jan. 2017). DOI: 10.1038/srep40643. URL: https://doi.org/10.1038/srep40643.

[69] Liu Fengchao and Zheng Bin. "The Linear Coefficient of Thermal Expansion of Silicon at Room Temperature". In: *Powder Diffraction* 6.3 (1991), pp. 147–152. DOI: 10.1017/S0885715600017292.

[70] Zemin Liu et al. "Creating three-dimensional magnetic functional microdevices via molding-integrated direct laser writing". In: *Nature Communications* 13.1 (Apr. 2022). DOI: 10.1038/s41467-022-29645-2.

A. Method 1: Masked pattern transfer-based process flow

A.1. Masks

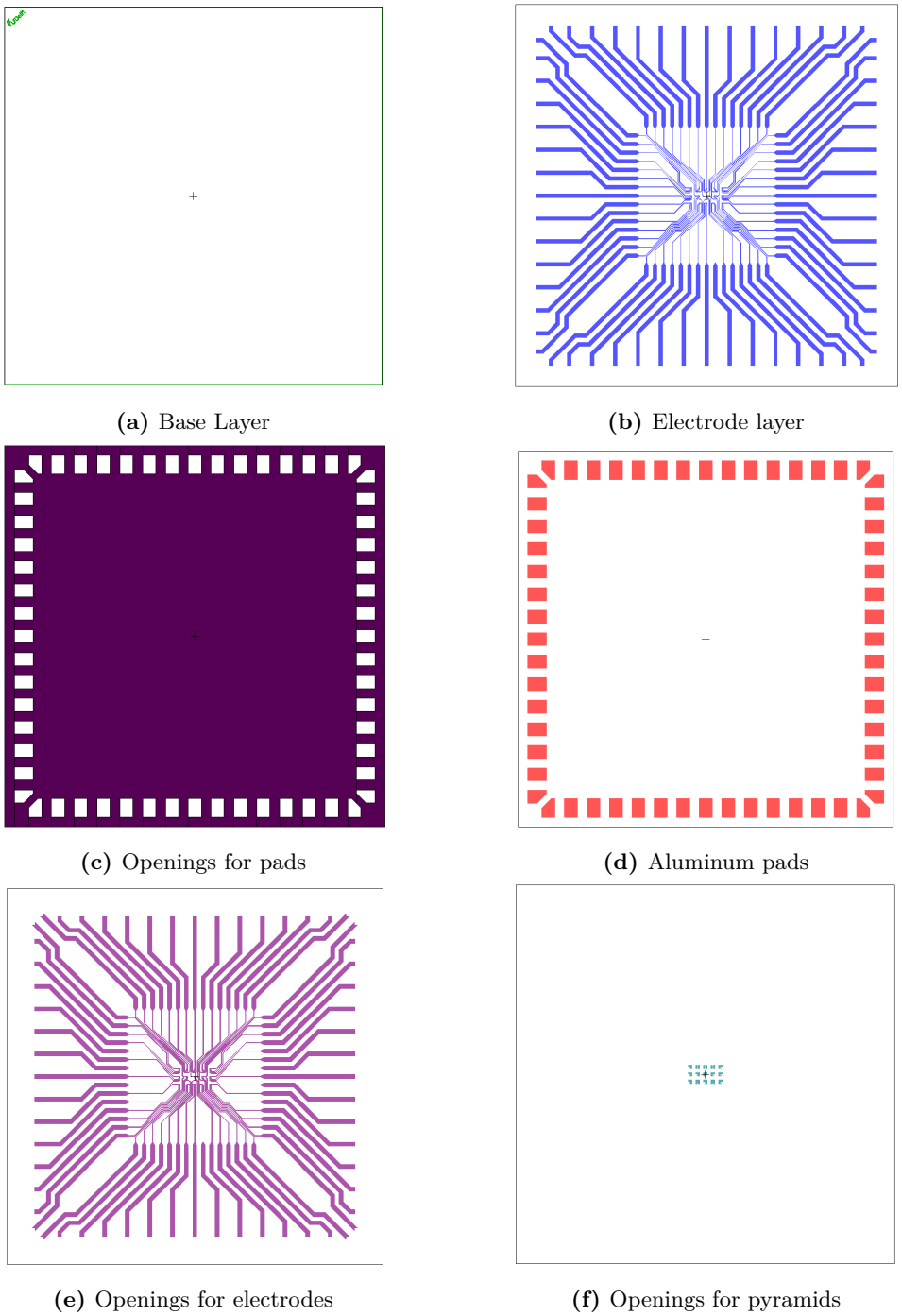

(a) Base Layer

(b) Electrode layer

(c) Openings for pads

(d) Aluminum pads

(e) Openings for electrodes

(f) Openings for pyramids

Figure A.1.: Masks (zoomed to die) for the masked pattern transfer based process flow

A.2. Flowchart

Else Kooi Laboratory

TU Delft

Polymeric 3D-multielectrode array

FLOWCHART

Masked pattern transfer-based process flow

VERSION 1.6

Valid from May 2022

BATCH INFORMATION			
NAME OF OWNER :	Thomas Michalica	**MASK SET :**	
NAME OF MENTOR :	Shriya Rangaswamy	**MASK BOX :**	
RUN NUMBER :		**DIE SIZE :**	
WAFER AMOUNT :		**START DATE :**	
SUBJECT TO PCC :		**PCC APPROVED :**	

DELFT UNIVERSITY OF TECHNOLOGY
ELSE KOOI LABORATORY

Adress : Feldmannweg 17, 2628 CT Delft, The Netherlands
P.O. Box : 5053, 2600 GB Delft, The Netherlands
Phone : +31 - (0)15 - 2783868
Fax : +31 - (0)15 - 2622163
Website : www.tudelft.nl/ewi/onderzoek/faciliteiten/else-kooi-lab

STARTING MATERIAL

Use **SINGLE SIDE** polished **LOW RESISTIVITY (LRES)** wafers,
with the following specifications:

Type:	n / phosphorus
Orientation:	<100>
Resistivity:	1-5 Ωcm
Thickness:	525 ± 15 µm
Diameter:	100 mm

Zero Layer

1. COATING

Use the coater station of the EVG120 system to coat the wafers with photoresist. The process consists of:
- a treatment with HMDS (hexamethyldisilazane) vapor, with nitrogen as a carrier gas
- spin coating of Shipley SPR3012 positive resist, dispensed by a pump
- a soft bake at 95 °C for 90 seconds

Always check the relative humidity (48 ± 2 %) in the room before coating, and follow the instructions for this equipment.
Use program "1-**Co - 3012 – 1.4 _no EBR**". There will be no edge bead removal.

2. ALIGNMENT AND EXPOSURE

Processing will be performed on the ASML PAS5500/80 automatic wafer stepper.
Expose masks COMURK and FWAM, with job "ZEFWAM" and the correct exposure energy (check the energy list).
This results in alignment markers for the stepper and contact aligner for wafers which will not get an EPI layer.

3. DEVELOPING

Use the developer station of the EVG120 system to develop the wafers. The process consists of:
- a post-exposure bake at 115 °C for 90 seconds
- developing with Shipley MF322 with a single puddle process
- a hard bake at 100 °C for 90 seconds

Use program "1-**Dev - SP**".

4. INSPECTION

Visually inspect the wafers through a microscope:
- No resist residues are allowed.
- Check the linewidth of the structures.
- Check the overlay of the exposed pattern if the mask was aligned to a previous pattern on the wafer.

5. WAFER NUMBERING

Use the glass pen in the lithography room to mark the wafers with the BATCH and WAFER number.
Write the numbers in the photoresist, just above the waferflat. Always do this after exposure and development !
It is NOT allowed to use a metal pen or a scriber (pen with a diamond tip) for this purpose.

6. PLASMA ETCHING: Alignment markers (URK's) into Silicon

Use the Trikon Ωmega 201 plasma etcher.
It is **not** allowed to change the process conditions and times from the etch recipe!
Use sequence **URK_NPD** (with a platen temperature of **20 °C**) to etch 120 nm deep ASM URK's into the Si.

Process conditions from chamber recipe URK_ETCH:						
Step	Gasses & flows	Pressure	Platen RF	ICP RF	Platen temp.	Etch time
1. breakthrough	CF_4/O_2 = 40/20 sccm	5 mTorr	60 W	500 W	20 °C	0'10"
2. bulk etch	Cl_2/HBr = 80/40 sccm	60 mTorr	20 W	500 W	20 °C	0'40"

7. LAYER STRIPPING: Photoresist

Strip resist — Use the Tepla Plasma 300 system to remove the photoresist in an oxygen plasma.
Follow the instructions specified for the Tepla stripper, and use the quartz carrier.
Use **program 1**: 1000 watts power and automatic endpoint detection + 2 min. overetching.

8. CLEANING: HNO_3 99% and 69.5%

Clean — 10 minutes in fuming nitric acid at ambient temperature. This will dissolve organic materials.
Use wet bench "HNO_3 99% (Si)" and the carrier with the red dot.
Rinse — Rinse in the Quick Dump Rinser with the standard program until the resistivity is 5 MΩ.
Clean — 10 minutes in concentrated nitric acid at 110 °C. This will dissolve metal particles.
Use wet bench "HNO_3 69,5% 110C (Si)" and the carrier with the red dot.
Rinse — Rinse in the Quick Dump Rinser with the standard program until the resistivity is 5 MΩ.
Dry — Use the "Avenger Ultra-Pure 6" rinser/dryer with the standard program, and the white carrier with a red dot.

Base alignment layer

9. COATING

Use the coater station of the EVG120 system to coat the wafers with photoresist. The process consists of:

- a treatment with HMDS (hexamethyldisilazane) vapor, with nitrogen as a carrier gas
- spin coating of Shipley SPR3012 positive resist, dispensed by a pump
- a soft bake at 95 °C for 90 seconds

Always check the relative humidity (48 ± 2 %) in the room before coating, and follow the instructions for this equipment.
Use program "1-**Co - 3012 – 1.4 _no EBR**". There will be no edge bead removal.

10. ALIGNMENT AND EXPOSURE

Processing will be performed on the SUSS MicroTec MA/BA8 mask aligner
Check if the mask is clean before usage; perform mask cleaning if necessary.
Expose mask ***1_base_layer***, with an exposure dose of xxx.
Use top side alignment program 1 with the "soft contact" option switched on.

11. DEVELOPING

Use the developer station of the EVG120 system to develop the wafers. The process consists of:

- a post-exposure bake at 115 °C for 90 seconds
- developing with Shipley MF322 with a single puddle process
- a hard bake at 100 °C for 90 seconds

Use program "1-**Dev - SP**".

12. INSPECTION: Linewidth and overlay

Visually inspect the wafers through a microscope, and check the line width and overlay. No resist residues are allowed.

13. PLASMA ETCHING: Base Layer into Silicon

Use the Trikon Ωmega 201 plasma etcher.
It is **not** allowed to change the process conditions and times from the etch recipe!
Use sequence **URK_NPD** (with a platen temperature of **20 °C**) to etch 120 nm deep into the Si.

Process conditions from chamber recipe URK_ETCH:						
Step	Gasses & flows	Pressure	Platen RF	ICP RF	Platen temp.	Etch time
1. breakthrough	CF_4/O_2 = 40/20 sccm	5 mTorr	60 W	500 W	20 °C	0'10"
2. bulk etch	Cl_2/HBr = 80/40 sccm	60 mTorr	20 W	500 W	20 °C	0'40"

Polymeric pyramid structures

External at the PME cleanroom of the 3ME faculty

14. Transfer wafer to PME-LAB::

Use wafer-box or wafer-disk with zip-bag to transfer wafer to PME

15. PME-LAB: Cleaning:

Bath wafer in petri-dish: 2 min in acetone

Rinse with iso-propanol
Air-dry for ca. 5 min, until no drops remain

16. **PME-LAB: Surface treatment:**
Oxygen plasma: Diener Femto: 100W / 15 min 5-6 sccm O_2
Silanization bath for >2h: 30mL ethanol mixed with 3mL MAPTMS (10%)
Rinse with acetone and deionized water
Blow dry if necessary
Dispose the solvents into the organic waste container

17. **PME-LAB: FABRICATION: Two-Photon-Polymerisation**
Use the Nanoscribe Photonic Professional GT+ with Large Feature Set (10x objective) to fabricate the structures.
Place wafer into wafer-holder, fixate carefully with the screws.
Use photosensitive resin IP-Q (methacrylate-based): deposit droplets on fabrication sites (center of each wafer die)
Load holder into 2PP machine and align coordinate system to wafer markers at (-45, 0) and (45,0).
Follow the operating instructions from the manual when using this machine.

18. **PME-LAB: RESIN DEVELOPMENT:**
Use the developer fume hood in the PME cleanroom
Development Bath in Propylene glycol methyl ether acetate (PGMEA) for 25min.
Clean Bath in isopropanol for 5min.
Dry Let the wafer rest under the fume hood until isopropanol has evaporated (5min)
Dispose the developer into the organic waste container

19. **PME-LAB: INSPECTION:**
Use Keyence Digital Microscope VHX-6000 to visually inspect the structures and verify their alignment

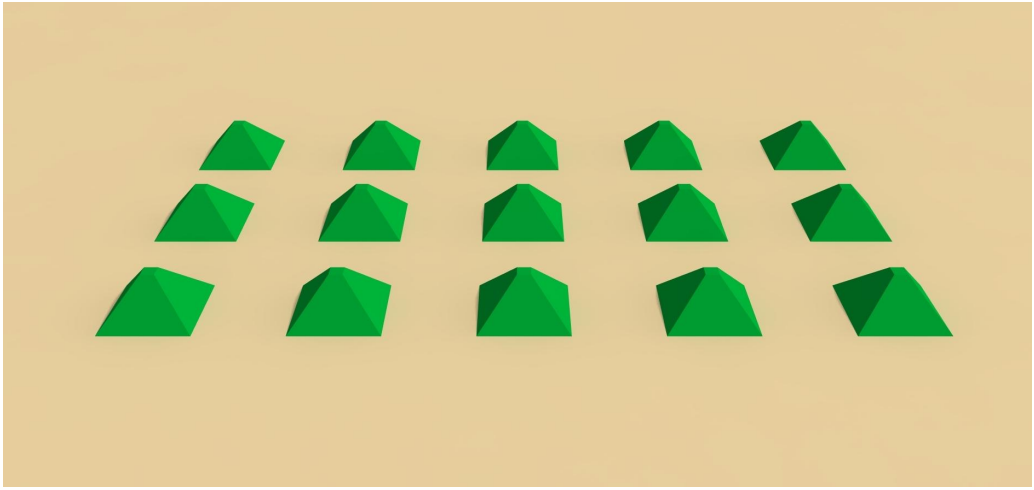

Passivation of pyramids

20. **Transfer wafer to KAVLI-LAB::**
Use wafer-box or wafer-disk with zip-bag to transfer wafer to KAVLI

21. **Kavli: SILICON NITRIDE ICPCVD: 500nm SiN 75°C**
External at the Kavli cleanroom
Oxford ICPCVD KavliLab to deposit **SiN** at low temperatures and passivate polymeric structures
Use Kavli low-temperature **SiN** recipe and adapt process time according to thickness.

22. **Transfer wafer to EKL-LAB::**
Use wafer-box or wafer-disk with zip-bag to transfer wafer to EKL.

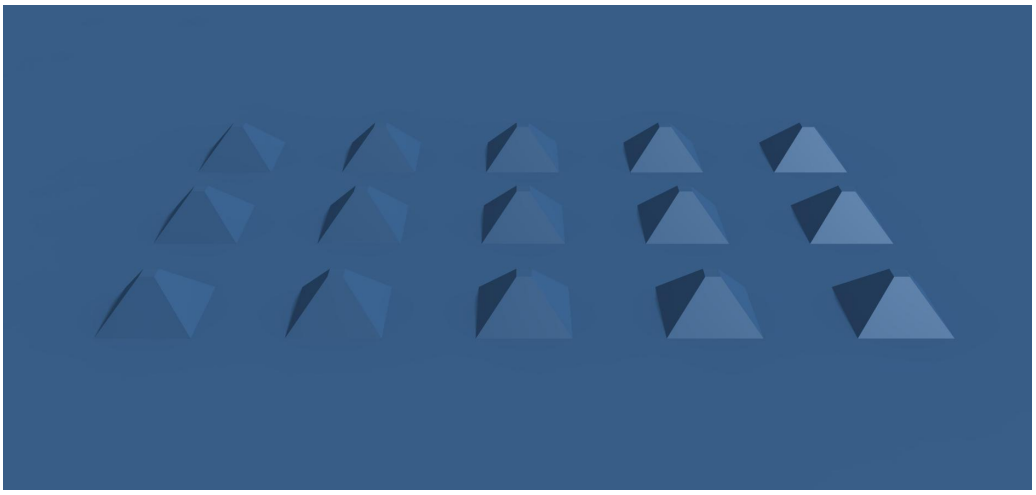

Electrode fabrication

23. **MANUAL Cleaning: Acetone and IPA**
Clean Wafer in Acetone bath
Rinse with DI water
Clean with IPA
Rinse with DI water

24. **TITANIUM SPUTTERING:100nm TiN@ 25°C (with Ti target)**
Use the TRIKON SIGMA 204 sputter coater for the deposition of a Titanium on the wafers.
The target must exist Ti and deposition must be done at 25°C with an Ar flow of ***xxx*** sccm.
Use carrier wafer
Follow the operating instructions from the manual when using this machine.
Use recipe ***xxx*** to obtain a 100 nm thick Ti layer.
Conduct a leak test if printed structure has changed

25. **Transfer wafer to KAVLI-LAB::**
Use wafer-box or wafer-disk with zip-bag to transfer wafer to KAVLI

26. **Kavli: SILICON NITRIDE ICPCVD: 200nm SiN 75°C**
External at the Kavli cleanroom
Oxford ICPCVD KavliLab to deposit **SiN** at low temperatures and passivate polymeric structures
Use Kavli low-temperature **SiN** recipe and adapt process time according to thickness.

27. **Transfer wafer to EKL-LAB::**
Use wafer-box or wafer-disk with zip-bag to transfer wafer to EKL.

28. **COATING**
Use the EVG101 spraycoater system to coat the wafers with photoresist. The process consists of:
- AZ 12XT-20PL diluted positive photoresist (ratio: 1:6:3.8)

Always check the relative humidity (48 ± 2 %) in the room before coating, and follow the instructions for this equipment.
Make sure to use the contaminated chuck and that the correct resist is loaded.
Use program "HP 1000mbar 5 ml 8 layers"
Softbake: 110°C/3min (Hot plate with carrier wafer)
Repeat Coating and Softbaking 2 times
Final Softbake: 110°C/6min (Hot plate with carrier wafer)

29. **ALIGNMENT AND EXPOSURE**
Processing will be performed on the SUSS MicroTec MA/BA8 mask aligner
Check if the mask is clean before usage; perform mask cleaning if necessary.
Expose mask ***2_electrodes***, with an exposure dose of xxx.
Use top side alignment program 1 with the "proximity" option switched on, set distance to pyramid height +20um.
Post-exposure bake: 90°C for 120seconds

30. DEVELOPING MANUAL

Use the developer fume hood in the polymer lab.

Developing with the AZ 326 MIF developer (3-4 min)
Rinse with DI water (1 min)
Blow or spin-dry wafer (**make sure to use the contaminated chuck**)

To ensure right development time it is recommended to optically inspect the wafer after 3min development time, and if necessary re-development the wafer further
Dispose the developer into the right container.

31. WET ETCHING: 200 nm silicon nitride (hard mask)

Prepare BHF bath in SAL-Lab: use buddy and neoprene gloves. All beakers must be made out of Teflon

Etch	Use "BHF 1:7 (SiO_2-ets)" at ambient temperature
Time	Submerge in BHF bath for 150sec
Rinse	Rinse with DI immediately, place in a Teflon beaker with a hole and let it rinse for 5 min.
Dry	Blow dry

32. WET ETCHING: 100 nm Titanium Nitride (sputtered at 25 °C)

Prepare RCA-1 bath in SAL-Lab: use buddy and neoprene gloves.

Etch	Use "RCA-1" at ambient temperature
Time	Submerge in bath for 2min
Rinse	Rinse with DI immediately for 5 min.
Dry	Blow dry

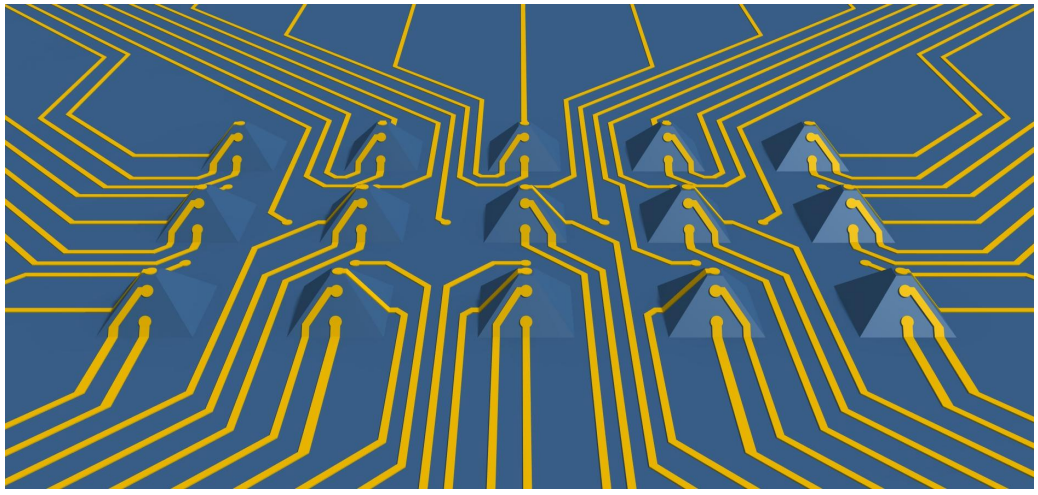

Aluminum Pads

33. MANUAL Cleaning: Acetone and IPA

Clean Wafer in Acetone bath
Rinse with DI water
Clean with IPA
Rinse with DI water

34. ALUMINIUM SPUTTERING: METALLIZATION FOR PADS

Use the TRIKON SIGMA sputter coater for the deposition of an aluminium metal layer on the wafers.
The target must exist of 99% Al and 1% Si, and deposition must be done at 25 °C. Follow the operating instructions from the manual when using this machine.

35. COATING

Use the EVG101 spraycoater system to coat the wafers with photoresist. The process consists of:

- AZ 12XT-20PL diluted positive photoresist (ratio: 1:6:3.8)

Always check the relative humidity (48 ± 2 %) in the room before coating, and follow the instructions for this equipment.
Make sure to use the contaminated chuck and that the correct resist is loaded.
Use program "HP 1000mbar 5 ml 8 layers"
Softbake: 110°C/3min (Hot plate with carrier wafer)
Repeat Coating and Softbaking 2 times
Final Softbake: 110°C/6min (Hot plate with carrier wafer)

36. ALIGNMENT AND EXPOSURE

Processing will be performed on the SUSS MicroTec MA/BA8 mask aligner
Check if the mask is clean before usage; perform mask cleaning if necessary.
Expose mask ***3_pads***, with an exposure dose of xxx.
Use top side alignment program 1 with the "proximity" option switched on, set distance to pyramid height +20um.
Post-exposure bake: 90°C for 120seconds

37. DEVELOPING MANUAL

Use the developer fume hood in the polymer lab.
Developing with the AZ 326 MIF developer (3-4 min)
Rinse with DI water (1 min)
Blow or spin-dry wafer (**make sure to use the contaminated chuck**)
To ensure right development time it is recommended to optically inspect the wafer after 3min development time, and if necessary re-development the wafer further
Dispose the developer into the right container.

38. INSPECTION: Linewidth and overlay

Visually inspect the wafers through a microscope, and check the line width and overlay. No resist residues are allowed.

39. WET ETCHING: 675 nm Aluminium (sputtered at 25°C)

40. MANUAL LAYER STRIPPING: Photoresist

Submerge the wafers in acetone then followed by IPA for 3 mins each to remove the remaining photoresist.
Manually rinse and then spin dry.

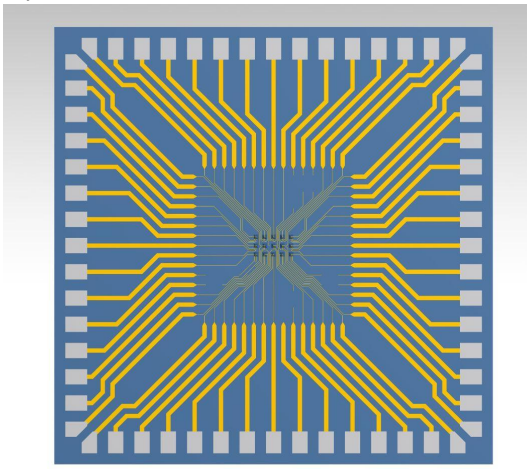

Passivation of electrode traces

41. MANUAL Cleaning: Acetone and IPA

Clean Wafer in Acetone bath
Rinse with DI water
Clean with IPA
Rinse with DI water

42. Transfer wafer to KAVLI-LAB::

Use wafer-box or wafer-disk with zip-bag to transfer wafer to KAVLI

43. Kavli: SILICON NITRIDE ICPCVD: 500nm SiN 75°C

External at the Kavli cleanroom
Oxford ICPCVD KavliLab to deposit **SiN** at low temperatures and passivate polymeric structures
Use Kavli low-temperature **SiN** recipe and adapt process time according to thickness.

44. Transfer wafer to EKL-LAB::

Use wafer-box or wafer-disk with zip-bag to transfer wafer to EKL.

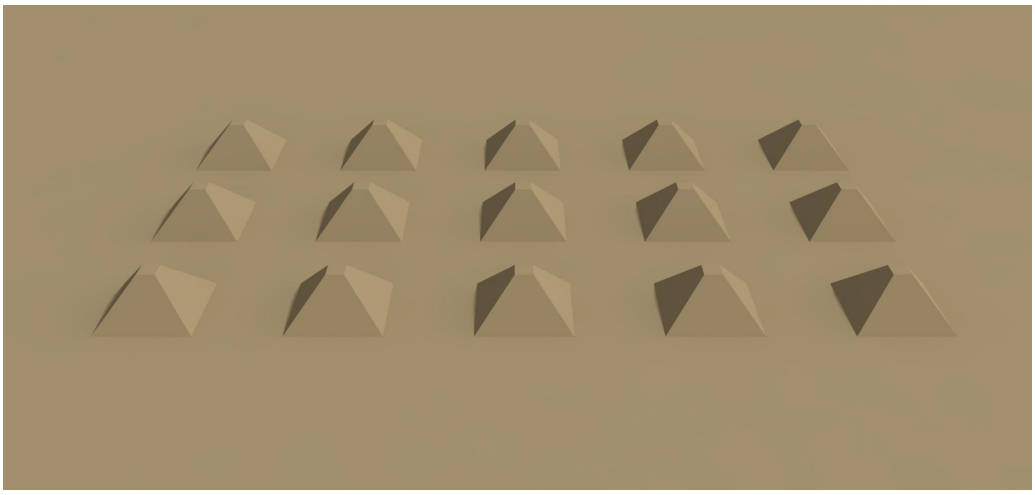

Electrode Openings

45. MANUAL Cleaning: Acetone and IPA
Clean Wafer in Acetone bath
Rinse with DI water
Clean with IPA
Rinse with DI water

46. COATING
Use the EVG101 spraycoater system to coat the wafers with photoresist. The process consists of:
- AZ 12XT-20PL diluted positive photoresist (ratio: 1:6:3.8)

Always check the relative humidity (48 ± 2 %) in the room before coating, and follow the instructions for this equipment.
Make sure to use the contaminated chuck and that the correct resist is loaded.
Use program "HP 1000mbar 5 ml 8 layers"
Softbake: 110°C/3min (Hot plate with carrier wafer)
Repeat Coating and Softbaking 2 times
Final Softbake: 110°C/6min (Hot plate with carrier wafer)

47. ALIGNMENT AND EXPOSURE
Processing will be performed on the SUSS MicroTec MA/BA8 mask aligner
Check if the mask is clean before usage; perform mask cleaning if necessary.
Expose mask ***4_open_electrodes***, with an exposure dose of xxx.
Use top side alignment program 1 with the "proximity" option switched on, set distance to pyramid height +20um.
Post-exposure bake: 90°C for 120seconds

48. DEVELOPING MANUAL
Use the developer fume hood in the polymer lab.
Developing with the AZ 326 MIF developer (3-4 min)
Rinse with DI water (1 min)
Blow or spin-dry wafer (**make sure to use the contaminated chuck**)
To ensure right development time it is recommended to optically inspect the wafer after 3min development time, and if necessary re-development the wafer further
Dispose the developer into the right container.

49. INSPECTION: Linewidth and overlay
Visually inspect the wafers through a microscope, and check the line width and overlay. No resist residues are allowed.

50. WET ETCHING: 200 nm silicon nitride

Prepare BHF bath in SAL-Lab: use buddy and neoprene gloves. All beakers must be made out of Teflon

Etch	Use "BHF 1:7 (SiO_2-ets)" at ambient temperature
Time	Submerge in BHF bath for 150sec
Rinse	Rinse with DI immediately, place in a Teflon beaker with a hole and let it rinse for 5 min.
Dry	Blow dry

51. MANUAL LAYER STRIPPING: Photoresist

Submerge the wafers in acetone then followed by IPA for 3 mins each to remove the remaining photoresist. Manually rinse and then spin dry.

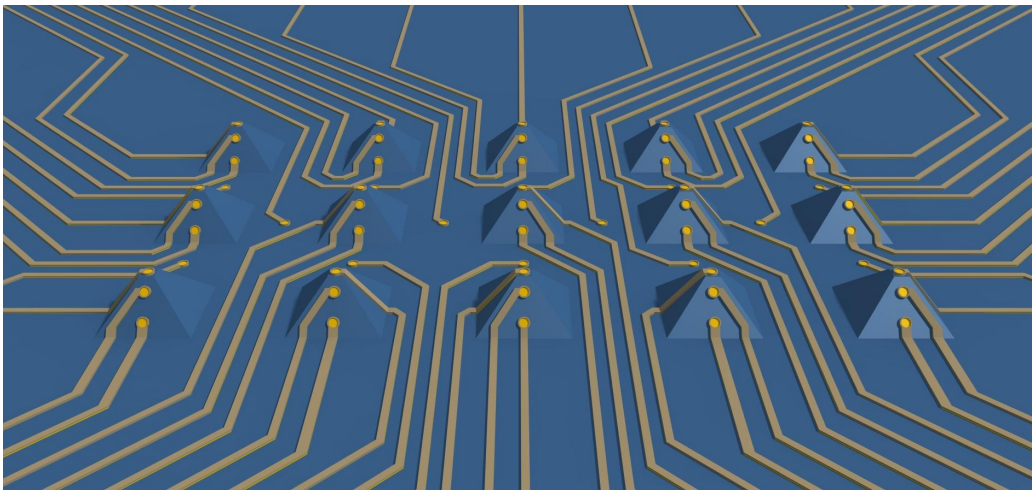

Pyramid Opening

52. MANUAL Cleaning: Acetone and IPA

Clean Wafer in Acetone bath
Rinse with DI water
Clean with IPA
Rinse with DI water

53. COATING

Use the EVG101 spraycoater system to coat the wafers with photoresist. The process consists of:

- AZ 12XT-20PL diluted positive photoresist (ratio: 1:6:3.8)

Always check the relative humidity (48 ± 2 %) in the room before coating, and follow the instructions for this equipment.
Make sure to use the contaminated chuck and that the correct resist is loaded.
Use program "HP 1000mbar 5 ml 8 layers"
Softbake: 110°C/3min (Hot plate with carrier wafer)
Repeat Coating and Softbaking 2 times
Final Softbake: 110°C/6min (Hot plate with carrier wafer)

54. ALIGNMENT AND EXPOSURE

Processing will be performed on the SUSS MicroTec MA/BA8 mask aligner
Check if the mask is clean before usage; perform mask cleaning if necessary.
Expose mask ***5_open_pyramids***, with an exposure dose of xxx.
Use top side alignment program 1 with the "proximity" option switched on, set distance to pyramid height +20um.
Post-exposure bake: 90°C for 120seconds

55. DEVELOPING MANUAL

Use the developer fume hood in the polymer lab.
Developing with the AZ 326 MIF developer (3-4 min)
Rinse with DI water (1 min)
Blow or spin-dry wafer (**make sure to use the contaminated chuck**)
To ensure right development time it is recommended to optically inspect the wafer after 3min development time, and if necessary re-development the wafer further
Dispose the developer into the right container.

56. INSPECTION: Linewidth and overlay

Visually inspect the wafers through a microscope, and check the line width and overlay. No resist residues are allowed.

57. WET ETCHING: 200 nm silicon nitride

Prepare BHF bath in SAL-Lab: use buddy and neoprene gloves. All beakers must be made out of Teflon

Etch	Use "BHF 1:7 (SiO_2-ets)" at ambient temperature
Time	Submerge in BHF bath for 150sec
Rinse	Rinse with DI immediately, place in a Teflon beaker with a hole and let it rinse for 5 min.
Dry	Blow dry

58. MANUAL LAYER STRIPPING: Photoresist

Submerge the wafers in acetone then followed by IPA for 3 mins each to remove the remaining photoresist. Manually rinse and then spin dry.

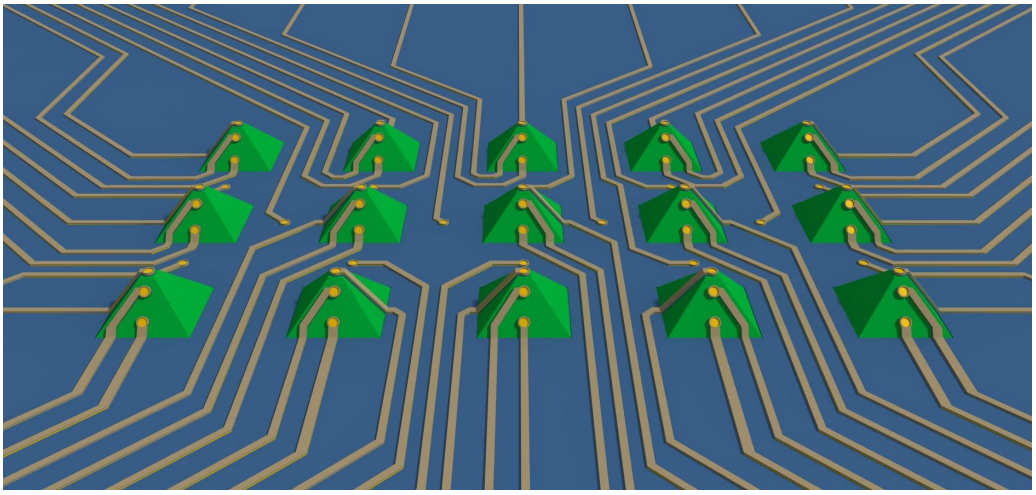

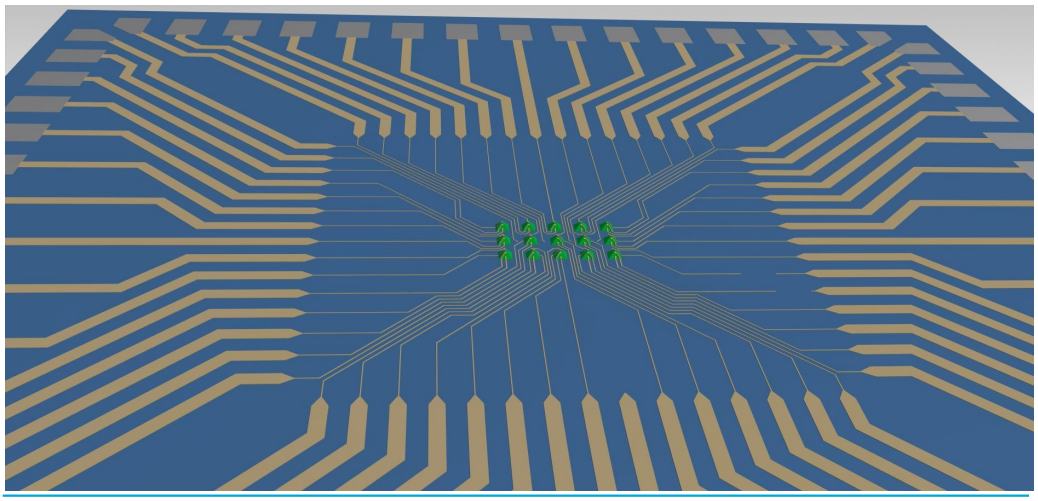

Packaging

59. Wafer Dicing for packaging

60. Wire bonding to pcb

B. Method 2: Two-photon polymerization-based process flow

B.1. Masks

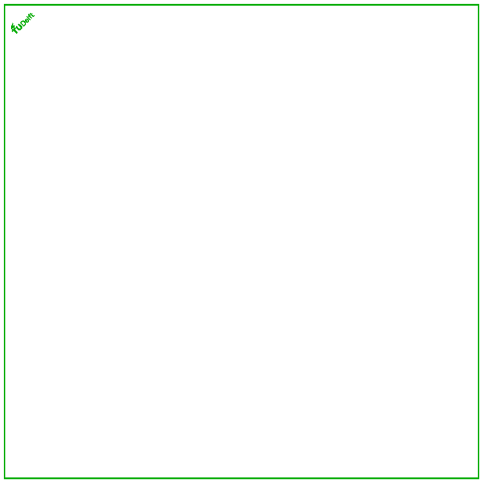

(a) Base Layer

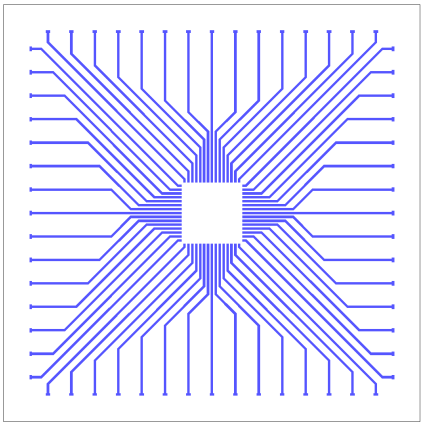

(b) Electrode layer

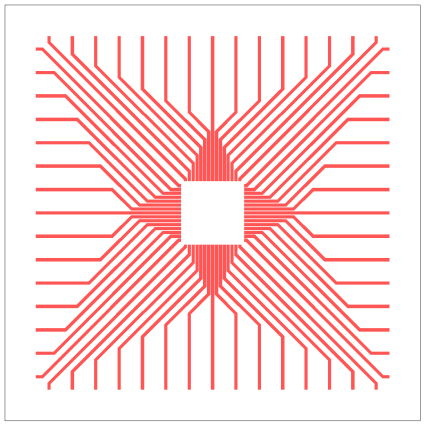

(c) Insulation layer

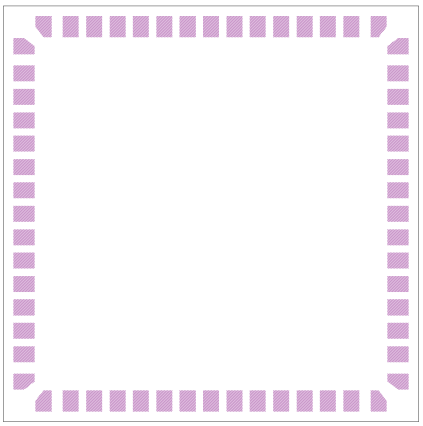

(d) Aluminium pads

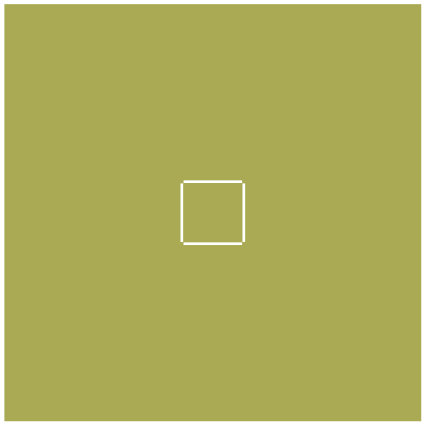

(e) Open back-end

Figure B.1.: Masks (zoomed to die) for the two-photon polymerization-based process flow

B.2. Flowchart

Else Kooi Laboratory

TU Delft

Polymeric 3D-multielectrode array

FLOWCHART

Two-photon polymerization-based process flow

VERSION 2.3

Valid from October 2022

BATCH INFORMATION			
NAME OF OWNER :	Thomas Michalica	**MASK SET :**	
NAME OF MENTOR :		**MASK BOX :**	
RUN NUMBER :		**DIE SIZE :**	
WAFER AMOUNT :		**START DATE :**	
SUBJECT TO PCC :		**PCC APPROVED :**	

DELFT UNIVERSITY OF TECHNOLOGY
ELSE KOOI LABORATORY

Adress : Feldmannweg 17, 2628 CT Delft, The Netherlands
P.O. Box : 5053, 2600 GB Delft, The Netherlands
Phone : +31 - (0)15 - 2783868
Fax : +31 - (0)15 - 2622163
Website : www.tudelft.nl/ewi/onderzoek/faciliteiten/else-kooi-lab

STARTING MATERIAL

Use **SINGLE SIDE** polished **LOW RESISTIVITY (LRES)** wafers,
with the following specifications:

Type:	n / phosphorus
Orientation:	<100>
Resistivity:	1-5 Ωcm
Thickness:	525 ± 15 µm
Diameter:	100 mm

Front-end process

Zero Layer

1. COATING

Use the coater station of the EVG120 system to coat the wafers with photoresist. The process consists of:

- a treatment with HMDS (hexamethyldisilazane) vapor, with nitrogen as a carrier gas
- spin coating of Shipley SPR3012 positive resist, dispensed by a pump
- a soft bake at 95 °C for 90 seconds

Always check the relative humidity (48 ± 2 %) in the room before coating, and follow the instructions for this equipment.
Use program "1-**Co - 3012 – 1.4 _no EBR**". There will be no edge bead removal.

2. ALIGNMENT AND EXPOSURE

Processing will be performed on the ASML PAS5500/80 automatic wafer stepper.
Expose masks COMURK and FWAM, with job "ZEFWAM" and the correct exposure energy (check the energy list).
This results in alignment markers for the stepper and contact aligner for wafers which will not get an EPI layer.

3. DEVELOPING

Use the developer station of the EVG120 system to develop the wafers. The process consists of:

- a post-exposure bake at 115 °C for 90 seconds
- developing with Shipley MF322 with a single puddle process
- a hard bake at 100 °C for 90 seconds

Use program "1-**Dev - SP**".

4. INSPECTION

Visually inspect the wafers through a microscope:

- No resist residues are allowed.
- Check the linewidth of the structures.
- Check the overlay of the exposed pattern if the mask was aligned to a previous pattern on the wafer.

5. WAFER NUMBERING

Use the glass pen in the lithography room to mark the wafers with the BATCH and WAFER number.
Write the numbers in the photoresist, just above the waferflat. Always do this after exposure and development !
It is NOT allowed to use a metal pen or a scriber (pen with a diamond tip) for this purpose.

6. PLASMA ETCHING: Alignment markers (URK's) into Silicon

Use the Trikon Ωmega 201 plasma etcher.
It is **not** allowed to change the process conditions and times from the etch recipe!
Use sequence **URK_NPD** (with a platen temperature of **20 ºC**) to etch 120 nm deep ASM URK's into the Si.

Process conditions from chamber recipe URK_ETCH:

Step	Gasses & flows	Pressure	Platen RF	ICP RF	Platen temp.	Etch time
1. breakthrough	CF_4/O_2 = 40/20 sccm	5 mTorr	60 W	500 W	20 °C	0'10"
2. bulk etch	Cl_2/HBr = 80/40 sccm	60 mTorr	20 W	500 W	20 °C	0'40"

7. LAYER STRIPPING: Photoresist

Strip resist — Use the Tepla Plasma 300 system to remove the photoresist in an oxygen plasma. Follow the instructions specified for the Tepla stripper, and use the quartz carrier. Use **program 1**: 1000 watts power and automatic endpoint detection + 2 min. overetching.

8. CLEANING: HNO_3 99% and 69.5%

Clean — 10 minutes in fuming nitric acid at ambient temperature. This will dissolve organic materials. Use wet bench "HNO_3 99% (Si)" and the carrier with the red dot.

Rinse — Rinse in the Quick Dump Rinser with the standard program until the resistivity is 5 MΩ.

Clean — 10 minutes in concentrated nitric acid at 110 °C. This will dissolve metal particles. Use wet bench "HNO_3 69,5% 110C (Si)" and the carrier with the red dot.

Rinse — Rinse in the Quick Dump Rinser with the standard program until the resistivity is 5 MΩ.

Dry — Use the "Avenger Ultra-Pure 6" rinser/dryer with the standard program, and the white carrier with a red dot.

Base alignment layer

9. COATING

Use the coater station of the EVG120 system to coat the wafers with photoresist. The process consists of:

- a treatment with HMDS (hexamethyldisilazane) vapor, with nitrogen as a carrier gas
- spin coating of Shipley SPR3012 positive resist, dispensed by a pump
- a soft bake at 95 °C for 90 seconds
- an automatic edge bead removal with a solvent

Always check the relative humidity (48 ± 2 %) in the room before coating, and follow the instructions for this equipment.
Use program "1-**Co - 3012 – 1.4 _no EBR**". There will be no edge bead removal.

10. ALIGNMENT AND EXPOSURE

Processing will be performed on the SUSS MicroTec MA/BA8 mask aligner
Check if the mask is clean before usage; perform mask cleaning if necessary.
Expose mask ***1_base_layer***, with an exposure dose of 950.
Use top side alignment program 1 with the "soft contact" option switched on.

11. DEVELOPING

Use the developer station of the EVG120 system to develop the wafers. The process consists of:

- a post-exposure bake at 115 °C for 90 seconds
- developing with Shipley MF322 with a single puddle process
- a hard bake at 100 °C for 90 seconds

Use program "1-**Dev - SP**".

12. INSPECTION: Linewidth and overlay

Visually inspect the wafers through a microscope, and check the line width and overlay. No resist residues are allowed.

13. PLASMA ETCHING: Base Layer into Silicon

Use the Trikon Ωmega 201 plasma etcher.
It is **not** allowed to change the process conditions and times from the etch recipe!
Use sequence **URK_NPD** (with a platen temperature of **20 °C**) to etch 120 nm deep into the Si.

Process conditions from chamber recipe URK_ETCH:						
Step	Gasses & flows	Pressure	Platen RF	ICP RF	Platen temp.	Etch time
1. breakthrough	CF_4/O_2 = 40/20 sccm	5 mTorr	60 W	500 W	20 °C	0'10"
2. bulk etch	Cl_2/HBr = 80/40 sccm	60 mTorr	20 W	500 W	20 °C	0'40"

Oxide layer

14. CLEANING: HNO_3 99% and 69.5%

Clean	10 minutes in fuming nitric acid at ambient temperature. This will dissolve organic materials. Use wet bench "HNO_3 99% (Si)" and the carrier with the red dot.
Rinse	Rinse in the Quick Dump Rinser with the standard program until the resistivity is 5 MΩ.
Clean	10 minutes in concentrated nitric acid at 110 °C. This will dissolve metal particles. Use wet bench "HNO_3 69,5% 110C (Si)" and the carrier with the red dot.
Rinse	Rinse in the Quick Dump Rinser with the standard program until the resistivity is 5 MΩ.
Dry	Use the "Avenger Ultra-Pure 6" rinser/dryer with the standard program, and the white carrier with a red dot.

15. PECVD DEPOSITION: 300 nm Silicon oxide

Use the Novellus Concept One PECVD reactor.
It is **not** allowed to change the process conditions and time from the deposition recipe!
Use recipe **".xxx_siostd"** to deposit a 300 nm thick SiO_2 layer.

Process conditions from recipe .xxx_siostd:					
Gasses & flows	Pressure	HF power	LF power	Temperature	Time
$N_2/SiH_4/N_2O$ = 3150/205/6000sccm	2.2 Torr	1000 W	0 W	400 °C	**variable**

Note:
- The layer thickness depends on the station deposition time (SDT), which can be calculated from the average deposition rate during recent recipe usage. This can be found in the logbook of the system.
- An extra test wafer can be deposited for measurements and etch tests.

Metal trace layer

16. CLEANING: HNO_3 99% and 69.5%

Clean	10 minutes in fuming nitric acid at ambient temperature. This will dissolve organic materials. Use wet bench "HNO_3 99% (Si)" and the carrier with the red dot.
Rinse	Rinse in the Quick Dump Rinser with the standard program until the resistivity is 5 MΩ.
Clean	10 minutes in concentrated nitric acid at 110 °C. This will dissolve metal particles. Use wet bench "HNO_3 69,5% 110C (Si)" and the carrier with the red dot.
Rinse	Rinse in the Quick Dump Rinser with the standard program until the resistivity is 5 MΩ.
Dry	Use the "Avenger Ultra-Pure 6" rinser/dryer with the standard program, and the white carrier with a red dot.

17. TITANIUM SPUTTERING: 200nm TiN@ 350°C (with Ti target)

Use the TRIKON SIGMA 204 sputter coater for the deposition of a Titanium on the wafers.
The target must exist Ti and deposition must be done at 350 °C with an Ar flow of *xxx* sccm.
Follow the operating instructions from the manual when using this machine.
Use recipe *xxx* to obtain a 200 nm thick Ti layer

18. COATING

Use the coater station of the EVG120 system to coat the wafers with photoresist. The process consists of:
- a treatment with HMDS (hexamethyldisilazane) vapor, with nitrogen as a carrier gas
- spin coating of Shipley SPR3012 positive resist, dispensed by a pump
- a soft bake at 95 °C for 90 seconds

Always check the relative humidity (48 ± 2 %) in the room before coating, and follow the instructions for this equipment.
Use program "1-**Co - 3012 – 1.4 _no EBR**". There will be no edge bead removal.

19. ALIGNMENT AND EXPOSURE

Processing will be performed on the SUSS MicroTec MA/BA8 mask aligner
Check if the mask is clean before usage; perform mask cleaning if necessary.
Expose mask ***2_electrodes***, with an exposure dose of xxx.
Use top side alignment program 1 with the "soft contact" option switched on.

20. DEVELOPING

Use the developer station of the EVG120 system to develop the wafers. The process consists of:
- a post-exposure bake at 115 °C for 90 seconds
- developing with Shipley MF322 with a single puddle process
- a hard bake at 100 °C for 90 seconds

Use program "1-**Dev - SP**".

21. INSPECTION: Linewidth and overlay

Visually inspect the wafers through a microscope, and check the line width and overlay. No resist residues are allowed.

22. PLASMA ETCHING: 200 nm Titanium Nitride

Use the Trikon mega 201 plasma etcher.
Follow the operating instructions from the manual when using this machine.
It is not allowed to change the process conditions and times from the etch recipe!
Use sequence ***xxx_TI*** (with a platen temperature of 25 ºC) to etch the titanium layer.

Process conditions from chamber recipe TiN:						
Step	Gasses & flows	Pressure	Platen RF	ICP RF	Platen temp.	Etch time
1. breakthrough	HBr/Cl_2 = 40/30 sccm	5 mTorr	50 W	500 W	25 °C	endpoint
2. bulk etch	HBr/Cl_2 = 40/30 sccm	5 mTorr	40 W	500 W	25 °C	endpoint
3. overetch	HBr/Cl_2 = 30/15 sccm	5 mTorr	40 W	500 W	25 °C	60% of bulk

23. INSPECTION: No titanium residues or undercut are allowed.

Visually inspect the wafers through a microscope.

24. LAYER STRIPPING: Photoresist

Strip resist — Use the Tepla Plasma 300 system to remove the photoresist in an oxygen plasma. Follow the instructions specified for the Tepla stripper, and use the quartz carrier. Use **program 1**: 1000 watts power and automatic endpoint detection + 2 min. overetching.

Insulation layer

25. CLEANING: HNO_3 99% and 69.5%

Clean — 10 minutes in fuming nitric acid at ambient temperature. This will dissolve organic materials. Use wet bench "HNO_3 99% (Si)" and the carrier with the red dot.
Rinse — Rinse in the Quick Dump Rinser with the standard program until the resistivity is 5 MΩ.
Clean — 10 minutes in concentrated nitric acid at 110 °C. This will dissolve metal particles. Use wet bench "HNO_3 69,5% 110C (Si)" and the carrier with the red dot.
Rinse — Rinse in the Quick Dump Rinser with the standard program until the resistivity is 5 MΩ.
Dry — Use the "Avenger Ultra-Pure 6" rinser/dryer with the standard program, and the white carrier with a red dot.

26. PECVD DEPOSITION: 300 nm Silicon oxide

Use the Novellus Concept One PECVD reactor.
It is **not** allowed to change the process conditions and time from the deposition recipe!
Use recipe **".xxx_siostd"** to deposit a 300 nm thick SiO_2 layer.

Process conditions from recipe .xxx siostd:					
Gasses & flows	Pressure	HF power	LF power	Temperature	Time
$N_2/SiH_4/N_2O$ = 3150/205/6000sccm	2.2 Torr	1000 W	0 W	400 °C	**variable**

Note: ▪ The layer thickness depends on the station deposition time (SDT), which can be calculated from the average deposition rate during recent recipe usage. This can be found in the logbook of the system.
▪ An extra test wafer can be deposited for measurements and etch tests.

27. COATING

Use the coater station of the EVG120 system to coat the wafers with photoresist. The process consists of:
- a treatment with HMDS (hexamethyldisilazane) vapor, with nitrogen as a carrier gas
- spin coating of Shipley SPR3012 positive resist, dispensed by a pump
- a soft bake at 95 °C for 90 seconds

Always check the relative humidity (48 ± 2 %) in the room before coating, and follow the instructions for this equipment.
Use program "1-**Co - 3012 – 1.4 _no EBR**". There will be no edge bead removal.

28. ALIGNMENT AND EXPOSURE

Processing will be performed on the SUSS MicroTec MA/BA8 mask aligner
Check if the mask is clean before usage; perform mask cleaning if necessary.
Expose mask ***3_insulation_open_frontend***, with an exposure dose of xxx.
Use top side alignment program 1 with the "soft contact" option switched on.

29. DEVELOPING

Use the developer station of the EVG120 system to develop the wafers. The process consists of:
- a post-exposure bake at 115 °C for 90 seconds
- developing with Shipley MF322 with a single puddle process
- a hard bake at 100 °C for 90 seconds

Use program "1-**Dev - SP**".

30. INSPECTION: Linewidth and overlay
Visually inspect the wafers through a microscope, and check the line width and overlay. No resist residues are allowed.

31. PLASMA ETCHING: 300 nm oxid
Use the Drytek Triode 384T plasma etcher.
It is **not** allowed to change the process conditions from the etch recipe, except for the etch time!

Use recipe **STDOXIDE** to etch the oxide layer. **Set the etch time to 33 seconds**.

Process conditions from recipe STDOXIDE:					
Step	Gasses & flows	Pressure	RF power	He pressure	Etch time
1. bulk etch (RIE)	C_2F_6/CHF_3 = 36/144 sccm	180 mTorr	300 W	12 Torr	variable

INSPECTION: No oxide residues are allowed on the etched areas.

32. LAYER STRIPPING: Photoresist
Strip resist Use the Tepla Plasma 300 system to remove the photoresist in an oxygen plasma.
Follow the instructions specified for the Tepla stripper, and use the quartz carrier.
Use **program 1**: 1000 watts power and automatic endpoint detection + 2 min. overetching.

Aluminum layer

33. CLEANING: HNO_3 99% and 69.5%
Clean 10 minutes in fuming nitric acid at ambient temperature. This will dissolve organic materials.
Use wet bench "HNO_3 99% (Si)" and the carrier with the red dot.
Rinse Rinse in the Quick Dump Rinser with the standard program until the resistivity is 5 MΩ.
Clean 10 minutes in concentrated nitric acid at 110 °C. This will dissolve metal particles.
Use wet bench "HNO_3 69,5% 110C (Si)" and the carrier with the red dot.
Rinse Rinse in the Quick Dump Rinser with the standard program until the resistivity is 5 MΩ.
Dry Use the "Avenger Ultra-Pure 6" rinser/dryer with the standard program, and the white carrier with a red dot.

34. METALLIZATION: 675 nm Al (with 1%Si) at 350 °C
Use the TRIKON SIGMA 204 sputter coater for the deposition of an aluminium metal layer on the wafers.
It is **not** allowed to change the process conditions and time from a sputtering recipe!

Use recipe **AlSi_675nm_350C** to obtain a 675 nm thick layer.

Process conditions from module recipe AlSi_675nm_350C:					
Module recipe	Target	Electrode temp.	Gasses & flows	Target power	Time
1. AlSi_675nm_350C	99% Al with 1% Si	350 °C	Ar = 100 sccm	10 kW	xx s

Visual inspection: the metal layer must look shiny.

35. COATING
Use the coater station of the EVG120 system to coat the wafers with photoresist. The process consists of:
- a treatment with HMDS (hexamethyldisilazane) vapor, with nitrogen as a carrier gas
- spin coating of Shipley SPR3012 positive resist, dispensed by a pump
- a soft bake at 95 °C for 90 seconds

Always check the relative humidity (48 ± 2 %) in the room before coating, and follow the instructions for this equipment.
Use program "1-**Co - 3012 – 1.4 _no EBR**". There will be no edge bead removal.

36. ALIGNMENT AND EXPOSURE
Processing will be performed on the SUSS MicroTec MA/BA8 mask aligner
Check if the mask is clean before usage; perform mask cleaning if necessary.
Expose mask ***4_pads***, with an exposure dose of 950.
Use top side alignment program 1 with the "soft contact" option switched on.

37. DEVELOPING
Use the developer station of the EVG120 system to develop the wafers. The process consists of:
- a post-exposure bake at 115 °C for 90 seconds
- developing with Shipley MF322 with a single puddle process
- a hard bake at 100 °C for 90 seconds

Use program "1-**Dev - SP**".

38. INSPECTION: Linewidth and overlay
Visually inspect the wafers through a microscope, and check the line width and overlay. No resist residues are allowed.

39. **WET ETCHING: 675 nm Aluminium (sputtered at 350 °C)**
Use wet etching line for aluminum etching

40. **LAYER STRIPPING: Photoresist**
Strip resist Use the Tepla Plasma 300 system to remove the photoresist in an oxygen plasma.
Follow the instructions specified for the Tepla stripper, and use the quartz carrier.
Use **program 1**: 1000 watts power and automatic endpoint detection + 2 min. overetching.

Back-end process

Contaminated wafer

Polymeric pyramid structures

External at the PME cleanroom of the 3ME faculty

41. **Transfer wafer to PME-LAB::**
Use wafer-box or wafer-disk with zip-bag to transfer wafer to PME

42. **PME-LAB: Cleaning:**
Bath wafer in petri-dish: 2 min in acetone
Rinse with iso-propanol
Air-dry for ca. 5 min, until no drops remain

43. **PME-LAB: Surface treatment:**
Oxygen plasma: Diener Femto: 100W / 15 min 5-6 sccm O_2
Silanization bath for >2h: 30mL ethanol mixed with 3mL MAPTMS (10%)
Rinse with acetone and deionized water
Blow dry if necessary
Dispose the solvents into the organic waste container

44. **PME-LAB: FABRICATION: Two-Photon-Polymerisation**
Use the Nanoscribe Photonic Professional GT+ with Large Feature Set (10x objective) to fabricate the structures.
Place wafer into wafer-holder, fixate carefully with the screws.
Use photosensitive resin IP-Q (methacrylate-based): deposit droplets on fabrication sites (center of each wafer die)
Load holde into 2PP machine and align coordinate system to wafer markers at (-45, 0) and (45,0).
Start wafer-level fabrication job, set variable **$FAB_STRUCTURE=1**, all other **$FAB variables** must be set to 0
Follow the operating instructions from the manual when using this machine.

45. **PME-LAB: RESIN DEVELOPMENT:**
Use the developer fume hood in the PME cleanroom
Development Bath in Propylene glycol methyl ether acetate (PGMEA) for 25min.
Clean Bath in isopropanol for 5min.
Dry Let the wafer rest under the fume hood until isopropanol has evaporated (5min)
Dispose the developer into the organic waste container

46. **PME-LAB: INSPECTION:**
Use Keyence Digital Microscope VHX-6000 to visually inspect the structures and verify their alignment

Passivation of pyramids

47. **Transfer wafer to KAVLI-LAB::**
Use wafer-box or wafer-disk with zip-bag to transfer wafer to KAVLI

48. **Kavli: SILICON OXID ICPCVD: 200nm SiO_2 @ 40 °C**
External at the Kavli cleanroom
Oxford ICPCVD KavliLab to deposit SiO_2 at low temperatures and passivate polymeric structures
Use Kavli low-temperature SiO_2 recipe and adapt process time according to thickness.

49. **Transfer wafer to EKL-LAB::**
Use wafer-box or wafer-disk with zip-bag to transfer wafer to EKL.

Open passivation for contact to front-end

50. MANUAL Cleaning: Acetone and IPA
Clean Wafer in Acetone bath for 2 min
Rinse with IPA for 30s
Rinse with DI water for 30s
Blow dry

51. MANUAL COATING
Manual HMDS treatment:
Hotplate: 110°C/ 5min
Manual HMDS for 10 min
Spin Coat in Polymer-Lab
Use spin-coater in polymer-lab: Shipley SPR3012 positive resist (3um recipe) (**use contaminated chuck**)
Soft bake at 95 °C for 90 seconds

52. ALIGNMENT AND EXPOSURE
Processing will be performed on the SUSS MicroTec MA/BA8 mask aligner
Check if the mask is clean before usage; perform mask cleaning if necessary.
Expose mask ***1_pads***, with an exposure dose of xxx.
Use top side alignment program 1 with the "proximity" option switched on, set distance to pyramid height +20um.
Post-exposure bake: 115 °C for 90 seconds

53. DEVELOPING MANUAL
Use the developer fume hood in the polymer lab.
Developing with the AZ 326 MIF developer (1-2 min)
Rinse with DI water (1 min)
Blow or spin-dry wafer (**make sure to use the contaminated chuck**)

54. WET ETCHING: 300 nm oxide
Prepare BHF bath in SAL-Lab: use buddy and neoprene gloves. All beakers must be made out of Teflon

Etch	Use "BHF 1:7 (SiO_2-ets)" at ambient temperature
Time	A short dip is enough to remove the ICPCVD SiO2 film
Rinse	Rinse with DI immediately, place in Teflon beaker with hole and let it rinse for 5 min.
Dry	Blow dry

55. LAYER STRIPPING: Photoresist
Strip resist in Acetone bath for 2 min.

Pattern electrodes

56. MANUAL Cleaning: Acetone and IPA
Clean Wafer in Acetone bath for 2 min
Rinse with IPA for 30s
Rinse with DI water for 30s
Blow dry

57. COATING
Use the EVG101 spraycoater system to coat the wafers with photoresist. The process consists of:
- AZ 12XT-20PL diluted positive photoresist (ratio: 1:6:3.8)

Always check the relative humidity (48 ± 2 %) in the room before coating, and follow the instructions for this equipment.
Make sure to use the contaminated chuck and that the correct resist is loaded.
Use program "HP 1000mbar 5 ml 8 layers"
Softbake: 110°C/3min (Hot plate with carrier wafer)
Repeat Coating and Softbaking 2 times
Final Softbake: 110°C/6min (Hot plate with carrier wafer)

58. Transfer wafer to PME-LAB::
Use wafer-box or wafer-disk with zip-bag to transfer wafer to PME-Lab.
Wrap box/disk with aluminum foil to avoid exposure from ambient light!

59. PME-LAB: EXPOSURE: Two-Photon-Polymerisation
Use the Nanoscribe Photonic Professional GT+ with Medium Feature Set (25x objective) to expose the electrode pattern.
Place wafer into wafer-holder, fixate carefully with the screws.
Use immersion medium: glycerol: deposit droplets on fabrication sites (center of each wafer die)
Load holder into 2PP machine and align coordinate system to wafer markers at (-45, 0) and (45,0).
Start wafer-level fabrication job, set variable **$FAB_ELECTRODES=1**, all other **$FAB variables** must be set to 0

60. **PME-LAB:: POST EXPOSURE**
Rinse wafer with DI-water to remove glycerol
Blow dry gently
Post exposure bake (PEB): 90 °C / 2 min (Hot plate with carrier wafer)

61. **Transfer wafer to EKL-LAB::**
Use wafer-box or wafer-disk with zip-bag to transfer wafer to EKL.
Wrap box/disk with aluminum foil to avoid exposure from ambient light!

62. **DEVELOPING MANUAL**
Use the developer fume hood in the polymer lab.
Developing with the AZ 326 MIF developer (3-4 min)
Rinse with DI water (1 min)
Blow or spin-dry wafer (**make sure to use the contaminated chuck**)
To ensure right development time it is recommended to optically inspect the wafer after 3min development time, and if necessary re-development the wafer further
Dispose the developer into the right container.

63. **INSPECTION: Linewidth and overlay**
Visually inspect the wafers through a microscope, and check the line width and overlay. No resist residues are allowed.

Deposit electrode material

64. **Transfer wafer to KAVLI-LAB::**
Use wafer-box or wafer-disk with zip-bag to transfer wafer to KAVLI

65. **GOLD DEPOSITION: 10 nm titanium / 100nm Gold**
Use electron beam evaporation: Temescal FC-20349
Check log-bug for deposition-rate and start-power
Wait until chamber pressure reached start-pressure before starting the recipe
Make sure enough material is in the crucible.

Lift-off electrode

66. **Transfer wafer to EKL-LAB::**
Use wafer-box or wafer-disk with zip-bag to transfer wafer to EKL.

67. **LIFT-OFF: Acetone bath**
Use Shaker and fume hut in polymer lab.
Place wafer up-side down into a petri dish, use spider-clamp from wafer-holder as spacer.
Fill petri dish with acetone and place inside a large beaker.
Put beaker on shaker and start, set to 60 rpm.
Wait 15-20 min, use acetone spray bottle to remove residues.
Clean with IPA
Blow or spin-dry wafer (**make sure to use the contaminated chuck**)

68. **INSPECTION: Linewidth and overlay**
Visually inspect the wafers through a microscope, and check the line width and overlay. No gold flakes are allowed.
SEM may be used as well.

69. **WET ETCHING: 300 nm oxide**
Prepare BHF bath in SAL-Lab: use buddy and neoprene gloves. All beakers must be made out of Teflon

Etch	Use "BHF 1:7 (SiO_2-ets)" at ambient temperature
Time	A short dip is enough to remove the ICPCVD SiO2 film
Rinse	Rinse with DI immediately, place in a Teflon beaker with a hole and let it rinse for 5 min.
Dry	Blow dry

Polymeric pyramid structures

External at the PME cleanroom of the 3ME faculty

70. **Transfer wafer to PME-LAB::**
Use wafer-box or wafer-disk with zip-bag to transfer wafer to PME

71. **PME-LAB: Cleaning:**
Bath wafer in petri-dish: 2 min in acetone
Rinse with iso-propanol
Air-dry for ca. 5 min, until no drops remain

72. **PME-LAB: Surface treatment:**
Oxygen plasma: Diener Femto: 100W / 30 sec 5-6 sccm O_2
Silanization bath for >2h: 30mL ethanol mixed with 3mL MAPTMS (10%)
Rinse with acetone and deionized water
Blow dry if necessary
Dispose the solvents into the organic waste container

73. **PME-LAB: FABRICATION: Two-Photon-Polymerisation**
Use the Nanoscribe Photonic Professional GT+ with Large Feature Set (10x objective) to fabricate the structures.
Place wafer into wafer-holder, fixate carefully with the screws.
Use photosensitive resin IP-Q (methacrylate-based): deposit droplets on fabrication sites (center of each wafer die)
Load holde into 2PP machine and align coordinate system to wafer markers at (-45, 0) and (45,0).
Start wafer-level fabrication job, set variable **$FAB_ISOLATION=1**, all other **$FAB variables** must be set to 0
Follow the operating instructions from the manual when using this machine.

74. **PME-LAB: RESIN DEVELOPMENT:**
Use the developer fume hood in the PME cleanroom

Development	Bath in Propylene glycol methyl ether acetate (PGMEA) for 25min.
Clean	Bath in isopropanol for 5min.
Dry	Let the wafer rest under the fume hood until isopropanol has evaporated (5min)

Dispose the developer into the organic waste container

75. **PME-LAB: INSPECTION:**
Use Keyence Digital Microscope VHX-6000 to visually inspect the structures and verify their alignment

Packaging

76. **Wafer Dicing for packaging**

77. **Wire bonding to pcb**

C. DeScribe Code for multi-step 2PP process

In the following listings, the most important code snippets for the *Nnanoscribe* 2PP-machine are shown. Since the used language (General Writing Language (GWL)) is limited in terms of commands, compromises and work-around were made. Most importantly, the language does not offer functions and all variables are floats. Therefore, functions were imitated by using the `include` command, which refers to other GWL-files. Since parameters cannot be passed to these include statements, unique, global variables were set prior the including the file, such the code inside the file can access them. The subroutines and custom functions are referred to via a relative path, therefore, the directory structure may not be changed. Some of the code was shortened to improve readability.

C.1. Multi-step fabrication

The main job-file is shown in Listing C.1, at the beginning various variables are defined or loaded via include statements. Thereafter, the movement stage is moved to every fabrication position and the subroutine `dice_job.gwl` (Listing C.2) is called.

Listing C.1: Main jobfile: `main_wafer_scale_fabV4.gwl`

```
% Wafer scale fabrication for 12 20mm x 20mm dices
% Thomas Michalica
% Version 4
% Movement compensation
% Multiprint fabrication process

% ____________________________________________________________________________%
% START SETUP
% DEBUG
include ..\custom_functions\cf_logger.gwl
var $debug = $LOG_INFO
TimeStampOn

% ____________________________________________________________________________%
% BOOLS to set fabrication step
var $FAB_DEBUG = 0              % Only for CAM, prints all steps
var $FAB_STRUCTURE =1           % Structure step (IP-Q)
var $FAB_ELECTRODES = 0         % Electrode pattern step (AZ 12XT)
var $FAB_ISOLATION = 0          % Insulation step (IP-Q)
var $FAB_MISC = 0               % Additional step at after Insulation - not used
var $FAB_STEP = 0               % Used internally
% init variables
include ..\custom_functions\cf_stand_aloneV2.gwl

var $b_giant_pyr = 0            % BOOL: 1 = fabricate giant pyramids
var $b_pyr =0                   % BOOL: 1 = fabricate pyramids/dices
var $b_stairs = 0               % BOOL: 1 = fabricate staircase tests
var $b_dose_test = 0            % BOOL: 1 = make a dose test?!
var $b_verbose_fab = 0          % BOOL: 1 = verbose start & end of struct fabrication
var $bool_photo = 0             % BOOL: 1 = take photo NOT IMPLEMENTED
var $b_center_stage = 0         % BOOL: 1 = center after print, else move to start

% SETUP Startposition for absolute coordinate system
var $start_pos_x = -45000           % x-coordinate of current position in um
var $start_pos_y = 0                % y-coordinate of current position in um

% FABRICATION ERROR OFFSETS (Wafer depended)
include fab_offsets.gwl %set global wafer offsets (shift structures a few um

% WAFER FABRICATION POSITIONS
include ..\custom_functions\cf_fab_positions.gwl
```

```
% SET STRUCTURES TO BE FABRICATED
include _fab_setter_lift_off.gwl

% Set current position for coordinate system
set $x_cur = $start_pos_x
set $y_cur = $start_pos_y


%_____________________________________________________________________________%
% INIT DONE

%_____________________________________________________________________________%
% START wafer-scale fabrication
%_____________________________________________________________________________%
% DICE 1
set $dice_number = 1
if $b_dice_01 > $FLOAT_RES
        NewStructure
        set $dice_count = $dice_count + 1
        MessageOut "Start Dice %u" # ($dice_number)
        MessageOut "%u / %u" # ($dice_count, $dice_target)
        % Move to dice position
        var $x_tar = $pos_d01_x
        var $y_tar = $pos_d01_y
        include ..\custom_functions\cf_move_abs_retract.gwl

        include jobs\dice_job\dice_job.gwl
end

%_____________________________________________________________________________%
% DICE 2
set $dice_number = 2
if $b_dice_02 > $FLOAT_RES
        NewStructure
        set $dice_count = $dice_count + 1
        MessageOut "Start Dice %u" # ($dice_number)
        MessageOut "%u / %u" # ($dice_count, $dice_target)
        % Move to dice position
        var $x_tar = $pos_d02_x
        var $y_tar = $pos_d02_y
        include ..\custom_functions\cf_move_abs_retract.gwl

        include jobs\dice_job\dice_job.gwl
end

%.............................................................................%
% CONTINUE WITH ALL OTHER DICE AND TEST POSITION
% OMMITED DUE TO LENGTH
%.............................................................................%

%_____________________________________________________________________________%
% DICE 12
set $dice_number = 12
if $b_dice_12 > $FLOAT_RES
        NewStructure
        set $dice_count = $dice_count + 1
        MessageOut "Start Dice %u" # ($dice_number)
        MessageOut "%u / %u" # ($dice_count, $dice_target)
        % Move to dice position
        var $x_tar = $pos_d12_x
        var $y_tar = $pos_d12_y
        include ..\custom_functions\cf_move_abs_retract.gwl

        include jobs\dice_job\dice_job.gwl
end

%_____________________________________________________________________________%
% Move back to start marker to be ready for additional jobs
if $debug <= $LOG_INFO
        MessageOut "Fabrication finished!"
        if abs($b_center_stage - 1) < $FLOAT_RES
                MessageOut "Fabrication finished! Centering Stage"
        else
                MessageOut "Moving back to start position!"
        end
end

if abs($b_center_stage - 1) < $FLOAT_RES
        % CENTER STAGE
        set $x_tar = 0
        set $y_tar = 0
else
        % back to marker
        set $x_tar = $start_pos_x
        set $y_tar = $start_pos_y
end
```

```
include ..\custom_functions\cf_move_abs_retract.gwl
SaveMessages "Log.txt"
```

The subroutine `dice_job.gwl` (Listing C.2) is called at the center of each dice location. It is a wrapper for future subroutines, to allow fast iterations of dice-jobs, without changing the main job-file.

Listing C.2: Subroutine dice-job: `dice_job.gwl`

```
% Dice job
% Name:          dice_job.gwl
% Author:        Thomas Michalica
% Version:       3
% Date:          2022/04/25
%
local $standAlone = 0 % If tested alone, set to 1
if  $standAlone > 0.01
        var $b_LIFT_OFF = 0
        var $b_DEBUG = 1
        include ..\..\..\custom_functions\cf_stand_alone.gwl
        include ..\..\..\custom_functions\cf_fab_positions.gwl
        include ..\..\..\custom_functions\cf_structures.gwl
        var $dice_number = 12
end
%_____________________________________________________________________________%
% Dice Job
% Current position is local die origin/ set local origin and move there
include ..\..\..\custom_functions\cf_set local_origin.gwl
include dice_job_v8\dice_job_v8.gwl
```

The subroutine `dice_job_v8.gwl` (Listing C.3), allows to set a different job-file for each dice locatation.

Listing C.3: Subroutine dice-job v8: `dice_job_v8.gwl`

```
% Dice job v8
% Name:          dice_job_v8.gwl
% Author:        Thomas Michalica
% Version:       8
% Date:          2022/09/01
%
% Gets called by dice job

%_____________________________________________________________________________%
% DICE 1
if abs($dice_number - 1) < $FLOAT_RES
        include pyramid\job_pyramid_array.gwl
end
%_____________________________________________________________________________%
% DICE 2
if abs($dice_number -2 ) < $FLOAT_RES
        include pyramid\job_pyramid_array.gwl
end

%.............................................................................%
% CONTINUE WITH ALL OTHER DICE POSITIONS
% OMMITED DUE TO LENGTH
%.............................................................................%

%_____________________________________________________________________________%
%_____________________________________________________________________________%
% DICE 12
if abs($dice_number - 12 ) < $FLOAT_RES
        include pyramid\job_pyramid_array.gwl
end
```

The subroutine `job_pyramid_array.gwl` (Listing C.4) is called at the center of each dice by the `dice_job_v8.gwl` (Listing C.3). Depending on which fabrication step (`$FAB_STRUCTURE` for pyramids, (`$FAB_ELECTRODES` for electrodes, (`$FAB_ISOLATION` for insulation) is selected, different subroutines are called. The pyramid structures are fabricated with a custom array function, while the other structures (electrodes, insulation) are split into two parts: (i) structures on top of the pyramid, and (ii) structures on the substrate.

Listing C.4: Subroutine: `job_pyramid_array.gwl`

```
% Set variables for array function
var $arr_space_x = 400                  % Spacing between structures in x
var $arr_space_y = 400                  % Spacing between structures in y
var $arr_size_x = 5                     % Number of structs in x
var $arr_size_y = 3                     % Number of structs in y
var $num_structs = $arr_size_y * $arr_size_x - 1
var $arr_init_retract = 0               % Retract between structures
var $arr_center_x = $local_origin_x     % x-coord of array center
var $arr_center_y = $local_origin_y     % y-coord of array center


if $FAB_STRUCTURE > $FLOAT_RES
        % IPQ PYRAMID ARRAY
        set $x_tar = $local_origin_x
        set $y_tar = $local_origin_y
        include ..\..\..\..\..\custom_functions\cf_move_abs.gwl
        set $FAB_STEP = 1

        var $arr_counter = 0 % reset array counter
        repeat $num_structs
        include array_caller_pyramids.gwl % Print pyramid array
end

if $FAB_ELECTRODES > $FLOAT_RES
        % LIFT OFF
        set $x_tar = $local_origin_x
        set $y_tar = $local_origin_y
        include ..\..\..\..\..\custom_functions\cf_move_abs.gwl
        set $FAB_STEP = 2

        var $arr_counter = 0
        repeat $num_structs
        include array_caller_pyramids.gwl % Print electrodes on pyramids

        set $x_tar = $local_origin_x
        set $y_tar = $local_origin_y
        include ..\..\..\..\..\custom_functions\cf_move_abs.gwl

        set $rel_interface_pos_x = 0
        set $rel_interface_pos_y = 1000
        include ..\..\..\..\..\custom_functions\cf_distance_interfaceV2.gwl
        include lo_electrode_selector.gwl % Print ground electrodes

        % Position for dice numbering
        var $dice_num_pos_x = 0
        var $dice_num_pos_y = -3150
end

if $FAB_ISOLATION > $FLOAT_RES
        % IP-Q Insulation
        set $x_tar = $local_origin_x
        set $y_tar = $local_origin_y
        include ..\..\..\..\..\custom_functions\cf_move_abs.gwl
        set $FAB_STEP = 3

        var $arr_counter = 0
        repeat $num_structs
        include array_caller_pyramids.gwl % print insulation on pyramids

        set $x_tar = $local_origin_x
        set $y_tar = $local_origin_y
        include ..\..\..\..\..\custom_functions\cf_move_abs.gwl

        set $rel_interface_pos_x = 0
        set $rel_interface_pos_y = -800
        include ..\..\..\..\..\custom_functions\cf_distance_interfaceV2.gwl
        set $s_selector = $S_GROUND_ISO_H6_OH10_z2_h05
        % print insulation on ground
        include ..\..\..\..\..\_structure_libary\structure_selector.gwl
end


if $FAB_MISC > $FLOAT_RES
        set $x_tar = $local_origin_x
        set $y_tar = $local_origin_y
        include ..\..\..\..\..\custom_functions\cf_move_abs.gwl
        set $FAB_STEP = 4
end
```

C.2. Custom functions and definitions

The following code listings will discuss the most important custom functions.

Custom coordinate system and movement commands

In order to position fabricated structures precisely on the wafer, a custom coordinate system was used together with the alignment routine discussed in Section 5.5.2. At the beginning of the print-job, the coordinate system is initialzed by setting the variables `$x_cur` and `$y_cur` to the current position of the stage with respect to the wafer (in µm). Since the stage is aligned to the alignment markers on the wafer, the start position is set to `-45000, 0` respectively. The origin of the virtual coordinate system coincides with the center of the wafer. Whenever the stage is repositioned, the current position of the stage (`$x_cur`, `$y_cur`) is updated.

Relative movements are done by calling (including) the custom function `cf_move_rel.gwl` (Listing C.5). The distance is defined by setting the variables `$x_rel` and `$y_rel` prior the include statement. The function takes care of mechanical backslash of the stage by making sure, that every position is reached from the same direction. After the movement, the current position is updated.

Listing C.5: Subroutine: `cf_move_rel.gwl`

```
% CUSTOM FUNCTION - no standalone
% Name:      cf_move_rel.gwl
% Author:    Thomas Michalica
% Version:   1
% Date:      2022/04/25
%
% Abstraction of relative movement with an absolute coordinate system
% Used for wafer-scale fabrication with custom origin
%
% INCLUDES
%    -)    cf_logger.gwl

% NESSESARY definitions
%    var $x_cur                 INT: x-coordinate of current position in um
%    var $y_cur                 INT: y-coordinate of current position in um
%    var $x_rel                 INT: x-distance for relative movement in um
%    var $y_rel                 INT: y-distance for relative movement in um
%    var $bool_compensate       BOOL: spindle backslash compensation: 0=no, 1=yes
%    var $bs_comp               INT: compensation movement (standard 50um)
%    var $debug                 INT: verbose debug messages

% SETUP
include cf_logger.gwl

if $debug <= $LOG_DEBUG
    MessageOut "  DEBUG: Move relative x_rel=%u | y_rel=%u" # ($x_rel, $y_rel)
end

MoveStageX $x_rel
MoveStageY $y_rel

if $bool_compensate > 0
        if $x_rel < 0
        MoveStageX (-1) * $bs_comp
        MoveStageX $bs_comp
    end
    if $y_rel < 0
        MoveStageY (-1) * $bs_comp
        MoveStageY $bs_comp
    end
end

% Update positions
set $x_cur = $x_cur + $x_rel
set $y_cur = $y_cur + $y_rel
```

Absolute movements of the stage can be executed by calling the custom function texttt`cf_move_abs.gwl` (Listing C.6). The function is calculating the relative distance and calls the relative movement function (Listing C.5).

Listing C.6: Subroutine: `cf_move_abs.gwl`

```
% CUSTOM FUNCTION - no standalone
% Name:          cf_move_abs.gwl
```

```
% Author:        Thomas Michalica
% Version:       2
% Date:          2022/04/22
%
% Abstraction of absolute movement with an absolute coordinate system
% Used for wafer-scale fabrication with custom origin
%
% INCLUDES
%     -)     cf_logger.gwl
%     -)     cf_move_rel.gwl
% NESSESARY definitions
%    var $x_cur                      INT: x-coordinate of current position in um
%    var $y_cur                   INT: y-coordinate of current position in um
%        var $x_tar                                  INT: x-coordinate of target position in um
%        var $y_tar                        INT: y-coordinate of target position in um
%    var $bool_compensate         BOOL: spindle backslash compensation: 0=no, 1=yes
%    var $bs_comp                 INT: compensation movement (standard 50um)
%        var $debug                                  INT: verbose debug messages

% SETUP
include cf_logger.gwl
if $debug <= $LOG_DEBUG
    MessageOut "  DEBUG: Move to x_tar=%u | y_tar=%u" # ($x_tar, $y_tar)
end
var $x_rel = $x_tar - $x_cur
var $y_rel = $y_tar - $y_cur

include cf_move_rel.gwl
```

A variation of the absolute movement function is shown in Listing C.7. Prior to the movement, the objective is retracted several milimeters from the wafer. The movement is then executed with increased velocity and after reaching the desired location the objective approaches the wafer again. The standard stage velocity is $0.2\,\mathrm{mm\,s^{-1}}$), travelling from one dice to the next would take 100 s, while the faster movement requires a fifth of the time. Retracting also prevents the objective to smear resin all over the wafer.

Listing C.7: Subroutine: `cf_move_abs_retract`

```
% CUSTOM FUNCTION - no standalone
% Name:          cf_move_abs_retract.gwl
% Author:        Thomas Michalica
% Version:       1
% Date:          2022/04/25
%
% Abstraction of relative movement with an absolute coordinate system
% Retracts z-Stage before movement to omit resin contact and approach afterwards
% used for long movements, eg. approaching a new dice position on a wafer

% INCLUDES
%     -)     cf_move_abs.gwl
%     -)     cf_logger.gwl
% NESSESARY definitions
%        var $z_retract              INT: relative z-retraction movement: !!!NEGATIVE!!! IF:
     InvertZAxis 0
%    var $z_approach          INT: relative z-approach movement: should be positive $zRetract
%    var $vel_fastStage       INT: fast stage velocity for the long movement in mm/sec
%    var $vel_slowStage       INT: slow stage velocity after the long movement in mm/sec
%    var $interfacePos        FLOAT: Interface position compensation (FindInterfaceAt)
%    var $settle_time         FLOAT: wait time for resin flow in seconds
%

include cf_logger.gwl

% Retract
if $debug <= $LOG_INFO
    MessageOut "  INFO: Retract z-Stage %d" # ($z_retract)
end
AddZDrivePosition $z_retract
StageVelocity $vel_fastStage
% Move
include cf_move_abs.gwl
% Approach

if $debug <= $LOG_INFO
    MessageOut "  INFO: Approach interface- move z-Stage %d" # ($z_approach)
end
StageVelocity $vel_slowStage
AddZDrivePosition $z_approach
% Wait
if $debug <= $LOG_INFO
    MessageOut "  INFO: Waiting %u seconds" # ($settle_time)
```

```
end
Wait $settle_time
if $debug <= $LOG_DEBUG
    MessageOut "  DEBUG: Finding interface"
end
%FindInterfaceAt $interfacePos
```

Custom coordinate system and movement commands

The wrapper for the automatic interface finder, which is called via `FindInterfaceAt`-command is shown in Listing C.8. For each fabrication step, a different offset can be defined (usually half the slicing distance). This wrapper allows users to add an additional offset in the z-direction, which can be helpful when the substrate consists of multiple layers, such as a spraycoated photoresist film, and the interface is found within the substrate.

Listing C.8: Subroutine: `cf_interfaceV2`

```
% CUSTOM FUNCTION - no standalone
% Name:       cf_interfaceV2.gwl
% Author:     Thomas Michalica
% Version:    2
% Date:       2022/08/23
%
% Wrapper for the interface finder
% In 20x Air mode, the interface is often find to low.
% $ZCOMP != 0 will move the zDrive $ZCOMP um after the interface routine.
% Basically $ZCOMP is the same as $interfacePos but for the z-drive.
% V2: adds multistep fabrication
% INCLUDES
%    -)    cf_logger.gwl

% NESSESARY definitions
%    var $ZCOMP                  Shift of z-drive after interface is found, in  um
%    var $FLOAT_RES              To make sure no FLOATing point error is made
%    var $interfacePos           Interface position in um, must be positive

% SETUP
include cf_logger.gwl

% SET Interface Position according to the fabrication step
if $FAB_STRUCTURE > $FLOAT_RES
        set $interfacePos = $INTERFACE_STRUCTURE
end
if $FAB_ELECTRODES > $FLOAT_RES
        set $interfacePos = $INTERFACE_ELECTRODES
end
if $FAB_ISOLATION > $FLOAT_RES
        set $interfacePos = $INTERFACE_ISOLATION
end
if $FAB_MISC > $FLOAT_RES
        set $interfacePos = $INTERFACE_MISC
end

if $debug <= $LOG_DEBUG
        MessageOut "  DEBUG: Finding interface at: %u" # ($interfacePos)
end

FindInterfaceAt $interfacePos

% Move Z-drive for $ZCOMP um
if abs($ZCOMP) > $FLOAT_RES
        if $debug <= $LOG_INFO
                MessageOut "  INFO: Add ZDrive Offset to interface pos: %u" # ($ZCOMP)
        end
        AddZDrivePosition $ZCOMP
end
```

If the current stage position is occupied by structures from a previous fabrication step, the interface finding routine may not work. To address this issue, users can define x- and y-offsets to move the stage to a nearby empty position, find the interface, and then move back to the previous position and start the fabrication. The code is shown in Listing C.9.

Listing C.9: Subroutine: `cf_distance_interfaceV2`

```
% CUSTOM FUNCTION - no standalone
% Name:         cf_distance_interfaceV2.gwl
% Author:       Thomas Michalica
% Version:      2
% Date:         2022/08/25
%
% Move to relative position, find interface, and move back to previous position
% Usefull if current position is populated by structures
% V2: interface pos is depended on fabrication step

% INCLUDES
%     -)      cf_move_abs.gwl
%     -)      cf_logger.gwl
%     -)      cf_interface.gwl
% NESSESARY definitions
%         var $rel_interface_pos_x
%    var $rel_interface_pos_y
%

include cf_logger.gwl

% Save current position
local $cur_loc_x = $x_cur
local $cur_loc_y = $y_cur

if $debug <= $LOG_DEBUG
        MessageOut "  DEBUG: Distance interface finder called"
        MessageOut "  DEBUG: Current Position: x_cur=%u | y_cur=%u" # ($x_cur, $y_cur)
end

set $x_tar = $cur_loc_x + $rel_interface_pos_x
set $y_tar = $cur_loc_y + $rel_interface_pos_y
include cf_move_abs.gwl

include cf_interfaceV2.gwl

% Move back to previous position
set $x_tar = $cur_loc_x
set $y_tar = $cur_loc_y
include cf_move_abs.gwl
```

D. Measurement of pyramid structures

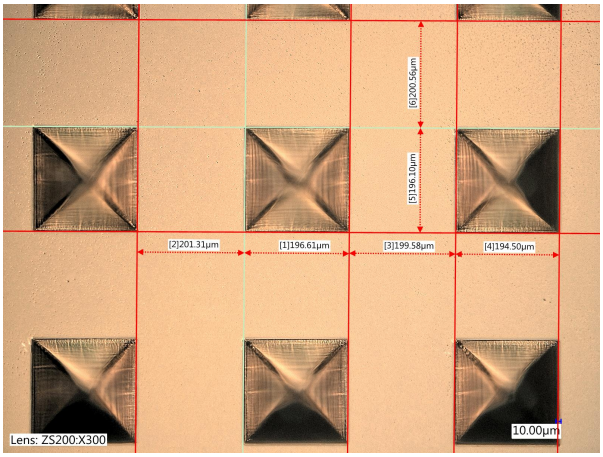

Figure D.1.: Measured dimensions of 3D-multi-electrode array (3D-MEA) pyramid structures

Table D.1.: Measured dimensions of 3D-MEA pyramid structures

Structure	**X**-dimension in µm	**Y**-dimension in µm
1	193.8	196.1
2	190.9	195.9
3	193.5	196.0
4	197.9	196.8
5	193.5	194.4
6	196.1	195.2
7	194.3	194.3
8	196.0	193.8
9	194.5	196.2
10	195.1	193.3
11	193.3	192.7
12	196.7	194.7
13	195.4	192.8
14	191.3	195.9
15	195.4	193.7
Nominal	200	200
Average	194.5	194.8
Std. dev	1.88	1.35